ISSN 2458-973X

JSCMT

Journal of Sustainable Construction Materials and Technologies

Volume 7
Issue 2
Year 2022

YTÜ PRESS

www.jscmt.yildiz.edu.tr

Journal of Sustainable Construction Materials and Technologies
Web page info: https://jscmt.yildiz.edu.tr

JSCMT
Journal of Sustainable Construction Materials and Technologies

Contact

Journal of Sustainable Construction

Materials and Technologies (JSCMT)

Yildiz Technical University
Civil Engineering Department, 34220 Esenler
Istanbul – Türkiye

Web: http://dergipark.gov.tr/jscmt/

E-mail: jscmt@yildiz.edu.tr

Journal of Sustainable Construction Materials and Technologies
Web page info: https://jscmt.yildiz.edu.tr

JSCMT
Journal of Sustainable Construction Materials and Technologies

Journal of Sustainable Construction Materials and Technologies
Web page info: https://jscmt.yildiz.edu.tr

Journal of Sustainable Construction Materials and Technologies
Web page info: https://jscmt.yildiz.edu.tr

JSCMT
Journal of Sustainable Construction Materials and Technologies

TABLE OF CONTENTS

Title Pages

Research Articles

Journal of Sustainable Construction Materials and Technologies
Web page info: https://jscmt.yildiz.edu.tr

Journal of Sustainable Construction Materials and Technologies
Web page info: https://jscmt.yildiz.edu.tr
DOI: 10.47481/jscmt.1114597

JSCMT
Journal of Sustainable Construction Materials and Technologies

Research Article

Analysis of alternative sustainable approach to concrete mixture design

Rebecca BABCOCK, Talat SALAMA*

Department of Manufacturing and Construction Management, Central Connecticut State University, New Britain, Connecticut, USA

ARTICLE INFO

Article history
Received: 10 May 2022
Accepted: 31 May 2022

Key words:
Admixture, concrete, fly-ash, ground glass concrete, sustainability, volcanic ash

ABSTRACT

Sustainability is a growing area of concern, especially amid the concrete industry. Concrete, especially traditional concrete, which contains Portland cement, is extremely harmful to the environment producing mass amounts of carbon dioxide. Additionally, the mining of the concrete materials, like lime, cause significant damage to waterways and ecosystems. For years, studies have found more sustainable alternatives that are structurally equivalent to traditional concrete. The Connecticut Department of Transportation does allow for the use of alternative "green" concretes if the mix designs meet the required specifications. Nevertheless, heavy highway construction seems reluctant to experiment with new substances and continues to fall back on the use of fly ash concrete. This solution, however, is not perfect, as fly ash is a finite material. By conducting a nationwide survey to the Departments of Transportation (DOT), the reliance on fly ash was evident. It was also found that the biggest concerns for DOTs was the cost and availability of the material. This study investigates presently accepted alternative concrete mixture designs and explores the solutions of volcanic ash concrete and ground glass concrete. Based on the results of the survey and construction practicality, this study suggests the incorporation of ground glass concrete for heavy highway construction. This solution provides the needed strength requirements per DOT specifications and is within the same price-range as fly ash concrete.

Cite this article as: Babcock, R., & Salama, T. (2022). Analysis of alternative sustainable approach to concrete mixture design. *J Sustain Const Mater Technol*, 7(2), 40–52.

1. INTRODUCTION

The Connecticut Department of Transportation currently adheres to the Federal Highway Administration's catchy slogan of "get in, get out, stay out", leaving them reluctant to experiment and possibly gamble with new concrete design mixtures that may not have the same longevity as traditional concrete mix designs or those that may require longer time to set risking unnecessary traffic delays. Current concrete mixture designs are up to the supplier who has the freedom to experiment as they see fit as long as they meet the strength specifications set by the Connecticut DOT [1]. Nevertheless, alternative concrete mixtures have been slow to make gains in heavy highway construction. Currently, the Connecticut DOT's most used sustainable concrete is fly ash concrete since it helps with concrete workability. However, while this is more eco-conscious than traditional concrete, it is not an in-

***Corresponding author.**
*E-mail address: talats@ccsu.edu

definite solution. As climate change is a growing concern, the burning of coal, which produces fly-ash has declined, as this process also causes significant harm to the environment [2]. Further, even if countries were to continue to burn coal, the current rate of consumption will likely deplete coal by 2090 [3]. In turn, coal slag will become scarcer, and the cost will inevitably increase as well.

Therefore, with this future date in mind, it is now more critical than ever to explore alternative concrete mixture designs that will prove to have similar material properties as traditional concrete but will be more sustainable in terms of the environment and economy. Two alternatives to be explored are volcanic ash concrete and ground glass pozzotive concrete. With strengths able to meet DOT specifications, it is surprising that Departments of Transportations have not attempted to use the material in their heavy highway builds [4]. This prompts questions involving practicality and supply to determine how these materials, or any other alternative materials, may become a solution for Connecticut highway infrastructure. By surveying the Departments of Transportation nationwide as well as investigating concrete suppliers, it may be possible to see if this reluctance is limited to Connecticut, or if it is nationwide. In all, this project attempts to gather data on alternative concrete mixtures used by the Departments of Transportation nationwide in an effort to offer more sustainable long-term solutions to the Connecticut DOT.

2. SYNOPSIS OF EXISTING LITERATURE

The plan for this project initially began as a survey to the Departments of Transportation nationwide to gain insight on concrete usage, specifically pertaining to cost and composition in the heavy highway construction industry. Following the surveys, this project's focus has morphed in response to the survey replies and targeted two alternatives for fly ash concrete. Of the two options discussed, ground glass pozzolan concrete is much more likely to take off in the New England and Tri-State regions compared to the volcanic ash concrete. To assess these mixture designs more clearly in comparison to fly ash concrete, a literature review was performed.

Fly ash, which is the resultant of burning coal, is one of the most frequently used additives in concrete composition to offset the amount of Portland cement, which not only makes concrete stronger, but also benefits the environment. Nevertheless, this material will not be around forever, as coal powered plants have experienced a severe decline. In the past 60 years alone, the coal production in the United States dropped 24%, with only 535 million short tons produced [5]. The labor force has shrunk as well, with only 37,000 coal miners working today, as compared to 178,000 miners in 1985 [6]. Figure 1 shows the drastic decline in coal plants from just 2007 to 2016 as wind, solar, natural gas, and hydrothermal plants have become more prevalent [7]. Further, recent environmental movements have pushed against coal production in support of greener energy sources [3, 8, 9]. Additionally, one study explains that the American coal supply has been largely overstated, and as coal production declines this will become more apparent, with the U.S. only recovering roughly 20% of the government's reported coal reserves [10]. This information is startling when considering the significant reliance on fly ash for so many concrete suppliers, and the apparent lack of acknowledgment of this information is just as worrisome. New studies are needed to gain industry insight on this decline and investigate alternatives that suppliers may be looking into to combat future shortcomings.

To underscore the significance of the need for an alternative concrete mix design that is more sustainable, one must recognize the damage of traditional concrete design, chiefly, the incorporation of Portland cement. The damage and devastation the Portland cement industry causes on the environment is well known. Research shows concrete production, specifically the Portland cement industry, to be one of the leading contributors of Carbon-Dioxide (CO_2) emissions, with estimates ranging roughly around 5% to 7% of global CO_2 emissions stemming from Portland cement production [11]. Author Jonathan Watts, of The Guardian, paints the picture of the crisis we face, stating: "If the cement industry was a country, it would be the third largest carbon dioxide emitter in the world with up to 2.8 billion tons, surpassed only by China and the US" [11]. Considering this fact, and how the construction industry is just one small facet of life, it is imperative we change.

Further, the making of cement is not the only factor in the concrete process that causes harm to the environment. The harvesting of natural materials causes significant irreparable damage to the Earth [12]. In one study, titled 'Green Concrete Mix Using Solid Waste and Nanoparticles as Alternatives- a Review,' the researchers argued for the implementation of natural waste materials to form Green Concrete [13]. Examining the currently used avenues of solid waste management, they focused on the harmful effects of landfills and recycling costs, as well as the harmful damage from cement manufacturing [12]. Breaking down the significant harmful effects of the concrete industry on the environment, it is clear the construction industry needs to strive for a more eco-conscious alternative concrete that will not wreak havoc on natural resources or pollute the Earth [13]. With these facts in mind, there is no turning back to traditional Portland cement concrete.

While States have their own specifications for concrete mixtures, the Federal Highway Administration (FHWA) sets general parameters that must be followed. The FHWA also advises on the general benefits of the incorporation of fly ash concrete, touching on improved workability, decreased water demand, reduced permeability, and improved durability [14]. While these points are all valid, it is important to address a difference between Connecticut State and

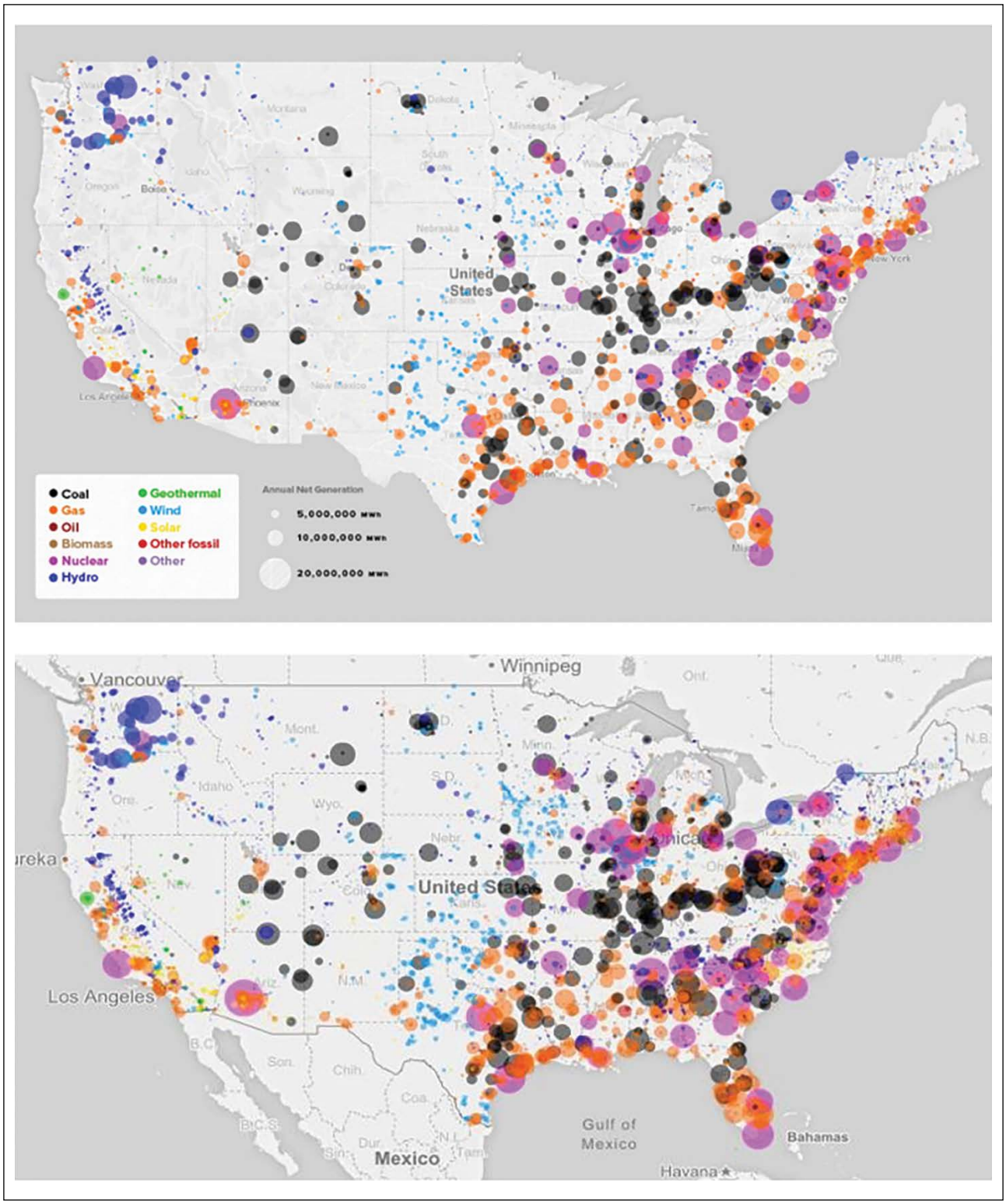

Figure 1. Map of Decline of Coal Power in the United States 2007 (top) and 2016 (bottom) [7].

Federal guidelines. Per the FHWA, "Fly ash is used to lower the cost and to improve the performance of PCC. Typically, 15% to 30% of the Portland cement is replaced with fly ash, with even higher percentages used for mass concrete placements. An equivalent or greater weight of fly ash is substituted for the cement removed. The substitution ratio for fly ash to Portland cement is typically 1:1 to 1.5:1" [14]. This is higher than the guidelines provided Connecticut.

Reviewing the DOT's specifications listed under section M.03.01 titled 'General Composition of Concrete Mixes,' the State of Connecticut allows any qualified composition of concrete if it meets the specifications listed per concrete grade. The design details are as follows: "Portland cement concrete shall consist of an intimate mixture of Portland cement, other approved cementitious material (when used), fine aggregate, coarse aggregate, water, and admixtures, if ordered or permitted by the Engineer, proportioned in accordance with the following requirements" [15]. Essentially, discussing strength alone, Class A and C concrete must meet 3,000 psi (20.7 MPa) compressive strength at 28 days, and Class F must meet 4,000 psi (27.6 MPa) at 28 days. Regarding fly ash replacement in the mixture, Connecticut allows for up to 15% replacement of Portland cement, pound for pound. Therefore, as long as the materials have been sourced and verified by the Division of Materials Testing, and the concrete meets the specified requirements, the engineer may choose any mixture design they deem suitable.

Additionally, it is important to point out the need for curing in Connecticut, especially in the colder months. While most concrete work is performed in the warmer months, CT DOT section 4.01 does specify supplemental needs including the laying of straw or hay for protection on days or nights where the temperatures may drop below 35 degrees Fahrenheit (2 degrees Celsius) [16]. Also, if any concrete freezes before it is fully cured, it must be removed and replaced at the contractor's expense [16]. Therefore, for any new concrete mixture designs to take off in New England, they must be suitable for work in colder temperatures, and not delay projects with longer cure times, which can lead to concrete damages if the material freezes before it is fully cured.

Fly ash concrete, either Class C or Class F types, is a commonly accepted alternative concrete mixture in which Portland cement is replaced partially with fly ash. The main difference between these two types of concrete is the chemical makeup of the ash itself. Boral Resources, a leading American supplier of coal combustion products, like fly ash, concisely summarizes these differences, explaining: "Class F fly ash is highly pozzolanic, meaning that it reacts with excess lime generated in the hydration of Portland cement, Class C fly ash is pozzolanic and also can be self-cementing" [17]. This manufacturer further explains specifications and requirements set forth by the American Society for Testing Materials [18]. This society per section ASTM C618 "requires that Class F fly ash contain at least 70% pozzolanic compounds (silica oxide, alumina oxide, and iron oxide), while Class C fly ashes have between 50% and 70% of these compounds. Typically, Class C fly ash also contains significant amounts of calcium oxide – over 20%. Most Class F fly ash contains little calcium oxide; however, some Class F fly ash sources may contain intermediate levels (8% to 16%) of calcium oxide" [17].

Fly ash concrete has long been studied and is widely accepted in the heavy highway industry [19–22]. However, none of these studies discuss the impending loss of the material or possible solutions. Notably though, one study in 2014 in Wisconsin did address the lack of the fly ash material (Class C) and suggested an expansion of their current specifications to allow for the incorporation of Class F fly ash concrete [23]. It is remarkable that this study was completed seven years ago, and the problem remains the same. Furthermore, it will not be feasible in the long run to adopt a different fly ash mixture since this would be a temporary fix; a permanent solution is needed for the heavy highway construction industry.

To expand further on the limitations and finite timeline of fly ash concrete, fly ash is the byproduct of burning coal for energy production, while energy production is becoming less reliant on coal. As the world moves greener and environmental crisis shapes the world, new initiatives are implemented to become more environmentally conscious in all areas of life, especially in significant areas such as electricity. In recent years the production of coal has declined due to shortages, as well as its harmful effects and toxicity. Even disregarding the environmental and health risks of coal consumption, research has shown coal supply is shrinking and may become extinct in the 70 years [8, 9, 24]. Therefore, as power plants move from burning coal to more environmentally friendly options like natural gas or hydroelectricity, the loss of fly ash might be sooner than predicted.

The future of sustainable alternative concrete must take into consideration materials that are in abundance and not comprised of finite resources, like fossil fuels. Natural pozzolans, like volcanic ash, have a great potential as a substitute for fly ash. The volcanic ash used for concrete mixtures can be obtained in several ways: explosive volcanic eruptions, phreatomagmatic eruptions, and the transports in pyroclastic density currents. However, it is important to note that these variations can result in different mechanical properties [25]. Nevertheless, harvesting this material is significantly less damaging to the environment in comparison to the mining of lime to create Portland cement. Collecting this material also eliminates the negative effects of volcanic eruption to human life [25]. In the United States alone, there are 169 volcanoes. Most are in Alaska, but they are across the U.S. as well. Harvesting this material is not damaging to the Earth in the same way that lime mining is, and the process for refining this ash to be useable in concrete does not release the same amount of carbon as Portland cement or burning coal [26, 27].

The chemical properties of this material make this a strong cementitious material with a comparable compressive strength to traditional concrete mixture designs with ranges of 6% to 10% replacement of Portland cement [28]. Interestingly, cure time for this material is roughly comparable to traditional concrete [29]. It is also important to note that one study identified volcanic ash as beneficial in improving the ability of concrete to resist freeze–thaw cycles with limited mass loss ratios

(2.1–2.3%) [30], which is extremely important in regions with fluctuating temperatures, like New England.

Another promising alternative to fly ash concrete is the supplementation of ground glass pozzolan as a partial replacement for Portland cement in concrete. Several studies have assessed this mix design and found it to be comparable, if not stronger than traditional Portland cement concrete [31–35]. For this mixture, 20% to 25% may be most optimal for heavy highway construction [31–33]. The chemical properties of this material make this a strong cementitious material with increased compressive strengths of 16% with only a 15% replacement of Portland cement [32], and increased compressive strength with 10% glass replacement [33]. Moreover, Khudair et al. [34] reason compressive strength could be the result of "pozzolanic activity", in which glass particles react with the cement hydrates forming new gel bonds, which can block the pores of the concrete, making pores smaller and not connected, which leads to greater density. Additionally, studies have also concluded this material to be longer lasting, with estimated service life five times greater than traditional concrete [36]. Cure time may be slightly longer than traditional concrete, however if protected properly from the elements and properly planned for in scheduling, this should not be a significant issue.

Silica Fume is another alternative mix concrete that has proven to increase strength and durability, while also reducing the carbon impact by replacing varying quantities of the Portland cement. Several studies have focused on this material, all finding it suitable for both lightweight and heavyweight concrete construction [37–40]. While this material has great benefit, there are drawbacks including potential cost increases or fluctuations in various regions where this material may not be readily available. The extra cost of the material is examined in one study in which quarry dust was incorporated as a filler in addition to silica fume, to strengthen the concrete mix while lessening the amount of silica fume or fly ash for regions that may not have as much access to these materials [41]. This information is useful as it shows that research is expressing concern over availability and cost of materials, however, there is not a similar study like it for just fly ash which is especially needed now as coal production declines.

It is also important to examine what other surveys and studies have assessed the current market of concrete production. Overall, there are relatively few studies in this regard. Most closely related is a survey completed in 2015. In this study, the scholars surveyed concrete suppliers and manufacturers to gain insight on the intersection of academic knowledge in comparison to industry production [42]. This study surveyed numerous suppliers, one trade organization, as well as the Ohio Department of Transportation. This study concluded that the most used concrete mixtures were fly ash (Class C and F), ground granulated blast-furnace slag (GGBFS), Silica fume, and shale. This study provided insight on manufacturers understanding and usage of alternative concrete mixture designs. Nevertheless, given how stringent state public jobs can be, more investigation is needed to see the concrete materials States would allow in their heavy highway jobs. Additionally, it would be useful to compare the results of the study that was done seven years ago with the results presented in this paper, specifically to evaluate if new concrete admixtures are being used by the various Departments of Transportations.

Table 1. Department of transportation concrete mixture survey

What is the traditional makeup of your concrete?		
What is your concrete budget?		
Do you use flyash?	Yes	
	Class C/Class F	No
How much does your flyash concrete cost?		
Do you use ground glass/ Pozzotive concrete?	Yes	No
Do you use Volcanic Ash?	Yes	No
Do you use other types of "green" admixtures to concrete?	Yes	No

3. STUDY METHODOLOGY

The primary goal of this study was to identify what concrete mixtures that are allowed by the Departments of Transportation across the nation. The secondary goal of this study was to evaluate the availability these materials, and hopefully highlight the practicality of these alternative compositions. To complete these tasks, a comprehensive literature review was completed that identified possible alternative mixture designs, as well as an investigation was performed that identified major suppliers, by state, of sustainable mixes currently produced in America. Then, with the aim of producing findings for the Connecticut DOT, a survey was sent out to the Departments of Transportation nationwide. To increase the likelihood of gaining information on concrete suppliers and materials currently in use while not being a customer, a thorough review of leading suppliers was completed to assess the materials they advertise and offer for more sustainable options.

Table 1, inserted below, shows the survey sent to the Departments of Transportation. This survey addressed questions regarding annual budget, concrete mixtures used, and concrete cost. To increase the likelihood of responses, the survey was kept short. Respondents did elaborate on their answers and provided further insight and thoughts on sustainable concrete mix designs. The survey was sent to the Materials Testing Divisions, and other relevant departments, listed publicly on the Departments of Transportation websites. If specific emails were not found, the survey was sent to the general forum in hopes of it being passed to the appropriate department.

The next step of this study was to interpret the various data these surveys provided. The results revealed information on various materials, costs, sale percentages, concrete usage and more. This information was illustrated by graphical representations. Additionally, the analysis of the data from the survey responses will lead to further

investigation of alternative materials and refine plausible solutions that is expected to be helpful to the Connecticut Department of Transportation to provide a more permanent sustainable alternative of concrete mixture for heavy highway construction.

4. RESULTS

This survey was sent out nationwide to multiple divisions of each the State's Departments of Transportation excluding Connecticut, as the information was obtained directly from the Connecticut DOT interviews. The authors received responses from 12 States. The data pooled revealed several important trends and identified more areas for future surveys to research. The results of the interview and the surveys are as follows.

4.1. Connecticut DOT Interviews

In effort to study sustainable construction and green alternatives for concrete specifically for heavy highway construction, interviews with the Connecticut DOT were conducted. The first interview was with the Pavement Design division, who explained that most of their work is rehabilitation and not new construction. It was explained that the DOT currently uses Recycled Asphalt Pavement (RAP), Recycled Asphalt Shingles (RAS), Ground Tire Rubber (GTR) in chip seals. Interestingly, this division will continue to use RAP, GTR as well as polymers and recycled plastics to improve the durability of mixes and reuse materials.

The second interview was with the Bridge Design division. It was explained that the Connecticut DOT does not use large concrete amounts to make a huge difference in carbon emissions, therefore low-embodied carbon concrete is not mandated from suppliers. However, the DOT is supportive of alternative mixes as long as they have the required strength at 28 days. It was also explained that DOT would use of pozzolan (recycled ground glass) in concrete mixes, but it was noted that the drawback is the longer curing time which is a significant disadvantage as it will slow down construction progress, causing delays and more expenses. It was also pointed out that the DOT references the work of organizations such as the Connecticut Green Building Council, the Connecticut Ready Mixed Concrete Association, and the Connecticut Concrete Promotion Council.

The third interview was with a Connecticut DOT Engineer, who discussed concrete alternatives for heavy highway construction, where the biggest concern is the long-term behaviour of green concrete. The DOT has the responsibility to ensure the continued performance of their projects and cannot risk having to go back and repair any damage or complications further delaying traffic. Therefore, significant research and experimentation needs to be conducted to address durability concerns. This stresses the need for an alternative concrete that is as strong or stronger than traditional concrete. Furthermore, it was explained that the leading cause of concrete damage is permeability. It was also clarified that fly ash is the most used substitute they worked with, however they do realize that this a limited resource and other alternatives must make way in the heavy highway construction industry to prevent any regression back towards traditional concrete.

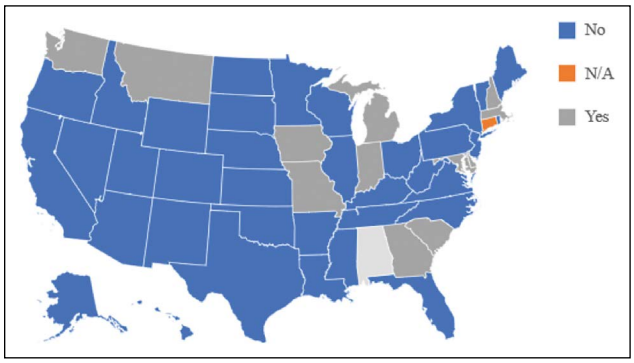

Figure 2. Geographic response rate.

The biggest concerns for the DOT are cost, strength, and durability. The insight gained from the Connecticut DOT interviews helped the researchers with the development of the survey questions, and the issues faced to adopt green alternative concrete mixtures. The interviews helped narrow down the project's objective.

4.2. Survey Response Rate

The survey (shown in Table 1) was sent out to 49 States, excluding Connecticut, and 12 states responded. The responses to the survey came from the following states: Georgia, Indiana, Washington, Delaware, Michigan, Montana, New Hampshire, Missouri, Iowa, South Carolina, Massachusetts, and Maryland. The response rate was 24%. It is also helpful to review the responses in a map formation (Fig. 2), as it will help identify any possible trends based off the region the responses are in. This may reveal common elements or shared concerns if the respondents expanded on the survey questions. Additionally, by looking at the responses geographically, it is more obvious which regions had no responses and areas that further investigative research would be needed to answer any specific questions this survey may have prompted.

By assessing this map, it is clear there was no reported data from the West Coast and South-West, as well as limited data from the South. Nevertheless, there is a wide range of responses scattered across the U.S., which does allow for a general nationwide interpretation of the results, as well as a look at the concerns that individual regions may be facing.

4.3. Survey Question Response – Concrete Composition

The first question addressed in the survey was the composition of each State's concrete in the hopes of being able to identify some common mixture design. Most of the re-

Table 2. Concrete composition

State	Georgia	Indiana	Washington	Delaware	Michigan	Montana
Makeup of concrete	Cement, sand, stone, air	Cement, sand, stone, air entrainment admixture, water reducing admixture, and depend on the type of structures and month of construction can include "additions" such as slag, fly ash, silica fume, and other "chemical admixtures".	Cementitious blends of portland cement, fly ash, slag, and limestone aggregate/water and chemical admixtures dependent on application. We see a lot of blended hydraulic cement such as type il cements with the use of fly ash and slag replacing portland cement	Our traditional concrete is made up of water, sand, stone, cement and flyash or slag. It also has the admixtures water reducer and aer in it. We add accelerating and retarding admixtures depending on outside temperatures	Natural fine aggregate and coarse aggregate, Type I (transitioning to Type IL) Portland cement, slag cement (ASTM C989)	Typically, is made of 1–2 coarse/medium aggregates, sand, cement, and admixtures dependent the producer.
Additives mentioned		Slag Fly ash Silica fume Chemical admixtures	Chemical admixtures	Fly ash Slag Admixture Retarding and accelerators	Slag	Admixture

Table 3. Concrete Composition (continued)

State	New Hampshire	Missouri	Iowa	South Carolina	Massachusetts	Maryland
Makeup of concrete	4000 psi with 50% slag or 25% fly ash	Average* 645 pounds per cubic yard of cementitious material (including fly ash, cement, etc.) and average w/c ratio of 0.41.///Average 76 pounds per cubic yard of fly ash counting all mixes, even ones without fly ash. Average fly ash content of 122 pounds per cubic yard counting only mixes containing fly ash	We use cement, coarse and fine aggregates, water, chemical admixtures and SCMs such as fly and GGBFS.	Our concrete is typically made up of cement (and often fly ash), water, fine aggregate, coarse aggregate, and chemical admixtures.	Cement, fly ash or slags, admixtures, aggregates and water	It can be 100% cement in concrete, or it can be 25% to 50% slag cement added, or 10% to 25% flyash added
Additives mentioned	Fly ash	Fly ash	Fly ash Ground granulated blast furnace slag (GGBFS)	Fly ash Chemical Admixtures	Admixtures	Slag Fly ash

sponses were in agreement with their concrete compounds consisting of crushed stone, sand, water, cement, air, and differing in terms of the addition of chemical admixtures or cement substitution admixture.

When the surveys were initially sent out, the question was intended to ask the participants to identify their percentage of concrete substitute used and what materials they often used. However, due to the open-ended nature of the question, the responses were rather general, with varying degrees of information provided from each state discussing the basic makeup of concrete. The results of this question are broken into two tables (Table 2, and Table 3) of six states each.

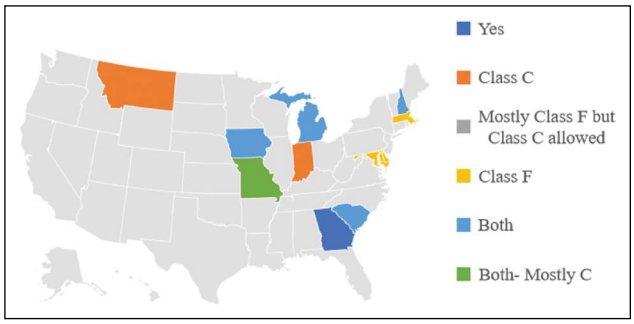

Figure 3. Geographic comparison of fly ash used.

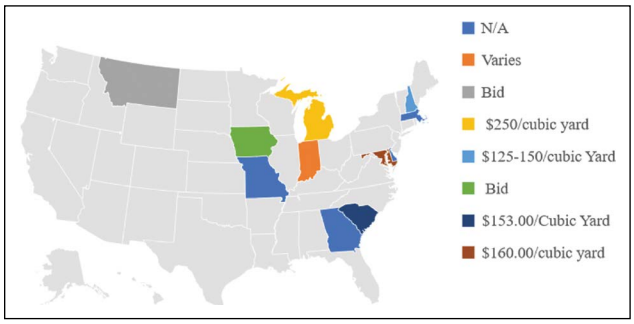

Figure 5. Fly ash cost by region.

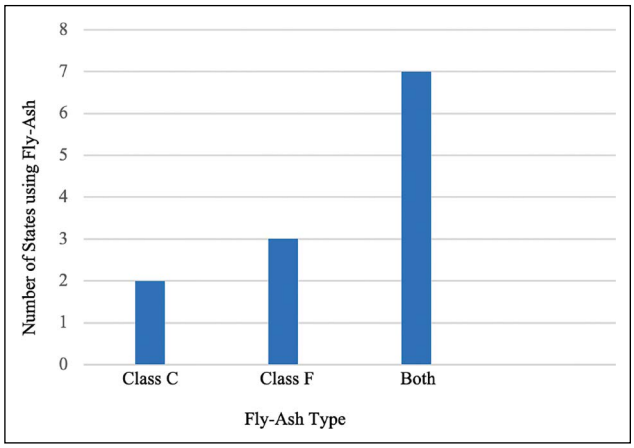

Figure 4. States fly ash usage by type.

Interestingly, several states, like Indiana, Washington, Delaware, and South Carolina reported usage of admixtures in their concrete. This is interesting as admixtures may serve several different functions and are classified by function, such as air-entraining, water-reducing, retarding, accelerating, and plasticizers [43]. However, only Delaware commented on the usage of the admixtures to influence acceleration or retardation depending on the weather. While the other states did not provide further insight on whether these admixtures were used in a similar fashion, or, in comparison, if they were to possibly inhibit corrosion, reduce shrinkage, influence silica reactivity, or improve workability. Overall, the bulk of the responses included the usage of some sort of cement substitution whether it be Fly Ash, Slag, or Silica Fume.

4.4. Survey Question Response – Concrete Budget

The second question in this survey was regarding the annual budget for concrete per state. It was assumed that most states would not have a strict annual budget as the amount of concrete work needed each year could change. Nevertheless, cost is a crucial concern, and it was important to inquire regardless of the anticipated answer. Fortunately, the received responses revealed some financial insight. Washington reported approximately a $200 million annual budget (including pavement, bridge structures, and other miscellaneous uses), and Iowa reported $23 to $30 million budget. The other responses were either not applicable or reported the budget changed annually due to the needs of the State and the various projects that are actively in the works. Additionally, Maryland reported that Districts have specified budgets and how they use their funds depends on the given project.

This data is useful as it shows most states do not provide a specific budget or limit of concrete usage but allow the districts or regions to determine their individual needs. Therefore, if there is no definitive cost cap, and a state may be able to petition for more funds than the previous year to switch to a more sustainable concrete material. For example, if the funds are received per job, if the cost of materials varied, or was slightly higher from one year to the next, it will not be obvious if it was due to the cost of the concrete itself, or if it was due to some other project factor.

4.5. Survey Question Response – Use of Fly Ash

The third question asked was to determine if all of the States are still using fly ash concrete and, if so, which class. Determining the current usage of fly ash concrete is imperative because if some states are not using fly ash, it is important to identify what they may have switched to, or if they are using it, do they have any plans to switch in the near future.

Of the responses received, every state responded yes to the use of fly ash. Figure 3 and Figure 4 depict the different fly ash class in use per state. In whole, most states allow both Class C and Class F fly ash in their projects, but Indiana and Montana reported only using Class C fly ash, and Delaware, Massachusetts, and Maryland reported only using Class F.

4.6. Survey Question Response – Fly Ash Cost

The fourth question in this survey was to investigate the cost of fly ash concrete (Fig. 5). The responses varied with some states being unaware since the cost is included in the project bid, but some states, including Michigan, South Carolina, Maryland, and New Hampshire, were able to provide an average cost per cubic yard. Michigan reported the highest cost out of the responses at roughly $250.00 per cubic yard (cy), while New Hampshire, South Carolina, and Maryland were closer together at $125.00 to $150.00/cy, $153.00/

Table 4. Use of ground glass concrete

State	Georgia	Indiana	Washington	Delaware	Michigan	Montana
Use of ground glass concrete	No	No	No	No	No	No

Table 5. Use of ground glass concrete (continued)

State	New Hampshire	Missouri	Iowa	South Carolina	Massachusetts	Maryland
Use of ground glass concrete	No	No	GGBFS concerns are there is not enough material available locally.	No	Allowed-Not used	Yes

cy and $160.00/cy, respectively. While the other States were unable to provide a definitive price range for material, it is interesting to see the varying cost range between just these three States. This does prompt further questions regarding why Michigan's cost might be so much higher, and if it could be due to a supply shortage in that area.

Interestingly, in response to this question, Montana stated that they do not often use fly ash concrete. Therefore, returning to their response to the first question, it is likely that the bulk of their concrete usage is Slag concrete mixtures rather than fly ash, as long as it reaches the required concrete strength of 4,000 psi (27.6 MPa).

4.7. Survey Question Response – Use of Ground Glass Concrete

The fifth question in this survey inquired on the usage of Ground Glass Concrete or Pozzotive. It was anticipated that this material has little usage, and this question would have a low response rate, but hopefully this question would prompt further discussion or insight on the material through the eyes of the Departments of Transportation. The responses are shown in Table 4 and Table 5.

The question did provide valuable insight. Only two States, Massachusetts and Maryland allow ground glass concrete, with only Maryland using the material so far. Additionally, Iowa commented on this material, stating that they use ground granulated furnace slag, but not ground glass as they are concerned about supply and need material that will be readily available. This is critical to note as Iowa is likely not the only state that would have this concern at the forefront of their minds. Low supply undoubtedly means higher costs and the potential risks of delays or failure to complete work. For ground glass concrete to become a first choice for DOTs, manufacturers must combat this fear and provide reassurance that there is enough material and long-term supply.

4.8. Survey Question Response – Use of Volcanic Ash Concrete

The sixth question in this survey was regarding volcanic ash concrete, another potentially viable replacement for fly ash concrete. The anticipated response was again low, but the hope was to receive insight on the material. It was also anticipated that this material will be used in regions with volcanos in proximity.

From the responses, 11 states replied that they do not use volcanic ash in concrete mix designs, with only Washington replying yes, allowing pumice natural pozzolan in their concrete mixtures. This is interesting as it shows more suppliers must be experimenting with more alternative materials in their projects and are opening the door for natural Pozzolans in heavy highway construction. This response from Washington is also in agreement that a region with volcanos in proximity would be more likely to begin working with the material rather than a region that may have to import the material.

4.9. Survey Question Response – Use of other "Green" Admixtures

The final question asked in this survey was regarding other "green" admixtures in concrete. This question was asked in the hopes of allowing the respondents the chance to expand on the survey or offer a material not explored in this survey. Of the responses, several states replied no other "green" admixtures were in use, while several states provided valuable insight shown in Table 6 and Table 7. In summary, several states, including Maryland, Missouri, and Michigan reported Silica Fume usage. Additionally, Georgia responded that they use recycled aggregate and Metakaolin. Also, Washington state expanded their response stating that they allow fly ash, slag, natural pozzolans, and blended cements, explaining that blended cements are most commonly used with fly ash and slag as replacement for Portland cement. Interestingly, Iowa, expanded their response as well, stating their long-standing use of ground granulated blast-furnace slag (GGBFS) and fly ash for over 40 years, with a significant decrease in their cement content, and have approved the use of CarbonCure with a 3% cement reduction.

5. REVIEW OF CONCRETE MANUFACTURERS

It was important to look to the leading concrete suppliers and evaluate the feasibility of different alternative mixture designs. For this study, four leading suppliers were researched: CalPortland and Cemex, Inc., each in a different region of the country, and two Connecticut suppliers, Tilcon and Urban Mining. Urban Mining was of particular interest, as they only manufacturer ground glass concrete.

Table 6. Other types of "green" admixtures in concrete

State	Georgia	Indiana	Washington	Delaware	Michigan	Montana
Other types of "green" admixtures in concrete	Slag, recycled agg, metakaolin	No	Fly ash, slag, natural pozzolans, and blended cementitious materials. We see a lot of blended hydraulic cement such as type IL cements with the use of fly ash and slag replacing portland cement	Slag	ASTM C595 blended cements and C1240 dry-densified silica fume	No

Table 7. Other types of "green" admixtures in concrete (continue)

State	New Hampshire	Missouri	Iowa	South Carolina	Massachusetts	Maryland
Other types of "green" admixtures in concrete	No	Ground granulated blast furnace slag, silica fume	We have been doing fly ash and GGBFS for over 40 years, we have optimized our gradations and reduced our cement contents, we use IL cements, we have approved the use of carbon cure with a 3% cement reduction	No	No	Silica fume and metakaolin

Urban Mining, in Beacon Falls, Connecticut is a local Connecticut concrete plant which has revolutionized the process of making ground glass concrete even more sustainable as it can accommodate all types of glass containers, including ceramic and other "nontraditional" glass bottles [44]. This is significant, as it maximizes the options of resources to make Pozzotive concrete, their brand of pozzolan. Recently, Connecticut has attempted to increase recycling statewide, specifically that of beverage bottles (and cans). To reduce littering and increase recycling, the state's legislature introduced the Connecticut Bottle Modernization Bill (Section 8 of PA 21-58) [45]. In 2020, Urban Mining commented on this bill, requesting the Department of Energy and Environmental Protection to make the Beacon Falls facility an important element of the in-state processing option for wine and liquor beverage containers sold in this state [44]. Urban Mining argued the addition of Pozzotive is aligned with the new bill's objectives of "finding 'the highest and best use' for glass, and the addition of Pozzotive to concrete mixes creates stronger and longer lasting concrete for our communities while reducing the carbon footprint of concrete on a nearly ton-for-ton basis" [44]. Urban Mining further explains that the use of Pozzotive ground glass concrete is "five times more impactful in reducing global CO_2 emissions than repurposing the glass back into bottles or fiberglass" [44]. Overall, this is promising, and this bill should increase the likelihood of recycling. By keeping the recycled glass in Connecticut and making it easier for people to participate, the amount of glass available will likely increase.

Tilcon is renowned as a reliable and long-standing concrete supplier in Connecticut. Comprised of 20 facilities, this company has supplied concrete, aggregates, and asphalt for 100 years, and provides a significant amount of the concrete for the Connecticut DOT's various concrete projects. In 2020, Tilcon's environmental report recorded 46% of their revenue came from sustainable products, 36.5 million tons of alternative materials and alternative fuels recycled, and 1 million tons of CO_2 emissions were prevented [46]. This information is significant and shows what great efforts for the environment have begun to take shape in leading plants, while still providing their high-quality products.

CalPortland is one of the largest suppliers on the West Coast with facilities in Oregon, Washington, California, Nevada, and Arizona. This supplier is a leading manufacturer of concrete and has worked to provide reliable and strong blended concretes with a variety of different materials including: limestone, slag, fly ash, and silica fume. Additionally, this company has introduced calcined clay as a natural pozzolan into their concrete mixes. Further, in 2020, this company released a new environmentally friendly ASTM C595 blended cement. This material offers greater Green House Gas and is comprised of a blend of SCMs including limestone, natural pozzolan, or other approved materials [47]. This reinforces the responses provided by Washington's survey as they commented on the frequent usage of ASTM C595. Between the survey responses and the information provided from CalPortland's website, it can be argued that ASTM C595 blended cement is a viable option for Connecticut as well. However, this material seems to rely on the addition of limestone. While this is a great solution, it stands to reason that Connecticut can progress further towards sustainable construction on all levels.

Cemex, Inc. is headquartered in Houston, Texas and readily serves the surrounding Southern region. This company advertises their sustainable progress in several ways, including safety actions, environment efforts, and their agreement with Climate Action policy. Their site details

their mixtures of fly ash and slag cement, along with their incorporation of chemical admixtures. However, there is no reported data on the use or incorporation of natural pozzolans or ground glass in their mixture designs. While this supplier is a leading supplier in the South and reinforces the sustainable efforts that other top suppliers are attempting, there was little additional data found.

6. CONCLUSION

In summary, this study provided further data on the current status of the Departments of Transportation concrete usage, materials used, cost, and use of alternative "green" mixtures. In comparison to the two studies completed in 2014 [23] and 2015 [42], it's clear how little has changed in the means of concrete manufacturing and how reliant states are on fly ash concrete especially. Nevertheless, by carefully analysing the answered surveys, and through careful investigation of these top suppliers, it can be argued that most states may be open to alternative mixture designs, if they meet the required build specifications, and that states are more concerned with product availability and means. Further, the survey responses received do correlate with the advertised materials from the several concrete manufacturers previously reviewed. This is interesting because, if the larger suppliers market this material more and continue to push it into production on projects, it is more likely that it will be fully accepted by government and state agencies overtime as the material will be less "new". This survey also expressed the significant amount of fly ash currently used, which raises red flags. This reinforces the concern and critical need for an alternative replacement compound that is fully sustainable on all levels to make its way into heavy highway construction. The time to begin the switch to this new mixture design is now, as the depletion of fly ash only continues with each build and with less availability comes increase in cost.

This study leaves room for future studies to attempt interviews with suppliers and investigate pipeline mixture designs as well as marketability for future mixture designs. The authors feel it is important to focus on the economics of alternative concrete use as it would have a major impact encouraging the States to use green concrete more frequently. It is thought provoking to look at the cost of alternative concrete and compare it with traditional concrete, comparing not only its cost of production, but the environmental savings from the recycled material and its lower carbon footprint. Sustainability is a growing area of concern, especially surrounding the concrete industry.

DATA AVAILABILITY STATEMENT

The authors confirm that the data that supports the findings of this study are available within the article. Raw data that support the finding of this study are available from the corresponding author, upon reasonable request.

CONFLICT OF INTEREST

The authors declare that they have no conflict of interest.

FINANCIAL DISCLOSURE

The authors declared that this study has received no financial support.

PEER-REVIEW

Externally peer-reviewed.

REFERENCES

[1] Larsen, D., Bernier, A., & Mahoney, J. (2020). *Connecticut annual pavement report* (Report No: CAPLAB 11-2019). Bureau of Engineering and Construction Pavement Unit. Connecticut Department of Transportation. https://portal.ct.gov/-/media/DOT/documents/dpavement/Connecticut-DOT-Annual-Pavement-Report_2019.pdf

[2] Perera, F. (2018). Pollution from fossil-fuel combustion is leading environmental threat to global pediatric health and equity: Solution exist. *International Journal of Environmental Research and Public Health*, 15, 16. [CrossRef]

[3] Kuo, G. (2021, October 11). *When fossil fuels run out, what then*? The Millennium Alliance for Humanity and the Biosphere (MAHB). https://mahb.stanford.edu/library-item/fossil-fuels-run

[4] Norton, S. (2011). *Pavement preservation manual* (Report No: 10/25/2011). Bureau of Engineering and Construction Pavement Unit. Connecticut Department of Transportation. https://portal.ct.gov/DOT/Engineering/Pavement-Design/Pavement-Preservation-Documents

[5] Berry, R. (2021). U.S. *Coal production fell to ıts lowest level since 1965*. U.S. Energy Information Administration - Today in Energy. https://www.eia.gov/todayinenergy/detail.php?id=48696

[6] U.S. Bureau of Labor Statistics - Statistics, Occupational Employment and Wage. (2021). NAICS 212100 - Coal Mining. Retrieved from https://www.bls.gov/oes/2020/may/naics4_212100.htm

[7] Desjardins, J. (2019). *Mapped: Every power plant in the United States*. https://www.visualcapitalist.com/mapped-every-power-plant-in-the-united-states/

[8] Lauren, B. (2015). Southeastern plants moving away from coal before EPA deadline. SNL Enery Power Daily. https://ccsu.idm.oclc.org/login?url=https://www.proquest.com/trade-journals/southeastern-plants-moving-away-coal-before-epa/docview/1671123393/se-2?accountid=9970

[9] Horwath, J. (2020). *Michigan town shuts power plant after running out of coal*. SNL Canada Energy Week. https://www.spglobal.com/commodityinsights/en/market-insights/latest-news/electric-pow-

er/021220-michigan-town-shuts-power-plant-after-running-out-of-coal

[10] Reaver, N. G., & Khare, S. V. (2014). Imminence of peak in US coal production and overestimation of reserves. *International Journal of Coal Geology*, 131, 90–105. [CrossRef]

[11] Damtoft, J., Lukasik, J., Herfort, D., Sorrentino, D., & Gartner, E. (2008). Sustainable development and climate change initiatives. *Cement and Concrete Research*, 38(2), 115–127. [CrossRef]

[12] Watts, J. (2019). Concrete: The most destructive material on earth. *The Guardian*. https://www.theguardian.com/cities/2019/feb/25/concrete-the-most-destructive-material-on-earth

[13] Vishwakarma, V., & Ramachandran, D. (2018). Green concrete mix using solid waste and nanoparticles as alternatives – A review. *Construction & Building Materials*, 162, 96–103. [CrossRef]

[14] Behera, M., Bhattacharyya, S., Minocha, A., Deoliya, R., & Maiti, S. (2014). Recycled aggregate from C&D waste & ıts use in concrete – a breakthrough towards sustainability in construction sector: A review. *Construction & Building Materials*, 68, 501–516. [CrossRef]

[15] Federal Highway Administration Research and Technology. (2016). *User guidelines for waste and byproduct materials in pavement construction* (Repot No: FHWA-RD-97-148). https://www.fhwa.dot.gov/publications/research/infrastructure/structures/97148/cfa53.cfm

[16] Connecticut Department of Transportation Section. (2022). *Portland cement concrete* (Report No: Section M.03). Connecticut Department of Transportation. https://portal.ct.gov/DOT/CONNDOT/SECTION-M03

[17] Connecticut Department of Transportation Section. (2006). *Concrete pavement concrete* (Report No: Section 4.01). (Connecticut Department of Transportation. https://portal.ct.gov/DOT/CONNDOT/SECTION-401

[18] Ecomatarial Technologies. (2021). *Boral resources*. https://flyash.com/

[19] ASTM International. (2019). Standard specification for coal fly ash and raw or calcined natural pozzolan for use in concrete. ASTM International. https://www.astm.org/c0618-19.html

[20] Karasin, A., & Dogruyol, M. (2014). An experimental study on strength and durability for utilization of fly ash in concrete mix. *Advances in Materials Science and Engineering*, 2014, Article 417514. [CrossRef]

[21] Liu, L., Wang, L., & Gong, Y. (2019). Strength time-varying and freeze-thaw durability of sustainable pervious concrete pavement material containing waste fly ash. *Sustainability*, 11(1), 176. [CrossRef]

[22] Thomas, M. (2007). *Optimizing the use of fly ash in concrete*. Portland Cement Association.

[23] Zhai, T., Thang, Y., Chen, S., Chen, H., Cheng, B., Cai, X., & Wei, Y. (2021). Experimental research on durability of fly ash pavement concrete and mix proportion optimization. *Advances in Materials Science and Engineering*, 2021, Article 8864706. [CrossRef]

[24] Gioietta, K. (2019). *When fossil fuels run out, what then*? MAHB. https://mahb.stanford.edu/library-item/fossil-fuels-run

[25] Sutter, L. L., Vruno, D. M., Anzalone, G. C., & Dong, J. (2014). *Laboratory study for comparison of class C versus class F fly ash for concrete pavement* [Unpublished Master Thesis]. Michigan Techological University, 1–154.

[26] Cai, G., Noguchi, T., Degee, H., Zhao, J., & Kitagaki, R. (2016). Volcano-related materials in concretes: A comprehensive review. *Environmental Science and Pollution Research International*, 23(8), 7220–7243. [CrossRef]

[27] Jativa, A., Ruales, E., & Etxeberria, M. (2021). Volcanic ash as a sustainable binder material: an extensive review. *Materials (Basel)*, 14(5), 1302. [CrossRef]

[28] Robayo-Salazar, R., Mejia-Arcila, J., Mejia de Gutierrez, R., & Martinez, E. (2018). Life cycle assessment (LCA) of an alkali-activated binary concrete based on natural volcanic pozzolan: A comparative analysis to OPC concrete. *Construction Building Materials*, 176, 103–111. [CrossRef]

[29] Susanti, D., Tambunan, R., Waruwu, A., & Syamsuddin, M. (2018). Studies on concrete by partial replacement of cement with volcanic ash. *Journal of Applied Engineering Science*, 16(2), 161–165. [CrossRef]

[30] Hossain, K. M., & Lachemi, M. (2010). Fresh, mechanical, and durability characteristics of self-consolidating concrete ıncorporating volcanic ash. *Jounal of Materials in Civil Engineering*, 22(7), 651–657. [CrossRef]

[31] Zhiguo, C. Z. (2009). Research on pavement performance of volcanic ash mixture as road base and mechanism. *Journal of Highway and Transportation Research*, 4(1), 18–23. [CrossRef]

[32] Guignone, V. G., Zulcao, R., Degen, M., de Moraes Mittri, S., & Baptista, G. (2020). Incorporation of glass powder and metakaolin as cement partial replacement to improve concrete mechanical properties and increase service life. *Journal of Composite Materials*, 54(21), 2965–2983. [CrossRef]

[33] Mohammed, Z. M. (2022). Behavior of sustainable reactive powder concrete by using glass powder as a replacement of cement. *IOP Conference Series. Earth and Environmental Science*, 961(1), Article 012022. [CrossRef]

[34] Khudair, A., Al-Ani, M., & Hama, S. (2020). Optimization of glass powder content in self-compacting concrete as partial replacement of cement. *IOP Conference Series Materials Science and Engineering*, 928(2), Article 022140. [CrossRef]

[35] Rashidian, D., & Rao Rangaraju, P. (2018). Evaluation of selected durability properties of portland cement concretes containing ground glass fiber as a pozzolan. *Transportation Research Record*, 2672(27), 88–89. [CrossRef]

[36] Paiva, H., Velosa, A., Cachim, P., & Ferreira, V. (2016). Effect of pozzolans with different physical and chemical characteristics on concrete properties. *Materiales De Construcción*, 66(322), e083. [CrossRef]

[37] Schrofl, C., Gruber, M., & Plank, J. (2012). Preferential adsorption of polycarboxylate superplasticizers on cement and silica fume in ultra-high performance concrete (UHPC). *Cement and Concrete Research*, 42(11), 1401–1408. [CrossRef]

[38] Tkach, E., Rudoy, D., & Murgul, V. (2019). Improvement of the modified heavy concrete properties based on the use of activated silica fume. *Web of Confrences*, 135, 3208. [CrossRef]

[39] Koksal, F., Altun, F., Yigit, I., & Sahin, Y. (2008). Combined effect of silica fume and steel fiber on the mechanical properties of high strength concretes. *Construction & Building Materials*, 22(8), 1874|1880. [CrossRef]

[40] Azunna, S. U., Aziz, F. N., Cun, P. M., & Elhibir, M. M. (2019). Characterization of lightweight cement concrete with partial replacement of coconut shell fine aggregate. *Applied Sciences*, 1(6), 1–9. [CrossRef]

[41] Dehwah, H. (2012). Mechanical properties of self-compacting concrete incorporating quarry dust powder, slica fume, or fly ash. *Construction & Building Materials*, 26, 547–551. [CrossRef]

[42] Jin, R., Chen, Q., & Soboyejo, A. (2015). Survey of the current status of sustainable concrete production in the U.S. *Resources, Conservation and Recycling*, 105, 148|159.

[43] PCA America's Cement Manufacturers. (2019). *Chemical admixtures*. https://www.cement.org/cement-concrete/concrete-materials/chemical-admixtures

[44] Urban Mining CT. (2020). *Urban mining CT, LLC comments on DEEP ımplementation of section 8 of public act* 21-58. https://portal.ct.gov/-/media/DEEP/reduce_reuse_recycle/bottles/Urban-Mining-CT-comments-27Aug-final.pdf.

[45] Connecticut Department of Energy and Environmental Protection. (2021). *The connecticut bottle bill*. https://portal.ct.gov/DEEP/Reduce-Reuse-Recycle/Bottles/Connecticut-Bottle-Bill.

[46] Tilcon. (2022). *Environmental sustainability*. https://www.tilconct.com/company/environmental-sustainability.

[47] CalPortland. (2022). *Concrete overview*. https://www.calportland.com/products/concrete/.

Journal of Sustainable Construction Materials and Technologies
Web page info: https://jscmt.yildiz.edu.tr
DOI: 10.47481/jscmt.1117139

JSCMT
Journal of Sustainable Construction Materials and Technologies

Research Article

Synthesis of pincer type carbene and their Ag(I)-NHC complexes, and their antimicrobial activities

Murat TÜRKYILMAZ*[1], Murat DÖNMEZ[1], Murat ATEŞ[2]

[1]*Department of Chemistry, Trakya University Faculty of Sciences, Edirne, Türkiye*
[2]*Department of Chemistry, Tekirdağ Namık Kemal University Faculty of Arts and Sciences, Tekirdağ, Türkiye*

ARTICLE INFO

Article history
Received: 16 May 2022
Accepted: 08 June 2022

Key words:
Antimicrobial activity, *candida albicans*, N-heterocyclic carbene (NHCs), SEM analysis, theophylline

ABSTRACT

In this study, theophylline (1) compounds were synthesized with addition of 2-bromoethanol, 2-bromoacetamide and methyl-2-bromoacetate to attain symmetric connections to *NHCs* (2a–c). New complexes containing the symmetric N-heterocyclic carbene (NHC) ligands were synthesized using azolium salts in dimethyl formamide (DMF). After the NHC predecessor compounds reacted with Ag_2O, Ag(I)-NHC complexes were synthesized in the following: 7,9-di-(2-hydroxyethyl)-8,9-dihydro-1,3-dimethyl-1*H*-purine-2,6(*3H,7H*)-dionedium silver(I)bromide (3a), 7,9-di(acetamide)-8,9-dihydro-1,3-dimethyl-1*H*-purine-2,6(*3H,7H*)-diondium silver(I)bromide (3b) and 7,9-di(methylacetate)-8,9-dihydro-1,3-dimethyl-1*H*-purine-2,6(*3H,7H*)-diondiumsilver(I)bromide (3c). Both synthesized NHC predecessors (2a-c) and Ag(I)-NHC complexes (3a-c) were described by FTIR, ^{1}H-NMR, ^{13}C-NMR, liquid and solid-state conductivity values, TGA analysis, melting point analysis and XRD spectroscopy. *In-vitro* antibacterial activities of NHC-predecessors and Ag(I)-NHC complexes were tested against gram-positive bacteria (*Staphylococcus Aureus* and *Bacillus Cereus*), gram-negative bacteria (*Escherichia Coli* and *Listeria Monocytogenes*), and fungus (*Candida Albicans*) in Tryptic Soy Broth method. Ag(I)-NHC complexes showed higher antibacterial activity than pure NHC predecessors. The lowest microbial inhibition concentration (MIC) value of compound 3a was obtained as 11.56 µg/ml for *Escherichia Coli* and 11.52 µg/ml for *Staphylococcus Aureus*. All tested complexes displayed antimicrobial activity with different results.

Cite this article as: Türkyılmaz. M., Dönmez, M, & Ateş, M. (2022). Synthesis of pincer type carbene and their Ag(I)-NHC complexes, and their antimicrobial activities. *J Sustain Const Mater Technol*, 7(2), 53–61.

1. STRUCTURE

Cyclic diamine carbenes allow the provision of σ-donor-π-receiver complexes [1, 2] that have powerful chemical stability in terms of water and oxygen tolerance according to complexes relying on phosphine ligands and they have generally lower toxicity [3]. After sporadic studies, concerning the cellular toxicity of these kind NHC compounds, the cytotoxic effects [4] and mechanisms of action against bacteria it was identified [5, 6].

***Corresponding author.**
*E-mail address: mturkyilmaz@trakya.edu.tr

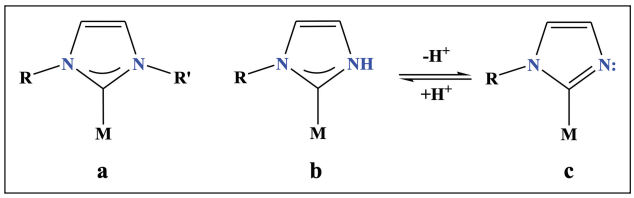

Figure 1. Complexes designed as general NHC **(a)**, pNHC **(b)**, and C-metalized azolato ligands **(c)**.

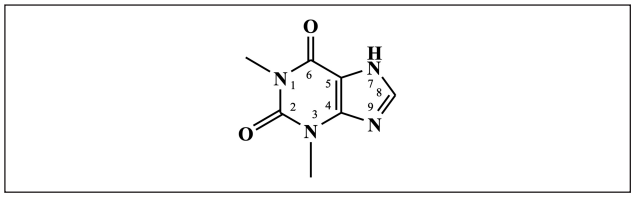

Figure 2. Numerical terminology of theophylline.

NHCs with minimum one NH functional group within the carbene heterocyclic structure are called protic NHCs or pNHCs [7]. These NHCs are not stable, in the free form because of rapid tautomerization to the suitable azole [8]. Additionally, they may be stabilized as ligands in different transition-metal complexes [9], and the synthesis of these pNHC complexes received interest and were prepared by many applications [10]. One feasible route for the adjustment of complexes with protic pNHC ligands is the oxidative supplementation of [11] *N*-alkyl halogen azoles [12] or unsubstituted azoles to different kind low-valent transition metals, such as Ni, Pd, and Pt. As a proton resource, this reaction gives pNHC complexes of type I, as an example [13].

While most NHCs used in inorganic chemistry act as observer ligands (Fig. 1a) that do not join directly in chemical transformations [14, 15], the development of NHCs exhibiting detrimental or assisting functionality were raised recently [16].

One lower class of these ligands are protic NHCs that have an acidic proton on one of the nitrogen atoms in the diamine heterocyclic compound [17]. In addition, they are deprotonated compounds containing a basic ring-nitrogen atom [18] (Fig. 1c).

The protonation method was extended to complexes of pNHC ligands, such as caffeine [19]. Even 2-halogenoazoles with a proton in place of an alkyl substituent on the azole ring nitrogen atom transport the protonation reactions with Pd (0) or Pt (0) to yield [19] the metal complexes with NH and NH-NHC ligands (IV) [20].

As model compounds, transition metal complexes of theophylline allow researched into the correlation between metal ions and nucleic acid oxo purine bases [21]. Theophylline is a monodentate ligand in a fundamental or neutral medium and it coordinates to metal ions through the N7 atom. In some samples, it functions as a bidentate N(7)/O(6) chelating ligand or as a bridging ligand with N(7)/O(6) chelation and N(9) coordination [22, 23].

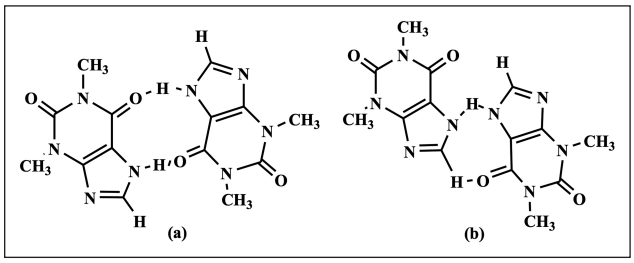

Figure 3. Hydrogen bond structure of theophylline.

Theophylline (1,3-dimethyl-3,7-dihydro-1*H*-purin-2,6-dione) is a natural *N*-methylated xanthine, consumed in beverages and food (Fig. 2). It is a purine alkaloid, 1,3-dimethylxanthine, with important biological properties [24]. It may be used as a respiratory stimulant for the treatment of lung disease and asthma [25]. Thanks to studies showed that theophylline will effectively block human immunodeficiency virus-1(HIV-1) [26].

Theophyllinium-derived compounds were obtained by binding tails with different properties to nitrogen atoms at positions 7 and 9 of the purchased theophylline compound, and their structure was characterized by spectroscopic methods. The XRD characterization of the theophylline molecule revealed strong interactions within crystal structures, such as, C–H···π, C=O···H and N···H···O (Fig. 3) [27].

Included among other health-related uses of theophylline, it has anti-inflammatory properties [28], antitumor potential [29, 30], and a role in neurodegenerative diseases [31]. In recent years, diverse fungi and bacteria have improved their resistance against drugs generally used in clinical studies; thus, there is a need to enhance the chemical and physical properties of drugs [32].

The synthesis and characterization of Ag (I) metal complexes with theophylline were investigated as a ligand for biological usage. Co-crystallization of a drug with another conformers greatly influences its physicochemical features, while it is hoped that metal complexes of theophylline will change the physiological structure of the drug by means of coordination bonds [33]. Alkali metal ions play a very important role in diverse biological subjects, such as within cellular diversity, pH, and tuning electrolyte balance [34–36]. In this study, it was proved that mono sodium salts possess a larger spectrum of antibacterial activity and they are effective especially against *Staphylococcus Aureus*, with over the range of pH 5.0 to 9.0 as bactericides.

Formation reactions for complex compounds involve the breaking of electron-rich olefins [37] by way of transition metals with low oxidation. The presentation of Ag(I)-NHC complexes, the transmetallation pathway [38] and stabilized *N*-heterocyclic carbine [39] make synthesis of functionalized carbene complexes possible in dissimilar studies. Amide, carbene donor polydentate ligand structures, pincer systems and tripodal have received great attention.

NHCs are synthesized in materials and modern medicine science because of their strong σ-transmitter and poor π-receiver characteristics. They were proven to be important compounds for coordination complexes with catalytic and medical activities [40].

Ag(I)-NHC complexes were recognized to have effective anticancer as antimicrobial agents not only with *in-vitro*, but also with *in-vivo* studies. In recent years, antimicrobial activities of Ag^+ ion against microorganisms have been used in medical studies. There are many studies about metal complexes of NHC compounds for dissimilar applications, including antimicrobial, antimitochondrial and anticancer studies in the literature [41, 42].

The synthesis and characterization of antimicrobial applications of new carbene complexes (3a-c) were presented in this paper. A number of bidentate theophyllinium, which are constitutional NHCs ligand pioneers, and their Ag(I)-NHC complexes were prepared. Sigma has a significant effect on reactivity due to electron-donating property in the environment where it is located. Ag(I) complexes were acquired by in-situ deprotonation of NHCs. Not only increasing chain length, but also methyl substituents in the theophylline ring increase the usage of Ag(I) complexes in bio-potential practice. Additionally, aryl bonding and two silver centers contributed to their antimicrobial action. Synthesized compounds were investigated with different techniques, such as FTIR, ^{1}H-NMR, ^{13}C-NMR, TGA, SEM, XRD, and elemental analysis [43].

Theophylline was acquired by the reaction of different substituents as ethanol, methyl acetamide and methyl acetate in a medium. Sodium carbonate was present as a base, and the theophyllinium cation resulted from this reaction. While 3a compound has small bulky bromide anion, 3b and 3c compounds have big bulky hexafluorophosphate anion. 3a, 3b and 3c compounds were obtained as Ag(I) complexes with interactions as a consequence of ligands 2a-c, with Ag_2O in C_2H_5OH or DMF. Ag(I)-NHC complexes, with symmetrical structure, were conjugated with hexafluorophosphate or bromine anions. Because of this arylation, compounds of theophylline derivatives with dissimilar properties were diverse in the sense of yield, conductivity, solubility and antimicrobial activity. NHCs and Ag(I)-complexes were tested against gram-positive and gram-negative bacteria, and fungi.

2. MATERIALS AND METHODS

2.1. Materials

Theophylline ($C_7H_8N_4O_2$, ≥99.00%), 2-bromoethanol (C_2H_5BrO ≥99.50%), 2-bromo acetamide (C_2H_4BrNO ≥99.50%) and methyl-2-bromo acetate ($C_3H_5BrO_2$ ≥97.00%) were supplied from Sigma-Aldrich (Poole, Dorset, UK). Dichloromethane (CH_2Cl_2 ≥99.9%), diethyl ether ($C_4H_{10}O$ ≥99.9%), deuterium oxide (D_2O ≥99.95%), deuterochloroform ($CDCl_3$ ≥99.80%), dimethyl formamide (DMF ≥99.80%), ethanol (C_2H_5OH ≥99.90%), potassium hexafluorophosphate (KPF_6 ≥99.50%), sodium carbonate (Na_2CO_3 ≥99.50%), and silver(I) oxide (Ag_2O ≥99.0%) were purchased from Merck (Germany). In addition, hexane (C_6H_{14} ≥99.00%) and ethyl acetate ($C_4H_8O_2$ ≥99.50%) were purchased at technical purity from local markets. All synthesized compounds were performed under Ar atmosphere using Schlenk line methods.

Minimum inhibition concentration (MIC) tests for each compound were investigated against reference bacterial strains: *Escherichia Coli* (ATCC 25922), *Listeria Monocytogenes* (ATCC 19115), *Salmonella Typhimurium* (ATCC 14028) as gram-negative bacteria, *Staphylococcus Aureus* (ATCC 25923), *Bacillus Cereus* (ATCC 11778), and a type of yeast *Candida Albicans* (ATCC 10231) [44]. Microorganisms were obtained from Technology Research-Development Application and Research Center in Trakya University (TUTAGEM, Edirne, Turkey). Bacterial strains and fungal strains were tested in sub-cultures.

2.2. Instrumentation

FTIR spectra were recorded with KBr pellets in an ATI Unicam 1000 spectrometer. Scanning electron microscope (SEM, Fei Quanta FEG 250) and Four-point probe device (Qiatek, FFP 4) were used to obtain surface images and solid state conductivity measurements, respectively. A pellet machine using a steel die (Desk-Top presser, Model: YLJ-24 MTI Corporation) under a pressure of ~10 tons was used to form a pellet. ^{1}H-NMR and ^{13}C-NMR spectra were recorded using a Varian As 300 Merkur spectrometer operating at 300 MHz (^{1}H-NMR) and 75 MHz (^{13}C-NMR) in $CDCl_3$.

Thermogravimetric analysis (TGA-DTA) TGA 400 was performed by using EXSTAR 6300 at Akkim Kimya Company. A vacuum oven (Nuve Company, vacuum capacity of 760 mmHg with adjustment of temperature of 250 °C) was used for synthesis procedures. X-ray diffraction (XRD) analysis was done by using a Malwern Panalytical Empryean (PANalytical Netherlands) at Ataturk University. Elemental analysis was done by using 836 Series Elemental Analyzer at Trakya University (TUTAGEM). Melting points were measured in open capillary tubes with an Electrothermal-9200 melting point apparatus.

2.3. Antimicrobial Activities of NHC Complexes

Antimicrobial activities of NHC complexes were tested using the agar dilution procedure proposed by the Institute of Clinical Laboratory Standards. For this purpose, *Escherichia Coli* (ATCC 25922), *Listeria Monocytogenes* (ATCC 19115), *Staphylococcus Aureus* (ATCC 25923), *Bacillus Cereus* (ATCC 11778), *Salmonella Typhimurium* (ATCC 14028), and a type of yeast *Candida Albicans* (ATCC 10231) were incubated in Tryptic Soy Broth (TSB) for 24 h at 37 °C. The McFarland Scale was set to 0.5 [45]. Ampicillin was used in cultures as antimicrobial control. Antimicrobial and soluble material stock solutions were filtered using 0.45

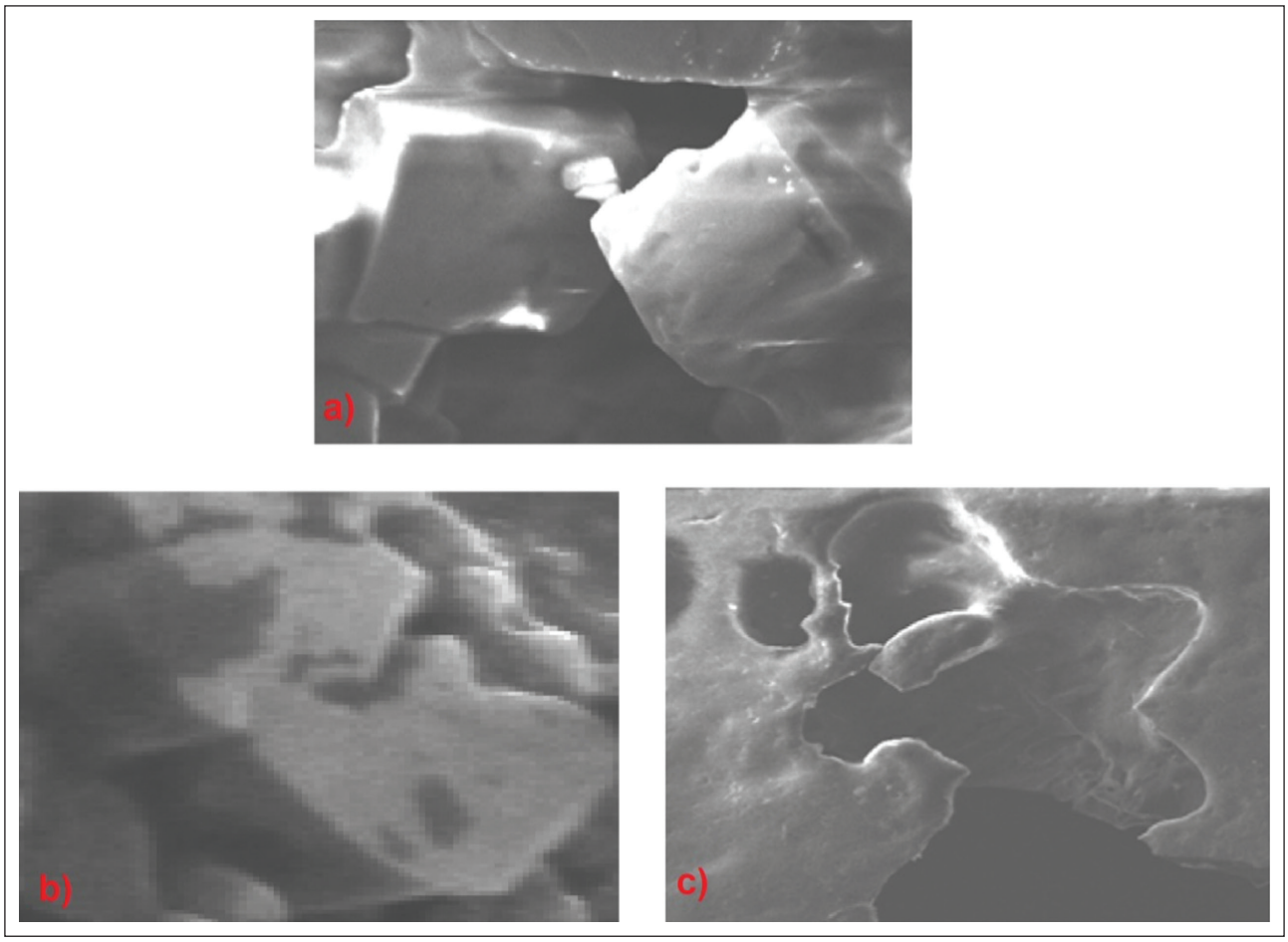

Figure 4. SEM images of NHC complexes, compounds (a) 3a, (b) 3b and (c) 3c. Inset: Time of sample gathering (days) **(a)** 500 µm, **(b)** 300 µm and **(c)** 500 µm scale bar.

µm sterile filter. The results were evaluated for bacteria and yeast after incubation periods of 24 and 48 h. Absorbance was measured at 600 nm and vitality % values were determined. Stock solutions of whole compounds were prepared in DMSO and dilutions were made with deionized water. Concentrations of tested whole compounds were prepared at 100, 50, 25 and 12.5 µg/mL. All inoculated plates were incubated and assessed for bacteria and yeast after incubation periods of 24 and 48 h. The lowest concentrations of compounds preventing growth were determined as MICs [46].

3. RESULTS AND DISCUSSION

3.1. Synthesis of NHCs

Theophylline (1) compound was added to 2-bromoethanol, ethyl-2-bromoacetate and methyl-3-bromopropanoate compounds, respectively. Each of these compounds were connected to NHCs for symmetrical attainment (2a-c). The obtained NHC predecessors (2a-c) were characterized by FTIR, ^{1}H-NMR, ^{13}C-NMR, melting point analysis, liquid and solid-state conductivity, TGA analysis, XRD spectroscopy and SEM analysis.

3.2. SEM Images of NHC Complexes

SEM images of NHC in NHC-Silver(I)-Bromide = 1:1 are illustrated in Figure 4a. The surface area relative to NHC and Ag(I)-bromide is given in Figure 6a. This uneven surface of bromide has many nucleation regions for the growth of silver bromide nanoparticles. SEM images of NHC in NHC-Silver(I)-Bromide = 1:1 are shown in Figure 4b. The large porous structures were enhanced on the surface area relative to NHC and Ag(I)-bromide. SEM images of NHC in NHC-Silver(I)-Bromide = 1:1 can be seen in Figure 4c. The porous spherical nanoparticles were enhanced on the surface area relative to NHC and Ag(I)-NHC bromide (compound 3c) [47].

3.3. TGA and XRD Analysis

Thermal gravimetric analysis (TGA) measurements of Ag(I)-NHC complexes (3a, 3b and 3c) and weight loss of compounds occurred in 4 steps (Fig. 5). In the first step, temperature was between 150 and 400 °C. The weight loss came from dehydration of components. In this step for water molecule lost is 2 mole. In the second step, the temperature was between 400 and 510 °C and is due to primary carbonization. There was higher weight loss (58.73%) at 510 °C due

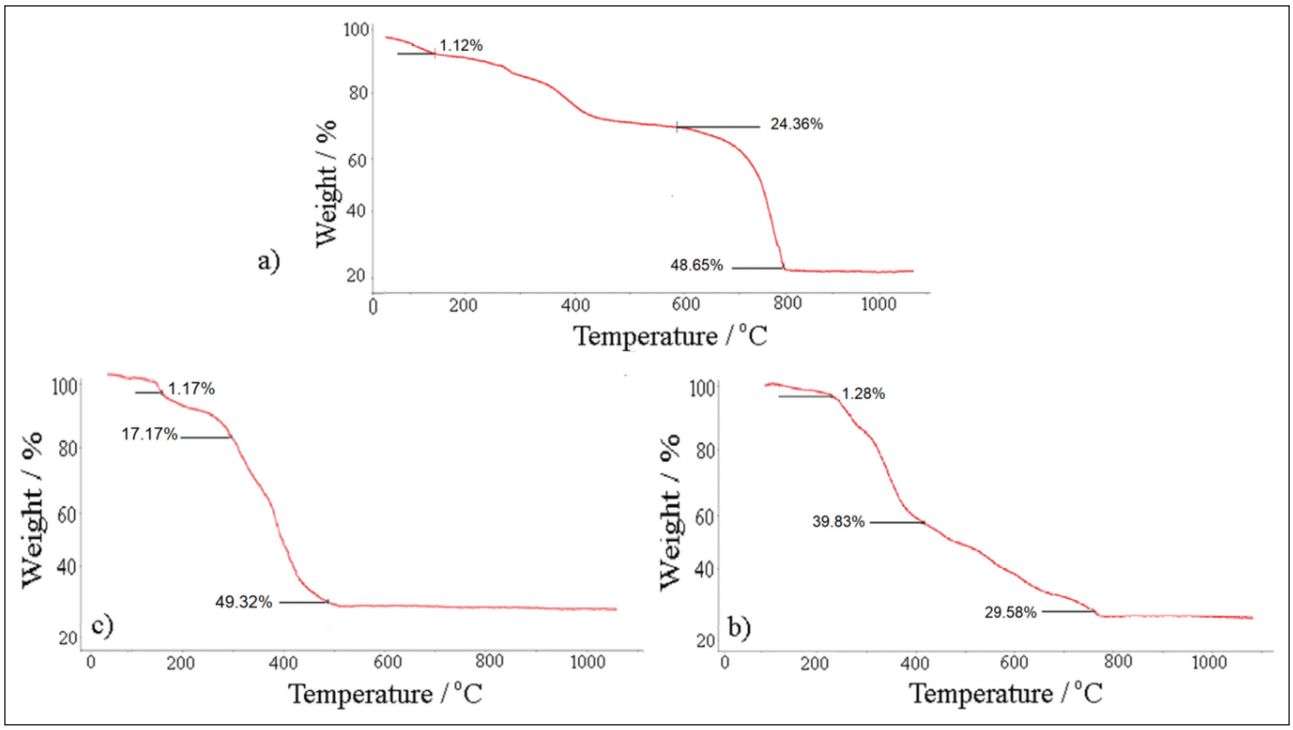

Figure 5. TGA measurements for NHC complexes, compounds **(a)** 3a, **(b)** 3b and **(c)** 3c.

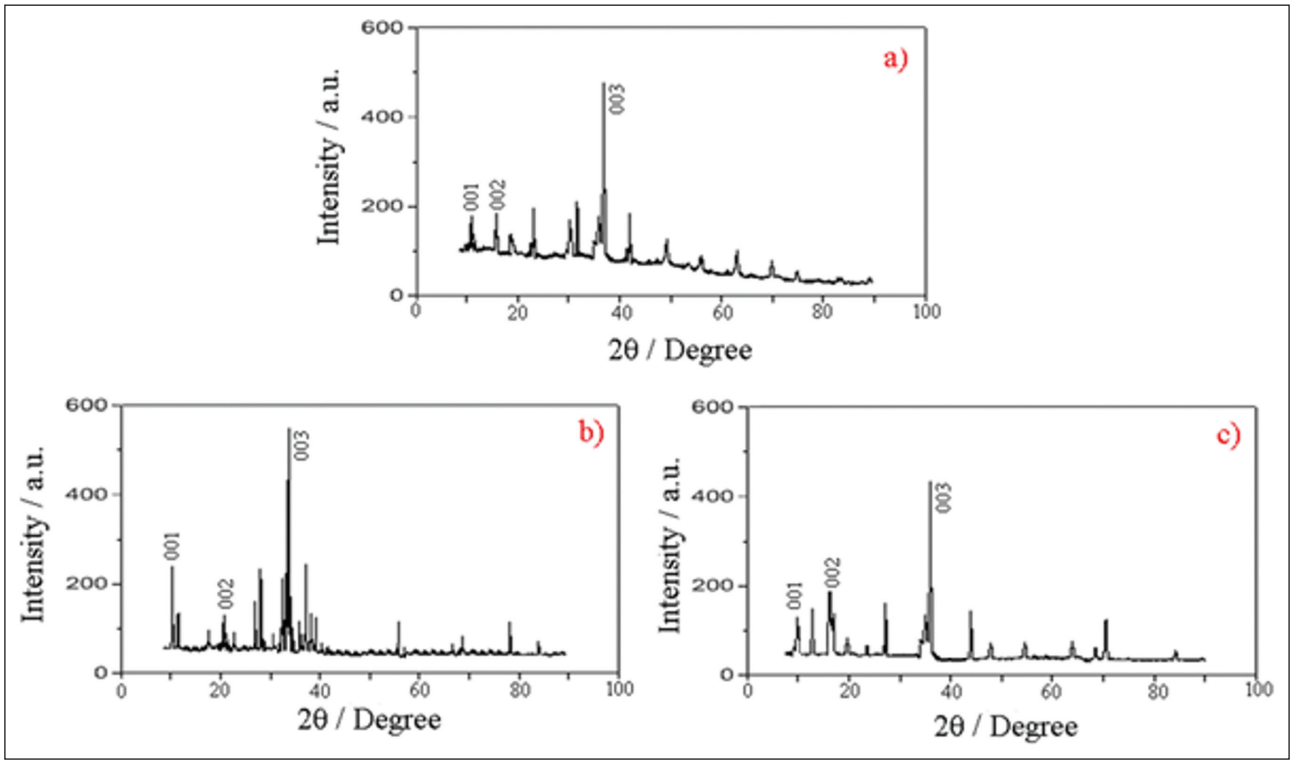

Figure 6. XRD measurements of NHC complexes, compounds **(a)** 3a, **(b)** 3b and **(c)** 3c.

to major volatiles and tar elimination. In the third step, the temperature was between 510 and 795 °C and the compound was nearly completely carbonized (weight loss = 39.83%). The ashes content of NHC is about 24.36%. The results of elemental analysis supported the TGA results. The weight loss of inorganic elements was obtained as 1–1.5% [48].

Table 1. MIC values of compounds (2a-c and 3a-c) for bacterial resistance in antimicrobial tests

	MIC (µg/ml)				
	Gram-negative		Gram-positive		Fungal
NHC complex	*Escherichia Coli*	*Listeria Monocytogenes*	*Staphylococcus Aureus*	*Bacillus Cereus*	*Candida Albicans*
2a	60.00	80.06	90.50	97.53	60.80
3a	11.56	28.36	11.52	44591	22.41
2b	99.02	52.50	85.03	99.00	53.95
3b	20,59	30.47	21.73	32.75	48.45
2c	87.10	58.29	99.00	99.20	57.65
3c	26.43	48.74	44.86	33.86	19.26
Ampicillin	5.00	5.00	10.00	10.00	–

In analysis of TGA plots of compounds 3a, 3b and 3c (Fig. 7a–c) were indicated an initial weight loss above 150 °C, based on the removal of water molecules. Respectively, this weight losses are higher than 1.12, 1.17 and 1.28% for impregnation degrees lower than 101% weight and reaches 8% for NHC, which confirms that these carbons are less hydrophilic in good agreement with their low oxygen surface contents. The second weight loss was followed on the step between 150 and 585 °C and is determined to decomposition of the oxygenated surface groups. In these step water losses for compounds are equivalent to 0.5, 1 and 2 moles, respectively. In the third step, when the temperature reached 500 to 800 °C, bigger weight loss occurred due to the carbonization of the NHC pioneer. Over generally 797 °C, the compound is nearly carbonized. In these step weight losses for compounds are equivalent to 74.13%, 67.66% and 70.69%, respectively.

XRD measurements of the NHC complexes of compounds 3a, 3b and 3c are illustrated in Figure 8. The XRD spectrum gives information depending on two phases with inorganic and organic structure for compound 3a. In this NHC-based Ag(I)-complex, hydrogen, nitrogen and carbon elements were pivotal components and silver and bromide ions were preserved compounds. The XRD peaks were acquired as 2θ= 12.78, 16.11 and 47.81°. In the designed NHC-based Ag(I)-complex of compound 3b, the hydrogen, nitrogen and carbon elements were central components and silver and hexafluorophosphate ions were preserved compounds. The XRD peaks at 2θ= 12.18, 12.84, 14.61 and 45.64° can be observed in Figure 8b. This can also be due to the structured formation of NHCs [49].

In the prepared NHC-based Ag(I)-complex of compound 3c, nitrogen, hydrogen and carbon elements were central components and silver and hexafluorophosphate ions were preserved compounds (Fig. 8c). The XRD peaks at 2θ= 12.36, 12.42, 14.81, and 45.27° were observed due to the structure of NHCs.

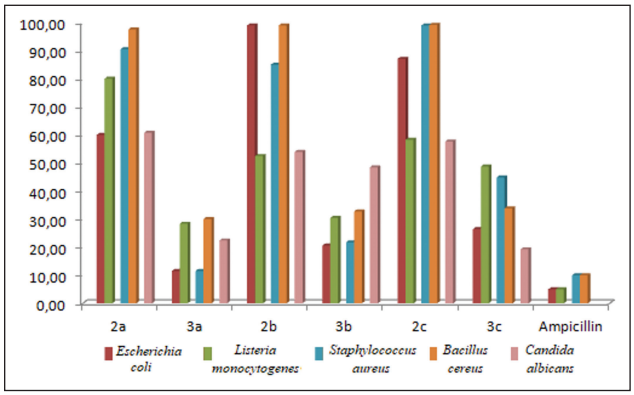

Figure 7. Antimicrobial activities of carbenes and Ag(I)-NHC ligands.

3.4. Conductivity Tests of NHCs and Their Complexes

Conductivity measurement tests of NHCs and their complexes were taken at molar concentration of 10^{-3} M in H_2O medium. The conductivity values for compounds 2a, 2b and 2c were acquired as 21.80, 23.20 and 25.90 µS/cm, respectively. But the conductivity values of NHC complexes increased to 78.25, 82.40 and 108.70 µS/cm for compounds 3a, 3b and 3c, respectively.

Solid-state conductivity of compounds 2a, 2b, 2c, 3a, 3b, and 3c was measured by Four-point probe device. All materials are pressed into a pellet form using the pellet machine. The highest conductivity was acquired as 5.94 $\mu S \times cm^{-1}$ for compound 2b. Other conductivity results are 0.36, 0.58, 4.10, 5.89 and 3.96 $\mu S \times cm^{-1}$ for compounds 2a, 2c, 3a, 3b and 3c, respectively. NHC complexes have conductivity of 4.10, 5.89 and 3.96 $\mu S \times cm^{-1}$ for compounds 3a, 3b and 3c, respectively. Inclusion of Ag metals in the complex form increases the conductivity results [50].

4.4. Microbial Activity of NHCs Complexed or Similar

The utility of Ag(I)-NHC complexes 3a, 3b and 3c for antimicrobial strains has been studied in more detail (Table 1). Compounds 3a, 3b and 3c displayed parallel activities

against both gram negative and gram positive bacteria and fungi. According to these results were more effective than the Ag(I)-NHC complexes carbenes of theophyllinium. Results are beneficial for synthesis of NHC compounds with high antimicrobial activities [51–54].

5. CONCLUSIONS

Thanks to the synthesis methods determined in the literature, derivatives of the theophyllinium cation were obtained by alkylation of theophyllinium. NHC cyclic complexes were synthesized as a result of the interaction of this theophyllinium cation with Ag_2O. The structural analyses of compounds 3a-c were performed with ^{1}H-NMR, ^{13}C-NMR, FTIR and mass spectrometry.

A serial of recent NHC predecessor complexes include symmetrical NHC ligands, which were obtained and characterized by various methods, such as ^{1}H-NMR, ^{13}C-NMR, FTIR liquid and solid-state conductivity, TGA analysis, XRD spectroscopy and melting point analysis. The antimicrobial activities of these Ag(I)-NHC complexes were published for the first time in the literature. NHC compound 3a displayed better antimicrobial activity against bacteria and fungi compared to another complexes, at lower concentrations.

DATA AVAILABILITY STATEMENT

The authors confirm that the data that supports the findings of this study are available within the article. Raw data that support the finding of this study are available from the corresponding author, upon reasonable request.

CONFLICT OF INTEREST

The authors declare that they have no conflict of interest.

FINANCIAL DISCLOSURE

The research grant (TUBAP-2014-106) from Trakya University Research Fund is gratefully acknowledged.

PEER-REVIEW

Externally peer-reviewed.

REFERENCES

[1] Hahn, F. E. & Jahnke, M. C. (2008). Heterocyclic carbenes: Synthesis and coordination chemistry. *Angewandte Chemie International Edition*, 47(17), 3122–3172. [CrossRef]

[2] Nam, D., Tinoco, A., Shen Z., Adukure R. D., Sreenilayam G., Khare S. D., & Fasan, R. (2022). Enantioselective Synthesis of α-Trifluoromethyl Amines via Biocatalytic N–H Bond Insertion with Acceptor-Acceptor Carbene Donors. *Journal of American Chemichal Society*, 144(6), 2590–2602. [CrossRef]

[3] Bakhonsky, V. V., Becker, J., Mlostoń, G., & Schreiner, P. R., (2022) N-Alkoxyimidazolylidines (NOHCs): nucleophilic carbenes based on an oxidized imidazolium core, *Chemical Communications*, 58(10), 1538–1541. [CrossRef]

[4] Adagu, I. S., Nolder, D., Warhurst, D. C., & Rossignol J. F. (2002). In vitro activity of nitazoxanide and related compounds against isolates of Giardia intestinalis, Entamoeba histolytica and Trichomonas vaginalis. *Journal of Antimicrobial Chemotherapy*, 49(1), 103–111. [CrossRef]

[5] Turkyilmaz, M., Ulucam, G., Aktas, S., & Okan, S E. (2017). Synthesis and characterization of new N-heterocyclic carbene ligands: 1, 3-Bis (acetamide) imidazol-3-ium bromide and 3-(acetamide)-1-(3-aminopropyl)-1H-imidazol-3-ium bromide. *Journal of Molecular Structure*, 5(15), 1136, 263–270. [CrossRef]

[6] Aktas, A., Taslimi, P., Gulcin, I. & Gok, Y. (2017). Novel NHC precursors: Synthesis, characterization, and carbonic anhydrase and acetylcholinesterase ınhibitory properties. *Archiv der Pharmazie Chemistry in Life Sciences*, 350(6), Article e201700045. [CrossRef]

[7] Anand, U., Carpena, M., Kowalska-Góralska M., Garcia-Perez, P., Sunita, K., Bontempi, E., Dey, A., Prieto, M. A., Proćków, J., Simal-Gandara. J. (2022). Safer plant-based nanoparticles for combating antibiotic resistance in bacteria: A comprehensive review on its potential applications, recent advances, and future perspective, *Science of The Total Environment*, 821, 153472. [CrossRef]

[8] Dong, M., Duan, X.-Y., Li, Y., Liu, B., & Qi, J., (2022). Highly enantioselective δ-protonation and formal [3+3] annulation promoted by N-heterocyclic carbene. *Organic Chemistry Frontiers*, 11(9), 3039–3044. [CrossRef]

[9] Klussmann, M., Breugst, M., Schlörer, N. E., & Berkessel, A. (2022). Formation of breslow intermediates from n-heterocyclic carbenes and aldehydes involves autocatalysis by the breslow intermediate, and a hemiacetal, 61(23), Article e202117682. [CrossRef]

[10] Kaloglu, M., Sémeril, D., Brenner, E., Matt, D., Ozdemir, I., & Toupet, L., (2016). The ınfluence of ımidazolylidene ligands with bulky resorcinarenyl substituents on catalysts for suzuki–miyaura coupling, *European Journal of Inorganic Chemistry*, 22(7), 1115–1120. [CrossRef]

[11] Ghosh, A., Shee,S., & Biju, A. T., (2022) A benzannulation strategy for rapid access to quinazoline-2,4-diones via oxidative N-heterocyclic carbene catalysis. Organic Letters, 24(14), 2772–2777. [CrossRef]

[12] Ghosh, D., Ghosh, S., Ghosh, A., Pyne, P., Majumder, S. & Hajra, (2022). A. Visible light-induced functionalization of indazole and pyrazole: a recent update, 28(58), 4435–4455. [CrossRef]

[13] Shi, Q., Pei Z., Song, J., Li, S., Wei, D., Coote, M. L., & Lan, Y. (2022). Diradical generation via relayed proton-coupled electron transfer. *Journal of the American Chemical Society*, 144(7), 3137–3145. [CrossRef]

[14] Pacholak, A., Burlaga, N., Frankowski, R., Zgoła-Grześkowiak, A., & Kaczorek, E. 2022. Azole fungicides: (Bio)degradation, transformation products and toxicity elucidation, *Science of The Total Environment*, 802, Article 149917. [CrossRef]

[15] Campillo, D., Escudero, D., Baya, M., & Martín, A. (2022). Heteropolymetallic architectures as snapshots of transmetallation processes at different degrees of Transfer. *Chemistry-A European Journal*, 28(7), Article e202104538. [CrossRef]

[16] Bourissou, D., Guerret, O., Gabbai, P.F., & Betrand, G. (2000). Stable carbenes. *Chemical Reviews*, 100(1), 39–92. [CrossRef]

[17] Seki, M., & Yoshida, K. (2022). Chiral bicyclic NHC/Rh complexes and their application to catalytic asymmetric ring-opening reaction of oxabenzonorbornadienes with amines. *The Journal of Organic Chemistry*, 87(5) 3007–3013. [CrossRef]

[18] Jahnke, M. C., Hahn, F. E., (2015) Complexes with protic (NH,NH and NH,NR) N-heterocyclic carbene ligands. *Coordination Chemistry Reviews*, 293–294, 95–115. [CrossRef]

[19] Das, R., Hepp, A., Daniliuc, C. G., & Hahn, F. E. (2014). Synthesis of complexes with protic NH,NH-NHC ligands via oxidative addition of 2-Halogenoazoles to zero-valent transition metals. *Organometallics*, 33(23), 6975–6987. [CrossRef]

[20] Haque, R. A., Asekunowo, P. O., Razali, M. R., & Mohammad, F. (2019). NHC–Silver(I) Complexes as Chemical Nucleases; Synthesis, Crystal Structures, and Antibacterial Studies. *Heteroatom Chemistry*, 253, 94–204.

[21] Edwards, P. G., & Hahn, F. E. (2011). Synthesis and coordination chemistry of macrocyclic ligands featuring NHC donor groups. *Dalton Trans*, 40(40), 10278–10288. [CrossRef]

[22] Marelius, D. C., Darrow E. H., Moore C. E., Golen, J. A., Rheingold, A. L., & Grotjahn, D. B. (2015). Hydrogen-bonding pincer complexes with two protic N-Heterocyclic carbenes from direct metalation of a 1,8-Bis(imidazol-1-yl)carbazole by Platinum, Palladium, and Nickel. *Chemistry A European Journal*, 21(31), 10988–10992. [CrossRef]

[23] Flowers, S. E., Johnson, M. C. Pitre B. Z., & Cossairt, B. M. (2018). Synthetic routes to a coordinatively unsaturated ruthenium complex supported by a tripodal, protic bis(N-heterocyclic carbene) phosphine ligand. *Dalton Transactions*, 47(4), 1276–1283. [CrossRef]

[24] Hussaini, S. Y., Haque, R. A., & Razali, M. R. (2019). Recent progress in silver(I)-, gold(I)/(III)- and palladium(II)-N-heterocyclic carbene complexes: A review towards biological perspectives. *Journal of Organometalic Chemistry*, 882, 96–111. [CrossRef]

[25] Uluçam, G., & Turkyilmaz, M., (2018). Synthesis, structural analysis, and biological activities of some imidazolium salts. *Bioinorganic Chemistry and Applications*, 2018, Article 1439810. [CrossRef]

[26] Nunnari, G., Argyris E., Fang, J., Mehlman, K. E., Pomerantz, R. J., & Daniel, R. (2005). Inhibition of HIV-1 replication by caffeine and caffeine-related methylxanthines. *Virology*, 335(2), 177–184. [CrossRef]

[27] Novena, L. M., Athimoolam, S., Anitha, R., & Bahadu S. A. (2022). Synthesis, crystal structure, hirshfeld surface analysis, spectral and quantum chemical studies of pharmaceutical cocrystals of a bronchodilator drug (Theophylline). *Journal of Molecular Structure*, 1249, Article 131585. [CrossRef]

[28] Habib A., Iqbal A. M., Bhatti H. N., Kamal A, & Kamal S. (2020) Synthesis of alkyl/aryl linked binuclear silver(I)-N-Heterocyclic carbene complexes and evaluation of their antimicrobial, hemolytic and thrombolytic potential. *Inorganic Chemistry Communications*, 111, Article 107670. [CrossRef]

[29] Lv, G., Guo, L., Qiu, L., Yang, H., Wang, T., Liu, H., & Lin, J. (2015). Lipophilicity-dependent ruthenium N-heterocyclic carbene complexes as potential anticancer agents. *Dalton Transactions*, 44(16), 7324–7331. [CrossRef]

[30] Iqbal, M. A., Umar, M. I., Haque, R. A., Ahamed, M. B. K., Asmawi, M. Z. B. & Majid, A. M. S. A. (2015). Macrophage and colon tumor cells as targets for a binuclear silver(I) N-heterocyclic carbene complex, an anti-inflammatory and apoptosis mediator. *Journal of Inorganic Biochemistry*, 146, 1–13. [CrossRef]

[31] Oñatibia-Astibia, A., Franco, R. & Martínez-Pinilla E. 2017. Health benefits of methylxanthines in neurodegenerative diseases. *Molecular Nutritoon & Food Research*, 61(6), Article 1600670. [CrossRef]

[32] Cherak, Z., Loucif L., Moussi, A., Bendjama E., Benbouza A., & Rolain, J.-M. (2022). Emergence of metallo-β-lactamases and oxa-48 carbapenemase producing gram-negative bacteria in Hospital Wastewater in Algeria: A potential dissemination pathway ınto the environment. *Microbial Drug Resistance*, 28(1), 23–30. [CrossRef]

[33] Dagi, H. T., Findik, D., Senkeles, C., & Arslan, U. (2016). Identification and antifungal susceptibility of Candida species isolated from bloodstream infections in Konya, Turkey. *Annals of Clinical Microbiology and Antimicrobials*, 15(1), 36. [CrossRef]

[34] Hu, J., Li, M., Wan J., Sun J.,Gao, H., Zhang, F., & Zhang, Z. (2022). Metal-free oxidative synthesis of benzimidazole compounds by dehydrogenative coupling of diamines and alcohols. *Organic & Biomolecular Chemistry*, 20, 2852–2856. [CrossRef]

[35] Hu, A., & Wilson, J. J. (2022). Advancing chelation strategies for large metal ıons for nuclear medicine applications, *Accounts Chemical Research*, 55(6), 904–915. [CrossRef]

[36] Augustine, R., Malik, H. N., Singhal, D. K., Mukherjee, A., Malakar, D., Kalarikkal, N., & Thomas, S. (2014). Electrospun polycaprolactone/ZnO nanocomposite membranes as biomaterials with antibacterial and cell adhesion properties. *Journal Polymer Research*, 21(3), 347. [CrossRef]

[37] Wang, P., Fitzpatrick, K. P., & Scheid, K. A. (2021). Combined Photoredox and Carbene Catalysis for the Synthesis of γ-Aryloxy Ketones, 364(3), 518–524. [CrossRef]

[38] Harper, M. J., Arthur, C. J., Crosby, J., Emmett, E. J., Falconer, R. L., Fensham-Smith, A. J., Gates PJ, Leman, T., McGrady, J. E., Bower, J. F., & Russell, C. A. (2018) Oxidative addition, transmetalation, and reductive elimination at a 2,2′-bipyridyl-ligated gold center. *Journal of the American Chemical Society*, 140(12), 4440–4445. [CrossRef]

[39] Çetinkaya, B., Demir, S., Özdemir, I., Toupet, L., Séméril, D., Bruneau, C., & Dixneuf, P. H. (2001) First ruthenium complexes with a chelating arene carbine ligand as catalytic precursors for alkene metathesis and cycloisomerisation, *New Journal of Chemistry*, 4(25), 519. [CrossRef]

[40] Özdemir, I., Gürbüz, N., Kaloglu, N., Dogan, Ö., Kaloglu, M., Bruneau, C., & Doucet, H. (2013). N-Heterocyclic carbene–palladium catalysts for the direct arylation of pyrrole derivatives with aryl chlorides. *Beilstein Journal of Organic Chemistry*, 9, 303–312. [CrossRef]

[41] Bertrand, B., Stefan, L., Pirrotta, M., Monchaud, D., Bodio, E., Richard, P., Le Gendre P., Warmerdam, E., de Jager, M. H., Groothuis, G. M. M., Picquet, M., & Casini, A. (2014). Caffeine-based gold(ı) n heterocyclic carbenes as possible anticancer agents: synthesis and biological properties. *Inorganic Chemistry*, 53(4), 2296–2303. [CrossRef]

[42] Chang, Y. L., Hsu, Y. J., Chen, Y., Wang, Y. W., & Huang S. M. (2017). Theophylline exhibits anticancer activity via suppressing SRSF3 in cervical and breast cancer cell lines. *Oncotarget*, 8(60), 101461–101474. [CrossRef]

[43] Chen, X., Wei, Z., Huang, K.-H., Uehling, M., Wleklinski, M., Krska, S., Makarov, A, A., Nowak, T., & Cooks, G. (2022). Pd Reaction Intermediates in Suzuki-Miyaura Cross-Coupling Characterized by Mass Spectrometry. *ChemPlusChem*, 87(3), Article 202100545. [CrossRef]

[44] Kaloglu, M., Kaloglu, N., Özdemir, I., Günal, S., & Özdemir, I. (2016). Novel benzimidazol-2-ylidene carbene precursors and their silver(I) complexes: Potential antimicrobial agents, *Bioorganic & Medicinal Chemistry*. 24(16), 3649–3656. [CrossRef]

[45] Ma, Q., Davidson, P. M., & Zhong, Q., (2013). Antimicrobial properties of lauric arginate alone or in combination with essential oils in tryptic soy broth and 2% reduced fat milk, *International Journal of Food Microbiology*, 166(1), 77–84. [CrossRef]

[46] Ragab, A., Elsisi, D. M,. Ali, O. A. A., Abusaif M. S., Askar, A. A., Farag, A. A., & Ammar, Y. A. (2022). Design, synthesis of new novel quinoxalin-2(1H)-one derivatives incorporating hydrazone, hydrazine, and pyrazole moieties as antimicrobial potential with *in-silico* ADME and molecular docking simulation, *Arabian Journal of Chemistry*, 15(1), Article 103497. [CrossRef]

[47] Jiang, X., Wang, Y., & Jiang, S. (2010). The effects of substitution of Cr for Mo on the mechanical properties of nanocrystalline Mo_5Si_3 films. *Nanoscale*, 2(3), 394–398. [CrossRef]

[48] Li, Y., Wang, J.-M., Kan, J.-L., Li, F., Dong, Y. & Dong, Y.-B. (2022). Combination of a Metal-*N*-Heterocyclic-Carbene Catalyst and a Chiral Aminocatalyst within a Covalent Organic Framework: a Powerful Cooperative Approach for Relay Asymmetric Catalysis, *Inorganic Chemistry Communications*, 61(5), 2455–2462. [CrossRef]

[49] Pei, X.-L., Zhao, P., Ube, H., Lei, Z., Nagata, K., Ehara, M., & Shionoya, M. (2022). Asymmetric twisting of *c*-centered octahedral gold(I) clusters by chiral *n*-heterocyclic carbene ligation. *Journal of the American Chemical Society*, 144(5), 2156–2163. [CrossRef]

[50] Peng, J., Wu, D., Song, F., Wang, S., Niu, Q. Xu, J., Lu, P., Li, H., Chen, L., & Wu, F. (2021) High current density and long cycle life enabled by sulfide solid electrolyte and dendrite-free liquid lithium anode, *Advanced Functional Materials*, 32(2), Article 2105776. [CrossRef]

[51] Günal, S., Kaloglu, N., Özdemir, I., & Demir, S. (2012). Novel benzimidazolium salts and their silver complexes: Synthesis and antibacterial properties. *Inorganic Chemistry Communications*, 21, 142–146. [CrossRef]

[52] Medici, S., Peana M., Crisponi, G., Nurchi, V. M., Lachowicz, J. I., Remelli M., & Zoroddu, M. A. (2016). Silver coordination compounds: a new horizon in medicine. *Coordination Chemical Reviews*, 327-328, 349–359. [CrossRef]

[53] Nikolić, M. V., Mijajlović, M. Ž., Jevtić, V. V., Ratković, Z. R., Radojević, I. D., Čomić, Lj. R., Novaković, S. B., Bogdanović, G. A., Trifunović, S. R., & Radić, G. P. (2014). Synthesis, characterization and antimicrobial activity of copper(II) complexes with some S-alkyl derivatives of thiosalicylic acid. Crystal structure of the binuclear copper(II) complex with S-methyl derivative of thiosalicylic acid. *Polyhedron*, 79, 80–87. [CrossRef]

[54] Balachandar, R., Navaneethan, R., Biruntha, M., Kumar, K. K. A., Govarthanan M., & Karmegam, N. (2022). Antibacterial activity of silver nanoparticles phytosynthesized from Glochidion candolleanum leaves. *Materials Letters*, 311, Article 131572. [CrossRef]

Journal of Sustainable Construction Materials and Technologies
Web page info: https://jscmt.yildiz.edu.tr
DOI: 10.47481/jscmt.1120446

JSCMT
Journal of Sustainable Construction Materials and Technologies

Research Article

Effect of cement and lime on strength and high-temperature resistance of class F and C fly ash-based geopolymer mortars

Işılay ÖZKUL[1], Adil GÜLTEKİN[2*], Kambiz RAMYAR[1]

[1]*Department of Civil Engineering, Ege University, İzmir, Türkiye*
[2]*Department of Civil Engineering, Düzce University, Düzce, Türkiye*

ARTICLE INFO

Article history
Received: 23 May 2022
Accepted: 02 June 2022

Key words:
Cement, fly ash, geopolymer mortar, high-temperature resistance, slaked lime

ABSTRACT

Geopolymers have advantages such as good high-temperature, acid and sulfate resistance. Recently, researchers have been working on cement-geopolymer hybrid materials. According to these studies, it is possible to adjust the setting times, to gain strength at ambient temperature and to increase the strength with the use of cement. However, it is known that the structural stability of cement deteriorates at high temperatures, lowering its strength. In this study, the effect of slaked lime and cement inclusion on the strength and high-temperature resistance of Class F and Class C fly ash-based geopolymer mortars was investigated. For this purpose, fly ash was replaced with 10, 20 and 30% cement or 5, 10, 20 and 30% slaked lime. The lime and cement substitutions decreased the compressive strength by 8.9–24.4% in Class F fly ash-based geopolymer mortars. In Class C fly ash, however, the cement addition increased the compressive strength up to 46.6%, but the lime inclusion decreased the strength slightly. There was no significant change in the high-temperature resistance of cement or lime-included Class F fly ash geopolymer mortars exposed to 900°C. However, serious decrease was recorded in the high-temperature resistance of Class C fly ash geopolymers upon partial replacement of the fly ash with either cement or lime.

Cite this article as: Özkul, I., Gültekin, A., & Ramyar, K. (2022). Effect of cement and lime on strength and high-temperature resistance of class F and C fly ash-based geopolymer mortars. *J Sustain Const Mater Technol*, 7(2), 62–69.

1. INTRODUCTION

Portland cement concrete is the most used building material in the world. However, in addition to the high amount of carbon dioxide emitted, several other harmful wastes such as sulphur dioxide and dust are released to the atmosphere during cement production. Due to the rapid population growth, cement requirement is increasing day by day, and the damage to the environment is also increasing [1]. Cement production not only releases high amounts of CO_2, but also causes soil and water pollution, high energy and natural resources consumption [2]. According to the International Energy Agency [3], approximately 4.3 billion tons of cement was produced in the world in 2020. Approximately 1 ton of CO_2 is emitted per ton of cement produced [4]. These figures draw attention to the damages caused by the cement industry.

***Corresponding author.**
*E-mail address: adilgultekin05@gmail.com

Table 1. Chemical composition and physical properties of fly ashes and cement

Compound (% by weight)	Class F fly ash	Class C fly ash	Cement
CaO	4.93	15.94	63.95
SiO_2	53.45	47.07	20.14
Al_2O_3	20.63	11.56	4.7
Fe_2O_3	9.79	7.22	3.2
MgO	1.95	7.77	1.41
SO_3	0.19	2.78	3.04
Na_2O	1.12	1.59	0.48
K_2O	2.07	3.04	0.63
Loss on ignition	4.46	0.42	2.43
Physical properties			
Specific gravity	2.32	2.55	3.11
% retained on 45 μm sieve	15.5	32.5	2.1
Blaine specific surface (cm^2/g)	5253	2980	4044

Alternative binders are being developed and used in order to reduce the disadvantages of cement production. Substituting pozzolans with cement or using binders other than portland cement are among the alternatives [5]. Geopolymers are materials produced by dissolving and reacting aluminosilicates in an alkaline environment. It is possible to use natural aluminosilicates such as kaolin or metakaolin, as well as industrial waste materials such as fly ash and slag. By using industrial wastes in the production of geopolymer, a construction material that is both cheap and environmentally friendly is obtained [6]. In their study, Lloyd and Rangan [7] reported that the use of fly ash-based geopolymer concrete would be 10–30% cheaper than conventional concrete. Owing to their sustainable character and outstanding properties, the interest in geopolymers is increasing day by day [8].

The presence of high amount of calcium in fly ash used in the production of geopolymer may result in C-S-H formation besides the geopolymer gel formation. The presence of C-S-H in the geopolymer structure seems to have a positive effect on the mechanical properties of geopolymers. It was also claimed that calcium can act as a balance-cation in the geopolymer structure [9]. Yip et al. [10] showed that in geopolymers produced with calcium-containing base materials, formation of C-S-H in addition to the geopolymer gel is possible. For this reason, researchers conducted studies on cement/geopolymer hybrid materials. Phoo-ngernkham et al. [9] investigated the effect of partial replacement of high-lime fly ash with cement on the compressive strength of geopolymer paste. For this purpose, 5, 10 and 15% of fly ash was replaced with cement. The cement substitution was considered to increase the compressive strength. The fact became more pronounced with the rising cement substitution level. Temuujin et al. [11] investigated the effect of CaO and $Ca(OH)_2$ replacement on the mechanical properties of fly ash-based geopolymer pastes. The rate of substitution ratios was 1, 2 and 3% by weight for CaO and 1.3, 2.6 and 3.9% for $Ca(OH)_2$. Ambient curing and 70°C oven curing were applied. It was reported that the effect of both CaO and $Ca(OH)_2$ on the geopolymer strength was significantly affected by the curing temperature and lime substitution level. Cao et al. [12] investigated the effect of calcium aluminate cement substitution on fly ash-based geopolymer concrete. 5, 10 and 20 wt.% of fly ash was replaced with cement and, activators produced with different NaOH concentrations were used. The positive effect of cement addition on the strength was emphasized and the optimum replacement ratio of cement reported as 10%.

Geopolymers have a lot of advantages such as good mechanical properties and excellent durability. It is reported that the high-temperature resistance of geopolymers is better than that of the portland cement [13]. The C-S-H and CH, the hydration products of ordinary portland cement, are not stable at high temperatures. The geopolymerization products, on the other hand, are more resistant to high temperatures [14]. However, C-S-H, which is likely to form in the structure of geopolymers containing high amounts of calcium, such as high-calcium fly ash or blast furnace slag, can reduce the high temperature resistance of the material.

In this study, the effects of calcium substitution from different sources (cement and slaked lime) on some properties of geopolymer mortars were investigated. It is well known that the increase in calcium content can cause the formation of additional phases such as C-S-H, C-A-S-H in the geopolymer matrix. To examine the effects of these possible new phases on compressive strength and high temperature resistance, cement and slaked lime, which are popularly used as building materials, were used. Either 10, 20 and 30 wt.% of the fly ash was replaced with cement or 5, 10, 20 and 30 wt.% of the fly ash was substituted by lime.

2. MATERIALS AND METHOD

2.1. Materials

Two types of fly ashes (F and C) were used as aluminosilicate sources in the study. The Class F fly ash was supplied from Izdemir Enerji/Izmir and the Class C fly ash was supplied from Cayirhan Thermal Power Plant/Ankara. An ordinary CEM I 42.5 R type cement and slaked lime were used as replacement materials. The chemical composition and some physical properties of fly ashes and cement are shown in the Table 1.

SEM images of fly ashes are shown in Figure 1. These images were obtained using by "Thermo Scientific Apreo S" device with the range of 5 and 7.5 kV. SEM images revealed that the Class F fly ash particles were more rounded than those of the Class C fly ash. Moreover, the particles of Class F fly ash were found to be more uniform in size than that of Class C fly ash particles.

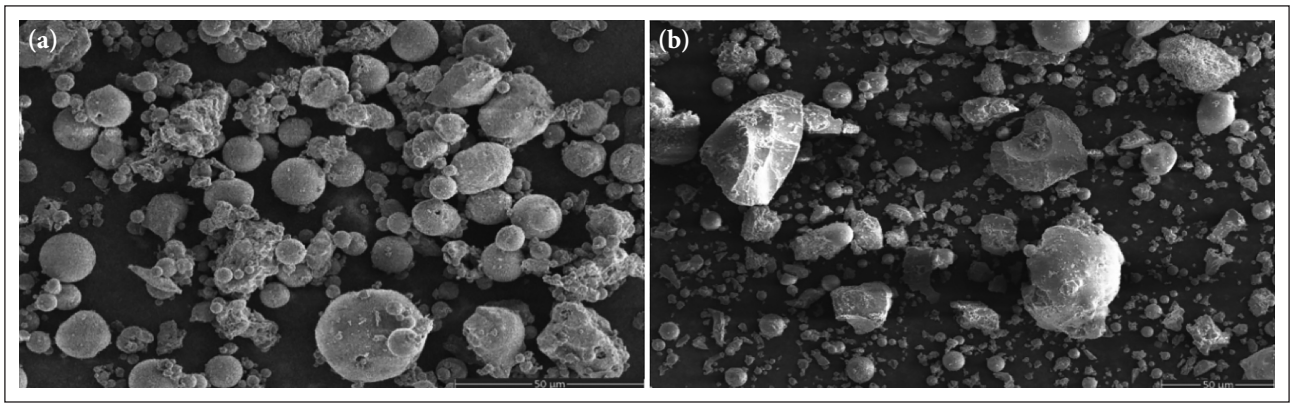

Figure 1. SEM images of fly ashes (a: Class F, b: Class C)

Sodium silicate solution, containing 11.32% Na_2O, 28.22% SiO_2 and 60.45% H_2O by weight, and sodium hydroxide in the form of pellets with 98% purity were used as activators. Sodium hydroxide pellets were dissolved in a given amount of sodium silicate solution to obtain the desired Ms ratio (total SiO_2 to Na_2O ratio by weight in activator). The obtained solution was used after 24 hours of rest.

Tap water and crushed limestone sand was used in the preparation of mortar mixes. The gradation of the sand is shown in the Figure 2.

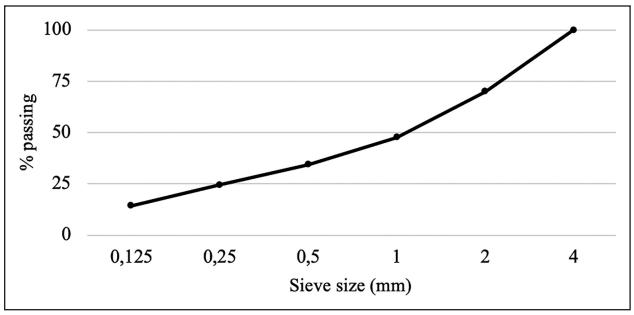

Figure 2. Gradation of sand.

2.2. Method

The experimental part of the study consisted of 2 stages.

At the first stage, the proportions of mixtures to obtain the highest compressive strength for each aluminosilicate were determined. For this purpose, 9 mortar mixtures were prepared with each aluminosilicate by using activators designed with 3 different Ms ratios and 3 different Na_2O percentages (total Na_2O ratio of the activator by weight of aluminosilicate). The compressive strengths as well as flow diameters of the mortar mixtures were determined. The flow diameters of the mortars were determined according to the ASTM 1437-20 [15] standard. In order for the mortars to have similar flow diameters, trail mixtures were prepared using different amounts of water. The target flow diameter for the mixtures was chosen as 18.5±1 cm. For the target flow value, Class C fly ash-based mortars water demand was higher than that of the Class F fly ash-bearing mixtures. The fact seems to be arisen from the morphological characteristics (angular shape) of the Class C fly ash particles which cause greater internal friction in the mixture reducing its consistency.

The ingredients were placed in the Hobart mixer bowl and mixed for 45 seconds at low speed. After scraping the materials adhering to the container, the mixer was operated for another 45 seconds at the same speed and the flow diameters were determined. The mortars were placed in the 50 mm cube molds in 2 layers and each layer was compacted by 25 drops in a jolting table. Immediately after preparing, the specimens were placed in an oven and cured at

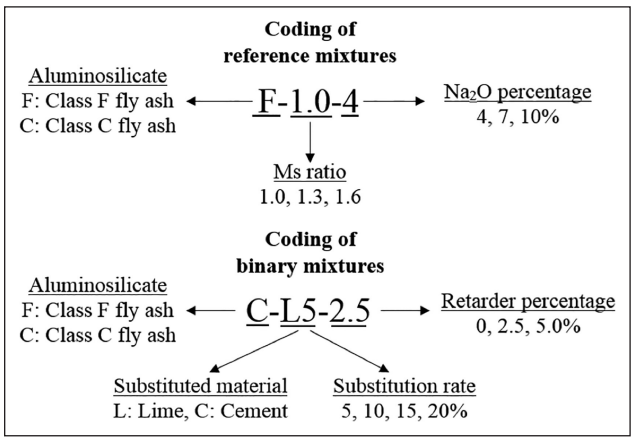

Figure 3. Designating of geopolymer mortar mixtures.

60°C for 1, 3 and 5 days. At this stage, the mixture giving the highest compressive strength for each fly ash was chosen as the reference mixture. The proportions of the mixtures produced at this stage are shown in the Table 2. Mixtures were designated as shown in Figure 3. The compressive strength tests were carried out in a 2000 kN capacity concrete press. The loading rate was set as 0.9 kN/s. The reported strength values are the average of 3 samples.

At the second stage, definite amounts of fly ashes were replaced with cement or slaked lime. The effects of substituted materials on the compressive strength and high-tem-

Table 2. Mix proportions and flow diameters of mixture

Code	Activator (g)	Water (g)	Flow diameter (cm)	Code	Activator (g)	Water (g)	Flow diameter (cm)
F-1.0-4	103.7	150.4	18.0	C-1.0-4	103.7	234.3	17.7
F-1.0-7	181.5	68.5	17.8	C-1.0-7	181.5	181.5	18.5
F-1.0-10	259.3	87.1	18.0	C-1.0-10	259.3	136.8	18.0
F-1.3-4	125.8	133.4	19.0	C-1.3-4	125.8	243.8	18.2
F-1.3-7	219.7	69.6	18.0	C-1.3-7	219.7	61.5	18.0
F-1.3-10	313.8	28.4	19.0	C-1.3-10	313.8	27.7	18.0
F-1.6-4	147.4	108.3	19.2	C-1.6-4	147.4	214.0	18.8
F-1.6-7	257.9	29.6	18.5	C-1.6-7	257.9	99.7	17.8
F-1.6-10	368.3	0	20.0	C-1.6-10	368.3	52.8	22.0

Sand: 1620 g, fly ash: 600 g for all mortar mixtures.

Table 3. Proportions and flow diameters of mixtures containing cement and lime

	Material (g)							Flow diameter (cm)
	Sand	Fly ash	Cement	Lime	Activator	Retarder	Water	
F-1.3-10 (R)	607.5	225.0	–	–	117.5	–	10.7	19
F-C10	607.5	202.5	22.5	–	117.5	–	12.4	
F-C20	607.5	180.0	45.0	–	117.5	–	21.8	
F-C30	607.5	157.5	67.5	–	117.5	–	20.6	19±0.3
F-L10	607.5	202.5	–	22.5	117.5	–	18.9	
F-L20	607.5	180.0	–	45.0	117.5	–	21.5	
F-L30	607.5	157.5	–	67.5	117.5	–	35.2	
C-1.3-10 (R)	607.5	225.0	–	–	117.5	–	10.4	18
C-C10	607.5	202.5	22.5	–	117.5	–	34.3	
C-C20	607.5	180.0	45.0	–	117.5	–	33.1	
C-C30	607.5	157.5	67.5	–	117.5	–	34.0	
C-L5	607.5	213.8	–	11.2	117.5	–	15.4	
C-L5-2.5	607.5	213.8	–	11.2	117.5	5.2	38.3	
C-L5-5	607.5	213.8	–	11.2	117.5	10.6	34.9	18±0.3
C-L10	607.5	202.5	–	22.2	117.5	–	32.0	
C-L10-2.5	607.5	202.5	–	22.2	117.5	5.0	39.1	
C-L10-5	607.5	202.5	–	22.2	117.5	10.1	40.3	
C-L20	607.5	180.0	–	45	117.5	–	40.5	
C-L20-2.5	607.5	180.0	–	45	117.5	4.5	53.0	
C-L20-5	607.5	180.0	–	45	117.5	8.9	52.9	

R: Reference mixture.

perature resistance (300, 600, 900°C) of geopolymer mortars were determined. At this stage, it was aimed to keep the flow diameters of the mixtures as close as possible to that of the reference mixture. For this purpose, differences between the flow diameters of cement- and lime-bearing mixtures and that of the control mixtures were kept within the range of ±0.3 cm. There was a rapid loss of consistency in some of the test mixtures. Thus, a retarder admixture was added to these mixtures. Trial and error were applied to determine the retarder admixture requirement of the mixtures. The proportions of the mixtures containing cement and lime are shown in Table 3.

Payakaniti et al. [13] investigated the high temperature resistance of Class C fly ash based geopolimer pastes and determined that the compressive strength starts to decrease after temperatures of 200°C, the rate of decrease was more considerable in the range of 400–600°C, and the rate of strength loss decreased after 600°C. Researchers also

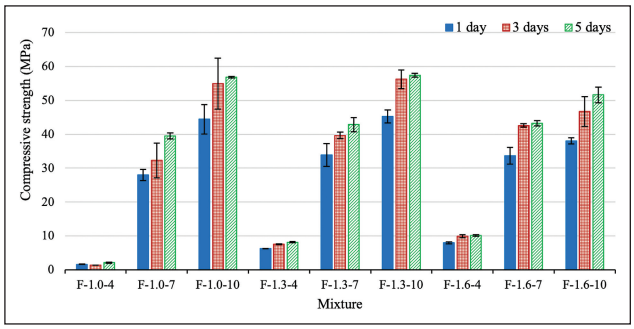

Figure 4. Compressive strength of class F fly ash-based geopolymer mortars.

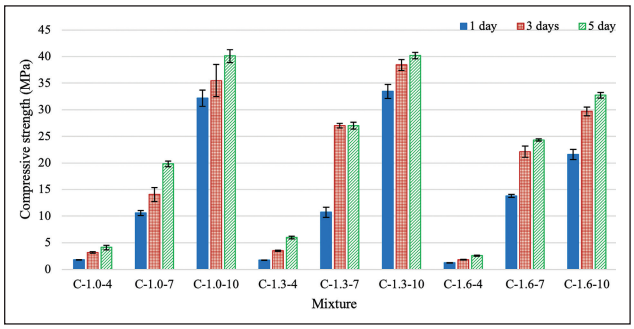

Figure 5. Compressive strength of class C fly ash-based geopolymer mortars.

reported that new crystalline phases appeared in the matrix 800°C and beyond that these crystalline phases had an positive or negative effect on the strength depending on the numbers of these new crystals. Lahoti et al. [16] stated that the first major shrinkage in geopolymers under the influence of high temperature starts at 150–300°C, and the second major shrinkage starts around 600°C in geopolymers produced with activators containing sodium ions. Regarding these findings and probability of presence of components such as C-S-H and CH in the matrix, it was decided to conduct high temperature resistance tests at 300, 600 and 900°C in the present study. The experiments were carried out in a muffle furnace. The temperature was increased at a rate of 20°C/min and the exposure time at the target temperature was set as 3 hours. At the end of this time, the samples were left to cool in the closed furnace. The compressive strength tests were applied immediately when the specimens cooled to the room temperature.

3. RESULTS AND DISCUSSION

3.1. Determination of Reference Mixtures

The compressive strength of Class F and C fly ash-based geopolymer mortars are shown in Figure 4 and Figure 5, respectively. With the increase in the curing time, the compressive strength of both Class C and Class F fly ash-based mortars increased. At the same Ms ratio and Na_2O percentage Class F fly ash mortars were found to be superior to the Class C fly ash mixtures. It is thought that the high water requirement of Class C fly ash-based mortars for a given flow is the cause of their low strength. The highest compressive strengths at all Ms ratios and Na_2O percentages were obtained with 5 days of curing. However, the increase in compressive strength was limited after 3 days. Chithambaram et al. [17] investigated the compressive strength of fly ash-based geopolymer mortars containing sodium silicate-sodium hydroxide activator in different concentrations at different curing times (3, 7, 28 days) and reported that the compressive strength increased with the increase in curing time, but the rate of gaining strength decreased in time. Bellum et al. [18] examined the 7, 14, 28, 60 and

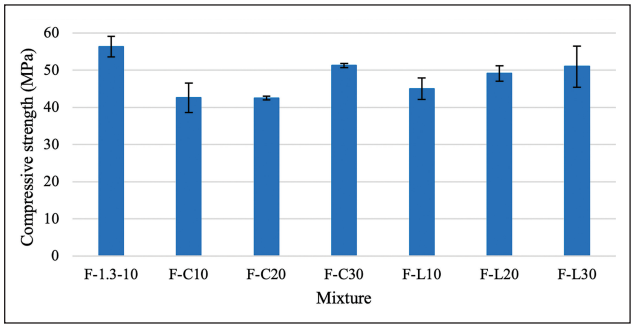

Figure 6. Compressive strength of Class F fly ash-based geopolymer mortars including cement and lime.

91- day compressive strength of slag-bearing fly ash-based geopolymers and stated that the increase in curing time had a positive effect on the compressive strength.

When the strengths of the mortars prepared with the same Ms ratio and cured for the same time are examined, it is seen that the compressive strengths of the geopolymers produced with both fly ashes increased significantly with the increase in the Na_2O percentage. The highest compressive strength achievable in mortars produced with activator having 4% Na_2O content was approximately 10 and 6 MPa for Class F and C fly ash mixtures, respectively. However, with the increase of Na_2O ratio, compressive strengths beyond 55 MPa in Class F fly ash geopolymers, and around 40 MPa in Class C fly ash mixtures were observed. Cho et al. [19] investigated the effect of sodium hydroxide concentration on geopolymers by using sodium hydroxide solution with 4, 6, 8 and 10 M concentrations and found that increasing the sodium oxide concentration improved the compressive strength. The researchers stated that this was due to the increased solubility of aluminosilicate with increasing alkalinity of the mixture.

Both Class F and Class C fly ash mortar mixtures with 1.3 Ms ratio and 10% Na_2O content subjected to 5 days curing showed the highest compressive strength. However, since the compressive strengths of the mixtures cured for 3 and 5 days were very close to each other, thus, 3 days was decided to be sufficient for the curing of the mixtures.

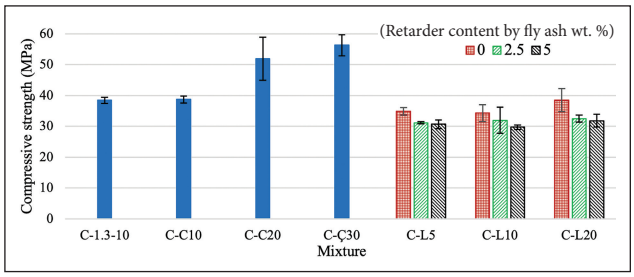

Figure 7. Compressive strength of Class C fly ash-based geopolymer mortars including cement, lime and retarder.

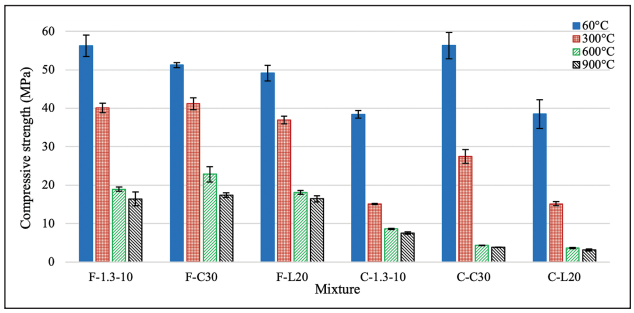

Figure 8. Compressive strength of geopolymer mortars exposed to high temperatures.

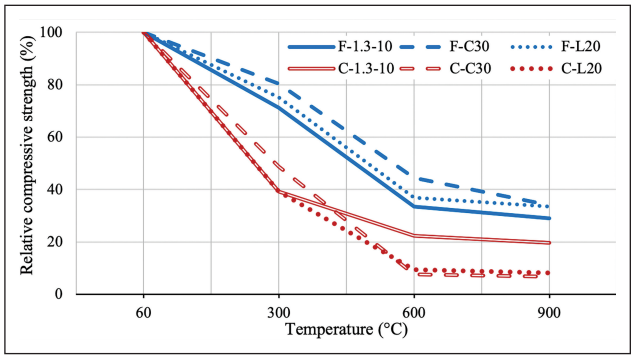

Figure 9. Relative compressive strength of geopolymer mortars exposed to high temperatures.

3.2. Determination of Effect of Cement and Slaked Lime Replacement

The effect of cement and lime on compressive strength of Class F and C fly ash-based geopolymer mortars are shown in Figure 6 and Figure 7, respectively. Within the scope of the study, 10, 20 and 30% lime and cement were replaced with Class F fly ash and the effect of the replacement of these materials on the compressive strength was investigated. The replacement levels of Class C fly ash with cement were same as those of Class F fly ash. However, the substitutions levels of lime with Class C fly ash was somewhat different, i.e., 5, 10, 20 and 30%. Since it was determined that the lime substituted Class C fly ash geopolymers set very quickly (with in 3–4 minutes), mixtures with set retarder were also produced with two different admixture dosages (2.5 and 5.0% by weight of fly ash). In spite of presence of set retarder admixture, the Class C fly ash-based geopolymer containing 30% lime showed flash set during mixing. Therefore, the mixture containing 30% lime could not be produced. Similarly, workability deficiencies were observed in Class F fly ash mixtures containing 30% lime.

Vafaei and Allahverdi [20] studied the effect of partial substitution of natural pozzolan with calcium aluminate cement on the compressive strength of geopolymer mortars. It was reported that the compressive strengths increased with calcium aluminate cement replacement. The strengths increased gradually further with increasing the cement replacement level. The researcher stated that the increased amount of alumina in the geopolymer mixture is important for the formation of N-A-S-H gel, and extra CaO in cement may react with SiO_2 and Al_2O_3 to form C-A-S-H. Yip and van Deventer [21] investigated the formation of C-S-H in geopolymers produced using metakaolin and blast furnace slag. Researchers reported that when calcium-containing aluminosilicates are used in the production of geopolymers, C-S-H could form in the matrix in addition to the geopolymer gel. However, the Ca/Si ratio of this C-S-H was found to be lower than that formed upon portland cement hydration. The increase in strength of the geopolymer mixtures observed in this study was attributed to the C-S-H formation. In the present study, it was observed that the compressive strength of Class F fly ash mortars decreased by 8.9 to 24.4% with cement and lime replacement. However, calcium inclusion was expected to improve strength by formation of additional phases (like C-S-H or C-A-S-H) in the matrix. The fact seems to be due to the effect of the extra water requirement of the mixture for the same workability. A similar situation was observed in Class C fly ash upon substitution of small amount of lime. With lime replacement, a strength loss of up to 10.9% occurred in the compressive strength of these mixtures. The addition of retarder resulted in a further reduction in strength. The water present in the retarder is thought to be the reason for the further strength reduction. However, in spite of its high water content, the compressive strength of cement-bearing Class C fly ash mixtures improved at all inclusion ratios reaching 34.5% and 46.6% upon 20% and 30% cement addition. The improvement in compressive strength of these mixtures, in spite of their high water content, was probably due to the presence of new phases in the matrix. Chindaprasirt et al. [22] also reported that calcium hydroxide and cement substitution improved the compressive strength of alkali-activated fly ash pastes. According to the researchers, this was related to the formation of additional C-S-H and C-A-S-H phases in the matrix and the shortening of the both initial and final setting times. Temuujin et al. [11] stated that the compressive strength of fly ash-based geopolymer pastes cured at ambient temperature increased with the inclusion of CaO and $Ca(OH)_2$, but on the contrary, the compressive strengths decreased upon curing at 70°C. The researchers attributed the fact to the increased rate of evaporation of water at high temperature increasing the porosity.

3.3. Determination of the Resistance of Selected Mixtures to High-Temperature

High- temperature resistance is also one of the important durability issues for geopolymers. There are many studies on the high- temperature resistance of geopolymers in the literature. F-C30, C-C30, F-L20 and C-L20 mixtures were selected for high-temperature resistance tests. Except for F-L20 mixture, the others showed the highest strength in their own group. Owing to its very short setting time, F-L30 mixture having the highest strength in its group was not selected.

The compressive strengths of the selected geopolymer mortars before and after exposure to 300, 600, 900°C are shown in Figure 8, and the relative compressive strengths are shown in Figure 9. The compressive strength of both Class C and Class F fly ash-based mortars decreased gradually with the increase in temperature. The reduction in strength of Class F fly ash mixtures after exposing to 300°C was in the range of 19.6 to 28.8%. The corresponding range was 51.2 to 60.7% in Class C fly ash mortars. The higher amount of calcium in Class C fly ash-based mixtures seems to be the reason for this situation. With the increase in temperature, the strength losses also increased so that upon exposure to 900°C the residual strengths in the Class F and C fly ash-based mortars were merely in the range of 29.1 to 34.0% and 6.8 to 19.7%, respectively. The presence of 16–17 MPa residual strength in Class F fly ash mixtures even after exposure to 900°C is a good measure of the high-temperature resistance of these mixtures. Klima et al. [23] stated that the evaporation of the water present in the geopolymers at high temperatures caused both thermal shrinkage and vapour pressure damaging the structure. Payakaniti et al. [13] reported that the compressive strength losses at temperatures higher than 400°C in geopolymers may be caused by thermal stresses, and the changes in the crystal structure at 1200°C was found to be responsible for further reduction of the mechanical properties. A very important part of the strength loss experienced within the scope of the present study was observed at temperatures up to 600°C. It is thought that the evaporation of water coupled with thermal shrinkage/stress are the causes of the strength loss.

As it can be seen from Figure 9, the loss in strength of Class F fly ash mixtures either with or without inclusions upon exposure to extreme temperatures are very close to each other, irrespective of the temperature level. This indicates that either the presence or type of the substitute has no significant effect on residual strength of Class F fly ash geopolymer exposed to high temperature. However, the opposite is true for Class C fly ash-based mortars. The cement and lime substituted Class C mixtures showed considerably higher loss in strength than their control mixture particularly when exposed to 600 and 900°C. The fact probably is arisen from the increase in the amount of C-S-H in the matrix due to the increased calcium content, which also negatively affects the compressive strength after exposing to high temperatures.

4. CONCLUSION

For the materials used and test methods applied the following conclusions were drawn:

- Class C fly ash had a lower fineness than Class F one. In spite of this, for a given flow, Class C fly ash geopolymer mortar showed a higher water requirement than Class F fly ash counterpart. The fact seems to be arisen from the angular shape of the Class C fly ash particles which cause greater internal friction.
- For a given activator composition, activator content and same curing conditions, Class F fly ash-based geopolymer mortars showed higher compressive strength than that of the Class C fly ash-based mortars. The fact most probably was arisen from the morphology of Class C fly ash particles which increased the water demand of the geopolymer mortar.
- In both Class C and F fly ashes, the highest mortar compressive strength was obtained at 1.3 Ms ratio and 10% Na_2O content. The highest average compressive strengths attained after 5 days of curing at 60°C were recorded as 57.4 and 40.2 MPa for Class F and C fly ash mixtures, respectively.
- The cement or lime substitution reduced the compressive strength of Class F fly ash-based mortars between 8.9 and 24.4%. On the contrary, in Class C fly ash mixtures, the cement replacement had a positive effect on the compressive strength and the strength increased by 46.6% upon 30% cement inclusion, while lime substitution reduced the strength slightly.
- The high-temperature resistance of Class F fly ash-based mixture was higher than that of its Class C fly ash counterpart.
- The high-temperature resistance of Class F fly ash geopolymer mortars did not changed considerably upon lime or cement substitution. On the other hand, in Class C fly ash geopolymer mortars containing either 20% lime or 20% cement the residual compressive strengths were only 6.8 and 8.2% upon exposure to 900°C, respectively.

DATA AVAILABILITY STATEMENT

The authors confirm that the data that supports the findings of this study are available within the article. Raw data that support the finding of this study are available from the corresponding author, upon reasonable request.

CONFLICT OF INTEREST

The authors declare that they have no conflict of interest.

FINANCIAL DISCLOSURE

The authors declared that this study has received no financial support.

PEER-REVIEW

Externally peer-reviewed.

REFERENCES

[1] Kaplan, G., Öz, A., Bayrak, B., Alcan, H. G., Çelebi, O., & Aydın, A. C. (2022). Effect of quartz powder on mid-strength fly ash geopolymers at short curing time and low curing temperature. *Construction and Building Materials*, 329, Article 127153. [CrossRef]

[2] Almutairi, A.L., Tayeh, B. A., Adesina, A., Isleem, H. F., & Zeyad A. M. (2021). Potential applications of geopolymer concrete in construction: A review. *Case Studies in Construction Materials*, 15, e00733. [CrossRef]

[3] International Energy Agency. (2022, May 17). Cement Report. https://www.iea.org/reports/cement

[4] Vikas, G., & Rao, T. D. G., Setting time, workability and strength properties of alkali activated fly ash and slag based geopolymer concrete activated with high silica modulus water glass. *Iranian Journal of Science and Technology, Transactions of Civil Engineering*, 45, 1483–1492. [CrossRef]

[5] Behforouz, B., Balkanlou, V. S., Naseri, F., Kasehchi, E., Mohseni, E., & Ozbakkaloglu, T. (2020). Investigation of eco-friendly fiber-reinforced geopolymer composites incorporating recycled coarse aggregates. *International Journal of Environmental Science and Technology*, 17, 3251–3260. [CrossRef]

[6] Nawaz, M., Heitor, A., & Sivakumar, M. (2020). Geopolymers in Construction - Recent Developments. *Construction and Building Materials*, 260, Article 120472. [CrossRef]

[7] Lloyd, N. A., & Rangan, B. V. (2010). Geopolymer Concrete with Fly Ash, *Second International Conference on Sustainable Construction Materials and Technologies*, Ancona, Italy. [CrossRef]

[8] Hui-Teng, N., Cheng-Yong, H., Yun-Ming, L., Abdullah, M. M. A. B., Rojviriya, C., Ken, P. W., Shee-Ween, O., Yong-Jie, H., & Wan-En, O. (2022). Thermo-mechanical behaviour of fly ash-ladle furnace slag blended geopolymer with incorporation of decahydrate borax. *Construction and Building Materials*, 331, Article 127337. [CrossRef]

[9] Phoo-ngernkham, T., Chindaprasirt, P., Sata, V., Pangdaeng, S., & Sinsiri, T. (2013). Properties of high calcium fly ash geopolymer pastes with portland cement as an additive. *International Journal of Minerals, Metallurgy and Materials*, 20(2), 214–220. [CrossRef]

[10] Yip, C. K., Lukey, G. C., & van Deventer, J.S.J. (2005). The coexistence of geopolymeric gel and calcium silicate hydrate at the early stage of alkaline activation. *Cement and Concrete Research*, 35, 1688–1697. [CrossRef]

[11] Temuujin, J., van Riessen, A., & Williams, R. (2009). Influence of calcium compounds on the mechanical properties of fly ash geopolymer pastes. *Journal of Hazardous Materials*, 167, 82–88. [CrossRef]

[12] Cao, Y-F., Tao, Z., Pan, Z., & Wuhrer, R. (2018). Effect of calcium aluminate cement on geopolymer concrete cured at ambient temperature. *Construction and Building Materials*, 191, 242–252. [CrossRef]

[13] Payakaniti, P., Chuewangkam, N., Yensano, R., Pinitsoontorn, S., & Chindaprasirt, P. (2020). Changes in compressive strength, microstructure and magnetic properties of a high-calcium fly ash geopolymer subjected to high temperatures. *Construction and Building Materials*, 265, Article 120650. [CrossRef]

[14] Choi, Y. C., & Park B. (2020). Effects of high-temperature exposure on fractal dimension of fly-ash-based geopolymer composites. *Journal of Materials Research and Technology*, 9(4), 7655–7668.

[15] ASTM International. (2020). ASTM 1437- *Standard test method for flow of hydraulic cement mortar*. https://www.astm.org/c1437-20.html

[16] Lahoti, M., Wong, K. K., Tan, K. H., & Yang, E-H. (2018). Effect of alkali cation type on strength endurance of fly ash geopolymers subject to high temperature exposure. *Materials and Design*, 154, 8–19. [CrossRef]

[17] Chithambaram, S. J., Kumar, S., & Prased, M. M. (2019). Thermo-mechanical characteristics of geopolymer mortar. *Construction and Building Materials*, 213, 100–108. [CrossRef]

[18] Bellum, R. R., Al Khazaleh, M., Pilla, R. K., Choudhary, S., & Venkatesh, C. (2022). Effect of slag on strength, durability and microstructural characteristics of fly ash-based geopolymer concrete. *Journal of Building Pathology and Rehabilitation*, 7, 25. [CrossRef]

[19] Cho, Y-K., Yoo, S-W., Jung, S-H., Lee, K-M., & Kwon S.-J. (2017). Effect of Na2O content, SiO2/Na2O molar ratio, and curing conditions on the compressive Strength of FA-based geopolymer. *Construction and Building Materials*, 145, 253–260. [CrossRef]

[20] Vafaei, M., & Allahverdi, A. (2016). Influence of calcium aluminate cement on geopolymerization of natural Pozzolan. *Construction and Building Materials*, 114, 290–296. [CrossRef]

[21] Yip, C. K., & Van Deventer, J. S. J. (2003). Microanalysis of calcium silicate hydrate gel formed within a geopolymeric Binder, *Journal of Materials Science*, 38, 3851–3860. [CrossRef]

[22] Chindaprasirt, P., Phoo-ngernkham, T., Hanjitsuwan, S., Horpibulsuk, S., Poowancum, A., & Injorhor, B. (2018). Effect of calcium-rich compounds on setting time and strength development of alkali-activated fly ash cured at ambient temperature. *Case Studies in Construction Materials*, 9, e00198. [CrossRef]

[23] Klima, K. M., Schollbach, K., Brouwers, H. J. H., & Yu, Q. (2022). Enhancing the thermal performance of class F fly ash-based geopolymer by sodalite. *Construction and Building Materials*, 314, Article 125574. [CrossRef]

Journal of Sustainable Construction Materials and Technologies
Web page info: https://jscmt.yildiz.edu.tr
DOI: 10.47481/jscmt.1116561

JSCMT
Journal of Sustainable Construction Materials and Technologies

Research Article

Numerical analysis of flexural and shear behaviors of geopolymer concrete beams

Ali İhsan ÇELİK[1*], Ahmet ÖZBAYRAK[2], Ahmet ŞENER[1], Mehmet Cemal ACAR[3]

[1]Department of Construction, Kayseri University, Tomarza Mustafa Akincioglu Vocational School, Kayseri, Türkiye
[2]Department of Civil Engineering, Erciyes University, Kayseri, Türkiye
[3]Department of Construction, Kayseri University, Vocational School of Technical Sciences, Kayseri, Türkiye

ARTICLE INFO

Article history
Received: 13 May 2022
Accepted: 31 May 2022

Key words:
Flexural and shear behavior of GPC, fly ash, geopolymer concrete, mechanical properties of GPC

ABSTRACT

Geopolymer concrete (GPC) is obtained by activating industrial wastes such as fly ash with chemical liquids such as sodium hydroxide (NaOH) and sodium silicate ($Na_2 SiO_3$). In order to use environmentally friendly GPC obtained from industrial wastes instead of Portland cement concrete (OPC), its behavior in structural elements is important and should be investigated in detail. Load-displacement characteristics, flexural and shear stiffnesses, and crack development of samples were obtained by numerical analysis. The GPC beams to be an alternative to OPC beams, their mechanical properties and fracture modes must be at least as much as OPC. As a result of the analyses, it was determined that the 110x20x15 cm GPC beams with compression reinforcements of 2Φ8 and tension reinforcements of 2Φ8, 3Φ14 and 2Φ18, respectively, showed similar flexural, shear and crack development with OPC beams. Simulations of GPC beams were made up to the breaking point, contributing to understanding its behavior. The ultimate load for both OPC and GPC beams in the FEM model was 45 MPa, while in the experimental model, the OPCB was 55 MPa and the GPCB was 60 MPa. While the first crack started at 1 mm in the OPCB-FEM model, the GPCB-FEM model showed a more elastic behavior, and the first crack started after 3.5 mm displacement. The load-displacement results for 2Φ8 compression and 3Φ14 tensile reinforced beams contain closer results in FEM and experimental. The ultimate load states are between 160 MPa and 180 MPa, but the maximum strengths of OPCBs are slightly higher. After 7.5 mm, crack formation continued to increase. Maximum strength in beams with 2Φ8 pressure and 2Φ18 reinforcement is in the range of 175–185 MPa. Although the values are very close to each other, it seems that they did not exceed the strengths of the previous 3Φ14 reinforced beams. On the other hand, it is seen that the plastic deformation of GPCBs starts from 7.5 mm, while OPCBs start after 10 mm. Observing the load-displacement graphs and the mobility of concrete and reinforcement, it can be said that the yield in the steel reinforcement and the crack development in the beams are simultaneous, and the crack development in GPCs starts a little earlier than the yield of the steel reinforcement.

Cite this article as: Çelik, A. İ., Özbayrak, A., Şener, A., & Acar, M. C. (2022). Numerical analysis of flexural and shear behaviors of geopolymer concrete beams. *J Sustain Const Mater Technol*, 7(2), 70–80.

***Corresponding author.**
*E-mail address: acelik@kayseri.edu.tr

1. INTRODUCTION

While modern building constructions continue worldwide, limestone calcination and carbon dioxide emissions caused by cement production, which is the primary concrete binding material, are considered the main causes of global warming. While humanity is looking for solutions to the world's climate crisis, scientists in civil engineering are working on an alternative to cementitious concrete and a more environmentally friendly concrete. Geopolymer Concrete (GPC), obtained by activating more environmentally friendly materials, has recently attracted great interest as an alternative to cementitious concrete. GPC is obtained by adding fly ash obtained as waste from the chimney of thermal power plants to coarse and fine aggregates and activating them with chemicals such as sodium hydroxide (NaOH) and sodium silicate (Na_2SiO_3). A lot of work has been done on the material properties, microstructure and compositions of GPC, which has not yet found application in practice. Research on the mechanical properties of GPCs remains more limited. From this point of view, the flexural and shear behavior of Geopolymer beams (GPCB) is among the important research topics. The structural behavior of GPCBs has been observed with experimental and numerical studies by Pham et al. (2021) [1]. Considering the linear elastic behavior of GPCs, flexural cracking and steel yielding, they revealed that GPCBs behave ductility. In addition, both experimental and numerical analysis results confirmed that the moment capacity increased when the steel reinforcement ratio increased. Hutagi et al. (2011) [2] studied the flexural behavior of GPC and Portland Cement concrete beams (OPCBs). As a result of the study, they revealed that the post-peak ductility of GPCBs is lower than that of OPC beams, while GPCBs behave in the same way as OPCBs in terms of load-deflection properties, cracking moment and service load moment. A similar statement in Kumar and Kumar (2016) found that the load deviation properties of OPCBs and GPCBs are almost the same. The cracking moment of GPCB was lower compared to OPCB [3]. However, the observed crack patterns and fracture modes for GPCBs were like OPCBs. The total number of felaxural cracks was nearly the same when all beam types were considered. The beams failed as their steel yield first, and then the concrete was crushed at the pressure zone of surface [3], GPCBs the flexural behavior, comparing the numerical simulation and analytic calculations OPCBs, concluded that they were more stringent than the theoretical calculation of GPCBs flexural behavior. In addition to the experimental investigation, they also performed numerical studies using ABAQUS finite element software to investigate the structural behavior of GPCBs [4]. Amiri et al. (2016) [5] examined the structural behavior of GPCBs in their study with the finite element method. They found that the experimental deviations differed from the ABAQUS simulations due to friction forces and sliding behavior at the beam-support contact. Uma et al. (2012) [6] tried to model the structural behavior of GPCBs using ANSYS 12.0 software. The authors showed a 20% difference between the experimental and numerical results in this comparative study.

There is little research to evaluate the shear behavior, crack shapes, and failure modes of reinforced GPCBs under bending load. Therefore, studies on the shear behavior of GPCBs are precious. Yost et al. [7] found that shear force transfer and shear strength were similar in both geopolymer and cement-based concrete beams. Yacob et al. [8] four GPCBs and one OPCB presented beams' strength, strains, deformations, and failure modes in their experimental study to determine shear strength. As a result of the research, it was found that the parameters that affect the shear strength of OPCBs, namely shear reinforcement, w/v and concrete compressive strength, also affect the shear strength of GPCBs. GPCB showed almost the same ductility behavior as OPCB with similar reinforcement in load-deflection response. Shear deformation and mean strain were more critical in beams that excel in shear and torsion-shear, while they were less important in beams that excel in shear-flexural. Visintin et al. [9] presented the low-level test results of eight reinforced concrete GPC beams without stirrups, along with the results of four direct shear tests. They determined that the shear friction properties for the GPC used in the experimental research were within the range of the shear friction properties of the OPC concrete. On the other hand, Mourougane et al. (2012) [10] observed that GPCBs showed higher shear strength in the range of 5–23% compared to OPCBs. However, Mourougane et al. [10] found that ACI 318 [11] gave a good estimate of the shear strength of GPCBs, with an average test prediction ratio of 0.96. Chang (2009) [12], based on research on GPCBs with varying longitudinal and transverse reinforcement ratios, that the calculation method for OPCBs is AS 3600 [13] and ACI318 [11], giving average test-to-estimate ratios of 1.70 and 2.55, respectively. They stated that GPCBs could be safely used to predict the shear strength of GPCBs. Ng et al. [14] found that shear cracking was delayed when steel fibers were added to GPC, but finer cracks were formed. It has been found that the crack width is reduced when smaller diameter straight steel fibers are used. As a result, steel fibers proved to increase the cracking load and ultimate strength of GPCBs.

Today, simulation of structural elements in computers with FEM plays a growing role in civil engineering studies. This software produces approximate solutions by making predictions and providing analysis. Comparably, FEM analysis yields 90% to 95% accurate results in analysis modes [15, 16]. Although the shear behavior of the beam provides the correct properties of the structure, the expense and time

Table 1. Beam geometry and reinforcement information

Group	Sample name	Beam dimensions (mm)	Reinforcement steel		Stirrup
			Pressure steel	Tension steel	
1	OPC1	150x200x1100	*2Φ8*	*2Φ8*	*Φ8/150*
	OPC2	150x200x1100	*2Φ8*	*3Φ14*	*Φ8/150*
	OPC3	150x200x1100	*2Φ8*	*2Φ18*	*Φ8/150*
2	GPC1	150x200x1100	2Φ8	2Φ8	Φ8/150
	GPC2	150x200x1100	*2Φ8*	*3Φ14*	*Φ8/150*
	GPC3	150x200x1100	*2Φ8*	*2Φ18*	*Φ8/150*

consumption during the experimental calibration are disadvantageous [17]. The results obtained from the ANSYS software, which digitally models the beam experiments, entirely depend on the mesh size, material properties, and load increases [18]. Rajhgopal et al. [19] modelled the concrete as a 3D solid65 element and the reinforcement as a Link 8 element for GPC beam via ANSYS software. As a result of nonlinear FEM analysis of geopolymer beams, load-deflection characteristics, fracture modes and crack states were observed together with experimental results. Modeling GPCBs that exhibit nonlinear behavior until failure with FEM reduces costs and produces results faster than laboratory testing. GPC preparation of concrete as environmentally friendly concrete still has many difficulties compared to casting and testing OPC concrete. Said beam denier is even more difficult. There are many experimental and FEM analysis studies on OPCBs and steel beams [20–30], but the study on GPC is very limited. Thanks to this study, the analysis of GPC beams in terms of both flexural and shear behavior is considered an innovation.

Most of the studies on GPCs are related to the microstructure and chemical composition of GPCs. However, studies on the structural behavior of GPCB still remain limited [7–10, 12, 31]. Examination of the real-time behavior of beams produced from GPC, obtained from strain and stretching in the laboratory environment, can be quite a time consuming, and materials can be quite expensive. To contribute to this limited area, ANSYS, finite element-based computer software with which nonlinear beam models can be defined easily due to its cost-effectiveness, was used in this study. This study aims to examine geopolymer concrete beams' flexural and shear behavior in various crack conditions such as crack initiation, propagation, flexural strength, load-deflection and structural failure modes using three-dimensional FEM analysis. At the same time, it is to reveal the time-dependent comprehensive behavior of the beam under the influence of increasing load until the moment of fracture under the critical distribution of stresses and effective strains in the steel reinforcement by comparing it with the results obtained from the calculations in the laboratory environment. Using software that performs finite element analysis makes it possible to simulate GPCBs up to the moment of fracture. This study aims to contribute significantly to the future development of this environmentally friendly concrete.

2. MATERIAL AND METHOD

2.1. FEM Development of GPC Beams

Observation of flexural and shear behavior of GPCBs was performed numerically with ANSYS Workbench (21.2) software. First, beams with a width of 150 mm, a height of 200 mm and a length of 1100 mm were drawn with Auto-Cad software, then ANSYS Workbench software was used in usable format. 2Φ8 longitudinal reinforcement is placed in the compression zone of all beams. The transverse reinforcement is adjusted to be 8Φ8/150 mm in each beam. In the research, a total of 6 beams were modeled and analyzed by using three different GPC and OPC beams matched with each other. The transverse reinforcements are sized so that the cover is 25 mm. The cross-section and reinforcement information of the modeled reinforced concrete samples are given in Table 1, and the longitudinal and transverse reinforcements placement are given in Figure 1.

According to the previous experimental study results for the concrete block, mechanical definitions were made in ANSYS. SOLID65-3D element is used while defining the concrete in ANSYS Workbench finite element model. SOLID65 is widely used for 3D concrete modeling of reinforced solids. The special cracking and crushing abilities of reinforced concrete elements, resembling a 3D structural solid, are very well represented by SOLD65. Thanks to this element, nonlinear material properties are defined and processed quite successfully. It can crack (in three vertical directions), crush, cause plastic deformation and creep into concrete. SOLD65 geopolymer is suitable for simulating the cracking behavior of concrete in the tensile zones (bottom) as well as the nonlinear performance of the concrete material in three orthogonal directions, such as crushing in the compression zones (top) by processing [32]. Rebar has to ability to tensile and compress but not cut. The LINK 180 element type used for modeling vertical and horizontal steel bars from the ANSYS 21.2 element library facilitates linear and nonlinear deformation in its

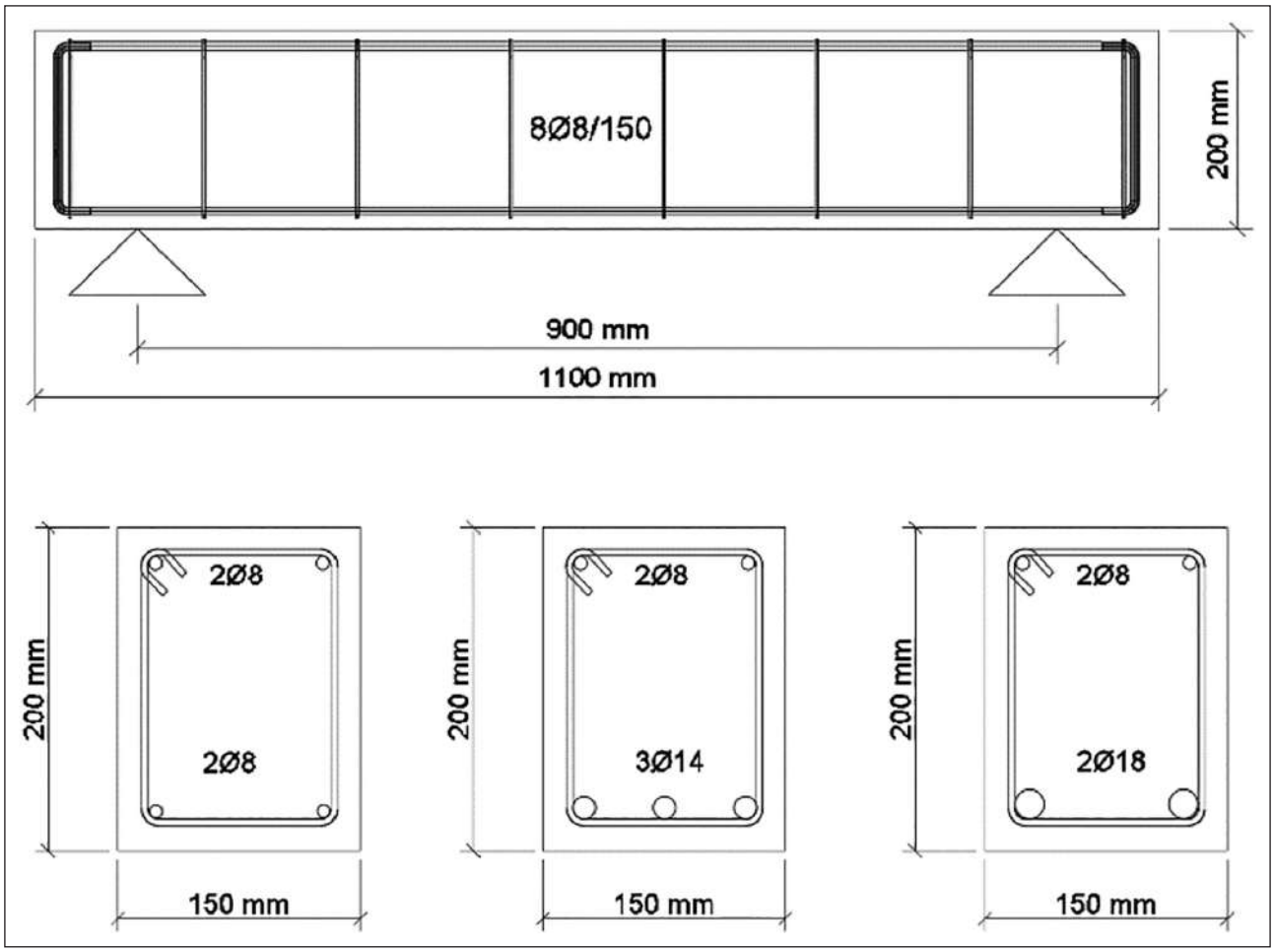

Figure 1. Beam sections and reinforcement placement.

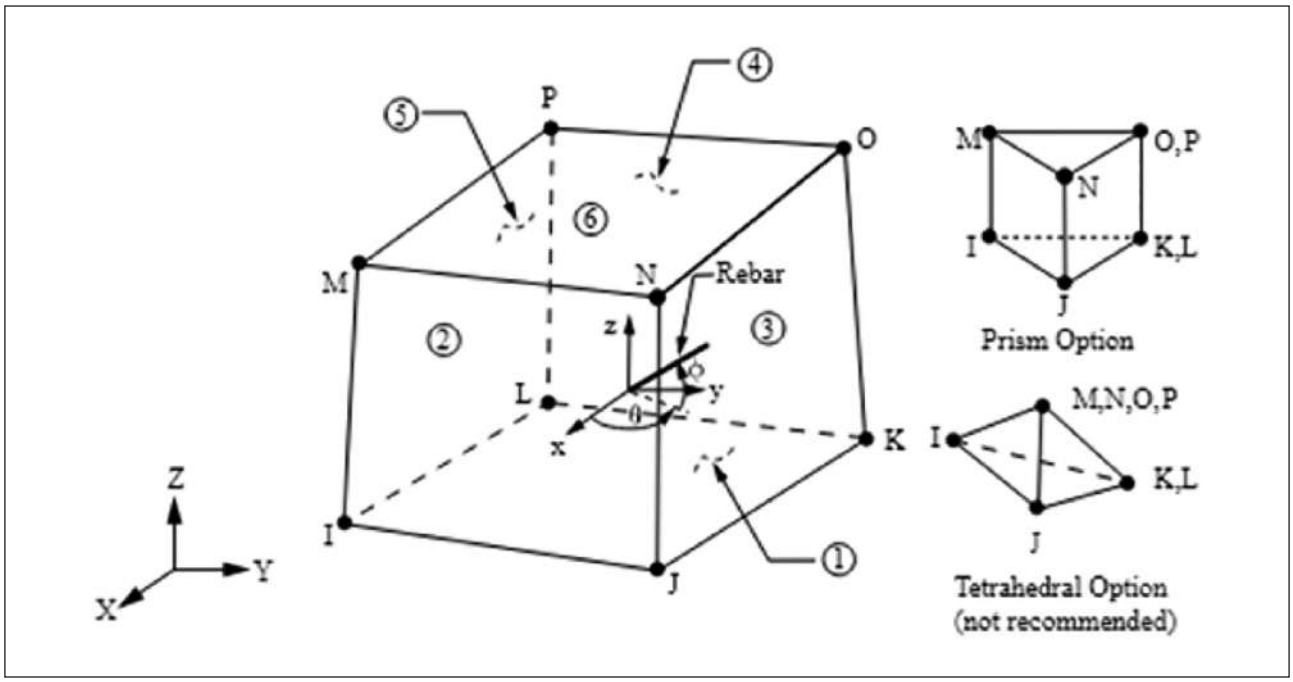

Figure 2. SOLID65 geometry.

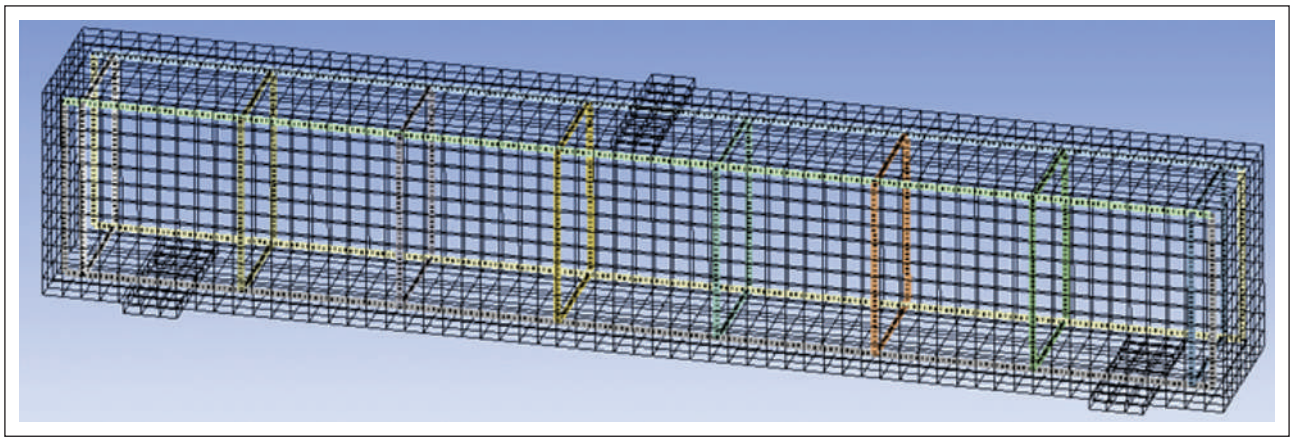

Figure 3. Reinforced Concrete Beam finite element mesh model.

Table 2. Reinforcement properties in axial tension

Rebar diameter (mm)	f_y (MPa)	f_u (MPa)	Elongation (%)	f_u/f_y
8	424	541	37.5	1.27
14	453	572	32.8	1.26
18	456	564	24.4	1.24

f_y: Yield strength; f_u: Tensile strength.

Table 3. Analytically results of flexural and shear load

Sample code	Longitudinal reinforcement	Beam flexural load capacity (kN)	Beam shear load capacity (kN)
(GPC-OPC) 1	2Φ8	27.35	119.5
(GPC-OPC) 2	3Φ14	106.3	119.5
(GPC-OPC) 3	2Φ18	114.3	119.5

plane. The described solid model can crack in tension and crush in compression. Each element of the SOLD65 that defines the concrete is represented by eight nodes with three degrees of freedom at each node: the nodes express the translations in the x, y, and z directions. The geometry, node positions and coordinate system for this element are shown in Figure 2 in SOLID65 geometry [33].

Inserted into the geometry defined as SOLID 65, With the commands, the mechanical properties previously determined by the experimental method were defined separately for GPC.

MPTEMP,,,,,,,
MPTEMP,1.0
MPDATA,EX,solid65_matid ,,16972
MPDATA,PRXY,solid65_matid ,,0.24
and for OPC
MPDATA,EX,solid65_matid ,,25256
MPDATA,PRXY,solid65_matid ,,0.2

The concrete body of the OPC beam is meshed with 18 mm and the reinforcements with 5 mm. It consists of a total of 12,252 nodes and 8681 elements. The transparent view of the finite element mesh model of the concrete body, reinforcement and support elements is shown in Figure 3.

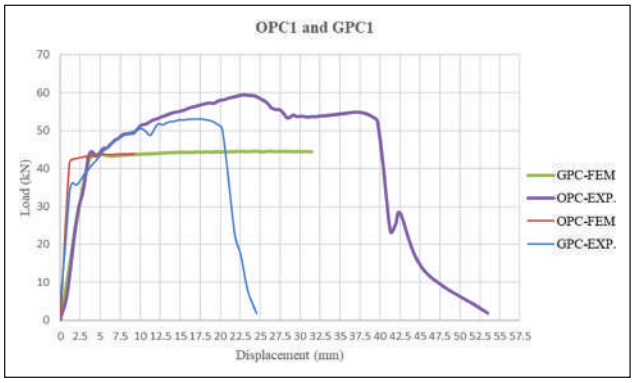

Figure 4. Stress-strain curves (OPC and GPC 8 mm).

The mechanical properties of steel reinforcement bars were determined due to the tensile test in the Kayseri University Tomarza Vocational School Construction laboratory. Then, definitions were made in ANSYS according to the results obtained. Values such as yield strength, tensile strength and elongation at break of longitudinal and transverse steel reinforcements defined while modeling in ANSYS Workbench are as in Table 2.

3. RESULTS AND DISCUSSION

In the beams used in the experimental study, flexural and shear behavior were investigated for three different longitudinal reinforcement ratios. In the analytical calculations, the shear bearing capacity of all beams is higher than the flexural bearing capacity. However, in beams 2 and 3, shear and flexural strengths are very close. Therefore, the expected failure of the beams is flexural in the first beam and flexural and shearing in the second and third beams, in the form of oblique shear failure. With

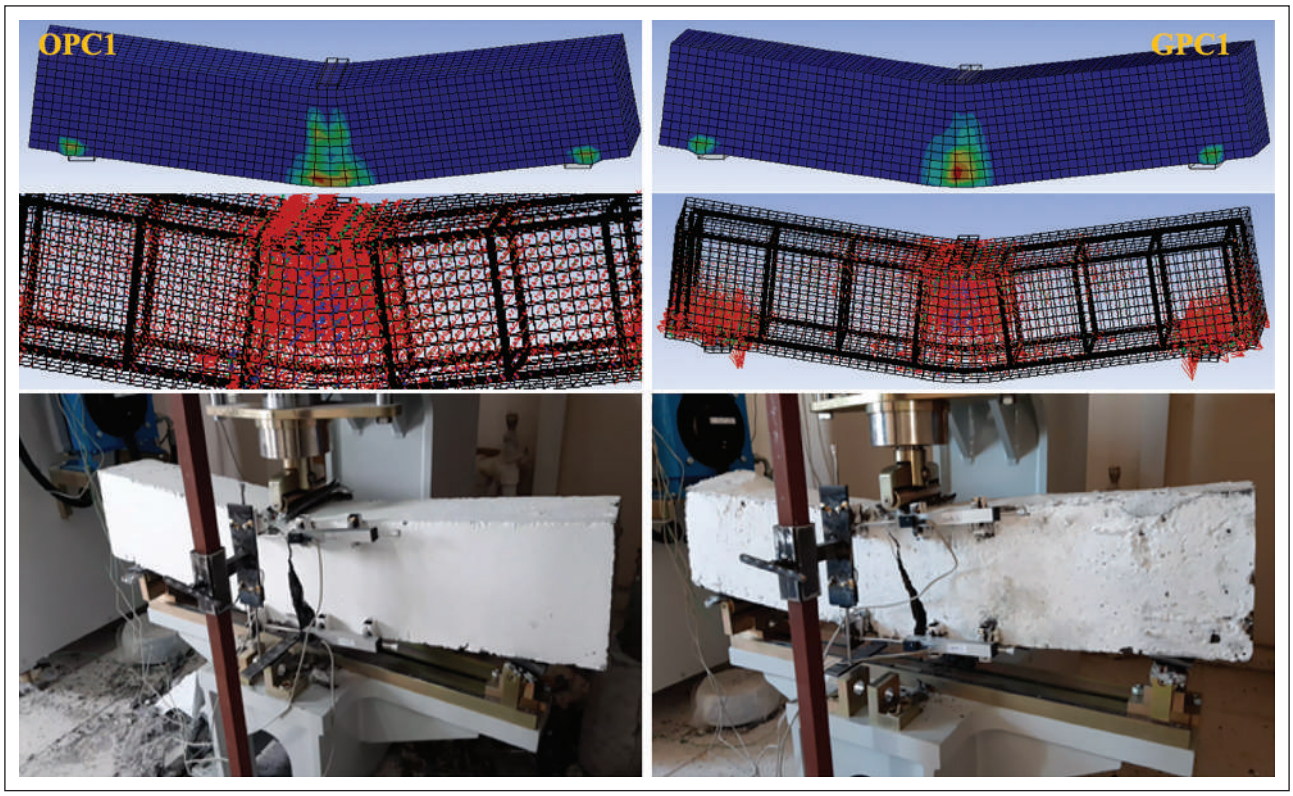

Figure 5. OPC and GPC beam flexural behavior (8 mm).

this aspect, both shear and shear behavior can be considered in the article. As stated in the title of the manuscript, the study aims to determine the shear and flexural behavior of geopolymer beams. In case the concrete strength is 30 MPa, analytically calculated flexural and shear load capacities are given in Table 3.

As a result, the flexural strength of all beams is lower than the shear strength. However, for the two samples, due to the flexural and shear strengths being close, the fractures occurred in a way that included both behavioral effects.

3.1. Material Test Results

According to the experimental study, the beams modeled with ANSYS Workbench were loaded with 50 mm displacement from a single point in the middle and analyses were carried out. Stress-strain curve, crack states and load-deflection graphs obtained as a result of simulations are presented in this section and comments are made on them.

3.2. Findings from Beams

The load-displacement graphs of OPC and GPC beams with 2Φ8 mm compression and tension reinforcement, which were analyzed numerically, are shown in Figure 4 compared to the previous experimental results. In the analysis made with the FEM model, the yield region is approximately the same as in the experimental model. There may be significant differences between the experimental study

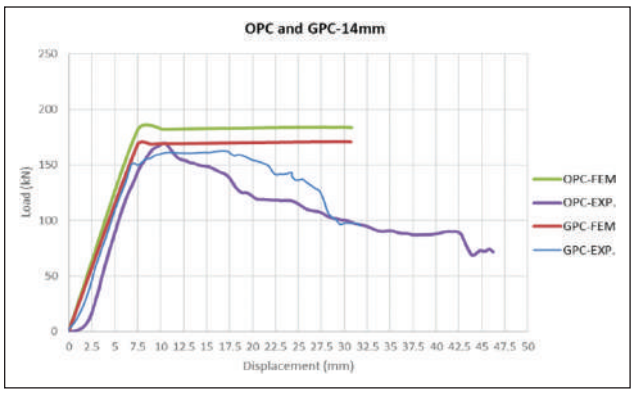

Figure 6. Stress strain curves (OPC and GPC 14 mm).

results and the FEM model. But it is an important result to reveal the yield strength limit, which is the end of the elastic behavior and the starting point of the plastic behavior, in the stress-strain curve. Although the graphical results obtained within the scope of this study do not match exactly with the experimental results, the yield strength points are approximated. With the development of the ANSYS finite element method, it will be possible to obtain results close to the experimental model over time.

The analysis images using the simply supported OPC and GPC FEM model under vertical load are shown in Figure 4. The final load for both OPC and GPC in the FEM model was 45 MPa, while in the experimental mod-

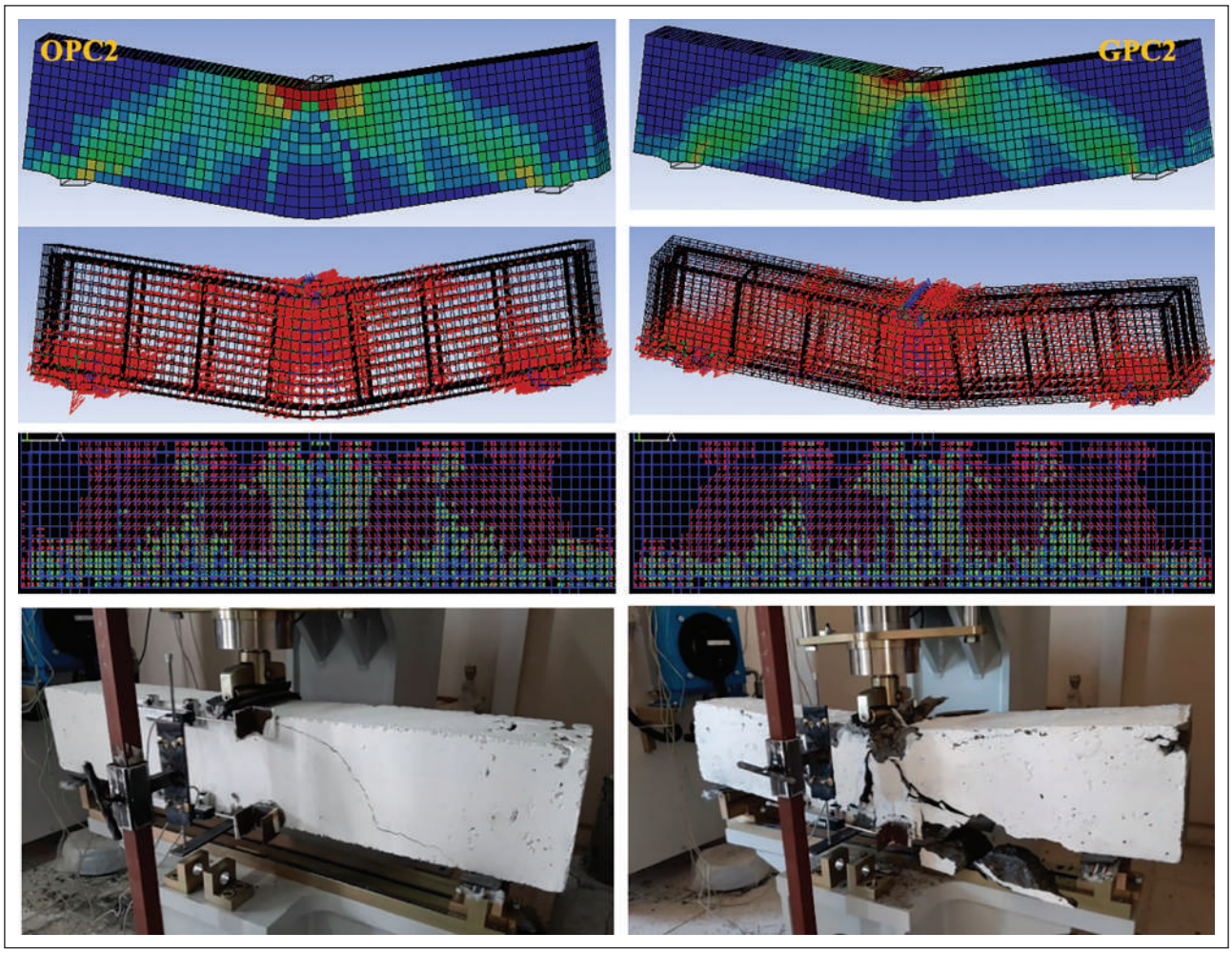

Figure 7. Stress strain states (OPC and GPC 14 mm).

el, the OPC was 55 MPa and the GPC 60 MPa. While the first crack started at 1 mm in the OPC-FEM model, the GPC-FEM model showed a more elastic behavior, and the first crack started after 3.5 mm displacement. In the experimental model, the opposite is the case; crack formation started after 1 mm displacement in GPC, whereas crack formation started after 3.5 mm in OPC. When the yield boundary states are observed in FEM and experimentally, progressively increasing cracks in the middle reveal the flexural behavior. Flexural cracks started in the lower part of the beam and gradually increased due to the increasing tensile load. The red-colored regions in Figure 5 clearly show the stress states and cracks pattern. The stress, strain and flexural cracks occurring in the middle of the beam are similar for GPC and OPC and prove the experimental images at the bottom.

It can be said that the graph in Figure 6 shows that the FEM and experimental results of beams with 2Φ8 compression and 3Φ14 tension reinforcement are more compatible. The FEM results were slightly above expectations for both OPC and GPC. The ultimate load states

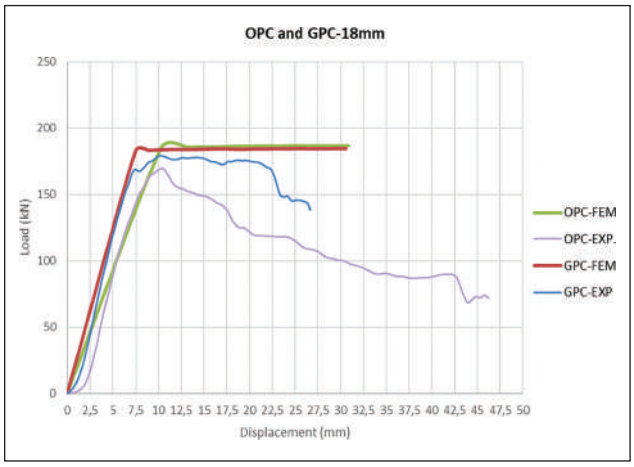

Figure 8. Stress-strain curves (OPC and GPC 18 mm).

are between 160 MPa and 180 MPa, although the maximum strengths of OPCs are slightly higher. After 7.5 mm, crack formation continued to increase. In their study, Venkatachalam et al. [32] stated that crack formation in-

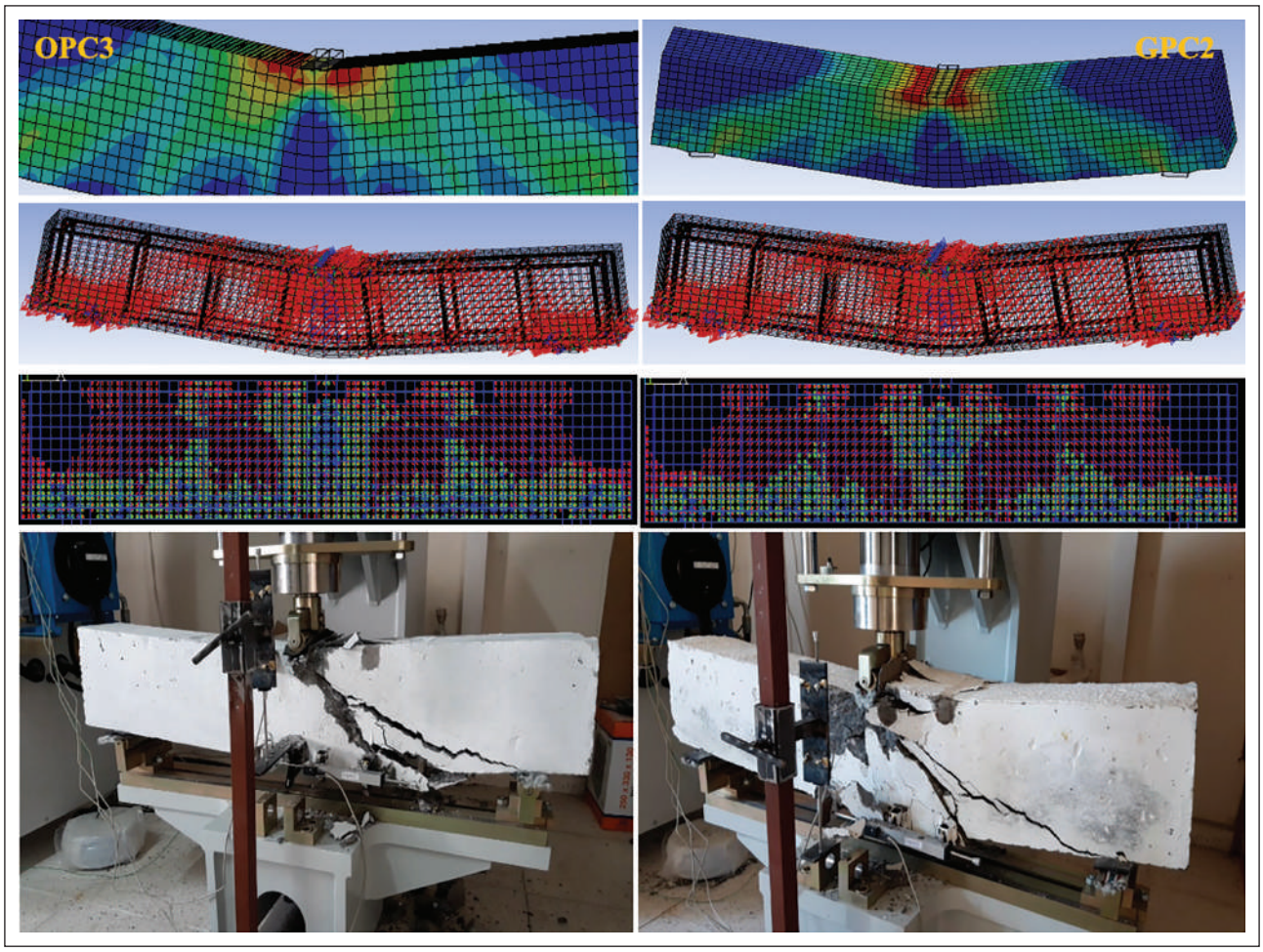

Figure 9. Stress-strain states (OPC and GPC 18 mm).

creased after 7.5 mm in the test of 1500 mm long beam with 8 mm shear and 10 mm flexural reinforcement. But, they stated that excessive flexural stress and cracks occur in the middle region of the beam [21].

It is seen that the flexural performances of OPC and GPC beams with 3Φ14 mm reinforcement in the tension region are excellent (Fig. 7). Especially in the FEM model, crack formations can be seen very well; OPC and GPC also show similarities. Cracks mainly formed towards the support points in the shear region, which confirms the experimental images.

Maximum strength in beams with 2Φ18 compression and 2Φ18 tension reinforcement is in the range of 175–185 MPa. Although the values are very close to each other, it seems that they did not exceed the strengths of the previous 3Φ14 reinforced beams. According to the FEM and experimental curve in Figure 8, the linear behavior of the beams appears to be coincident. On the other hand, while the plastic deformation of GPCs started at 7.5 mm, it was seen that OPCs started after 10 mm.

In Figure 9, crack formation is observed in accordance with the experimental result with the FEM model. The cracks formed are mostly in the shear region. While excessive stress is seen around the force application point in the compression region, less stress is seen in the tensile region. With the increase in longitudinal reinforcement, the flexural strength of both OPCs and GPCs increases, while crack formation in the shear region shows similarities.

When the load-displacement graphs and the mobility of concrete and reinforcement are observed. It can be said that the yield in the steel reinforcement and the crack development in the beams are simultaneous. However, it can be said that crack development in GPCBs starts a little earlier than in steel reinforcement. Figure 10 shows the stress and plastic deformation of the tensile and compressive reinforcement of the reinforcements in the GPC beams. Tensile and compressive reinforcements are equal in Figure 10a. In the beam, which is designed as 2Φ8, stresses also occur in the pressure bars. It is observed that the tensile reinforcement of the beam is designed as Figure 10b. 3Φ14 works well, and the compressive reinforcement has less stress. It is observed in Figure 10c. 2Φ18 that the tension reinforcement works well and the compressive reinforcement remains more rigid.

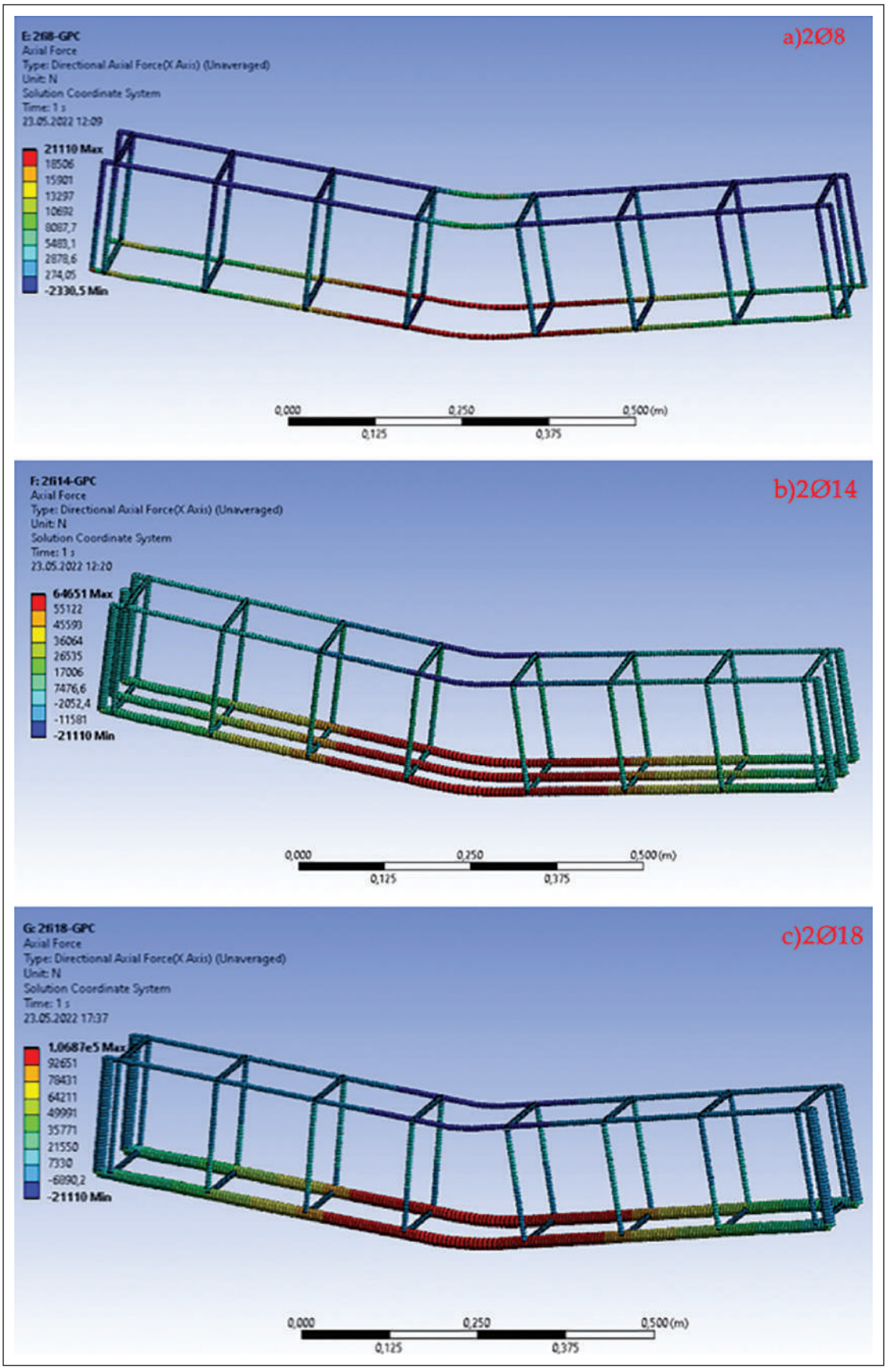

Figure 10. Elastic and Plastic behaviour of steel reinforcement.

4. CONCLUSION

As a result of GPC beam analysis via ANSYS Workbench, it gave similar values to the analysis of OPC beams. The results yielded from the numerical study are consistent with the previous experimental study results, showing that the investigation is reliable. The significant findings and results obtained as a result of the study are as follows. This study yielded results consistent with other studies in the literature.

- In the beams with 2Φ8 compression and tensile reinforcement, flexural cracks were formed mostly in the middle region up to the bottom of the beam. In the FEM model, the final load for both OPC and GPC beams was very close, while the last load derived from the experimental results of OPCBs was higher than the GPCBs with 0.9%. While the first crack started at 1 mm in the OPCB-FEM model, the GPCB-FEM model showed a more elastic behavior, and the first crack started after 3.5 mm displacement. In the experimental model, the opposite is the case; crack formation started after 1 mm displacement in GPCB, whereas crack formation started after 3.5 mm in OPCB.
- The load-displacement results for 2Φ8 compression and 3Φ14 tensile reinforced beams contain closer results in FEM and experimental. The ultimate load difference between the two beams is approximately 12%, but the maximum strengths of OPCBs are slightly higher. After 7.5 mm, crack formation continued to increase.
- The maximum strength difference in beams with 2Φ8 pressure and 2Φ18 reinforcement is around 0.57%. Although the values are very close to each other, it seems that they did not exceed the strengths of the previous 3Φ14 reinforced beams. On the other hand, it is seen that the plastic deformation of GPCBs starts from 7.5 mm, while OPCBs start after 10 mm. Observing the load-displacement graphs and the mobility of concrete and reinforcement, it can be said that the yield in the steel reinforcement and the crack development in the beams are simultaneous, and the crack development in GPCs starts a little earlier than the yield of the steel reinforcement.
- Since the mechanical behavior of GPCBs shows similar behavior to OPCBs. This study, which will be an essential reference in terms of supporting experimental studies and conducting theoretical studies quickly, that GPCBs analysis can be easily done with the FEM model.
- Finally, simulations of Geopolymer concrete beams were made up to the moment of fracture and it was tried to contribute to the understanding of the behavior of this environmentally friendly concrete under flexural.

DATA AVAILABILITY STATEMENT

The authors confirm that the data that supports the findings of this study are available within the article. Raw data that support the finding of this study are available from the corresponding author, upon reasonable request.

CONFLICT OF INTEREST

The authors declare that they have no conflict of interest.

FINANCIAL DISCLOSURE

This research was financially supported by the FKB-2020-1013 Scientific Research Project of Kayseri University.

PEER-REVIEW

Externally peer-reviewed.

REFERENCES

[1] Pham, D. Q., Nguyen, T. N., Le, S. T., Pham, T. T., & Ngo, T. D. (2021). The structural behaviours of steel reinforced geopolymer concrete beams: An experimental and numerical investigation. *In Structures* (Vol. 33, pp. 567–580). Elsevier. [CrossRef]

[2] Hutagi, A., & Khadiranaikar, R. B. (2016). Flexural behavior of reinforced geopolymer concrete beams. In 2016 International Conference on Electrical, *Electronics, and Optimization Techniques (ICEEOT)* (pp. 3463-3467). [CrossRef]

[3] Kumar, P. U., & Kumar, B. S. C. (2016). Flexural behaviour of reinforced geopolymer concrete beams with GGBS and metakaoline. *International Journal of Civil Engineering and Technology*, 7(6), 260–277.

[4] Nguyen, K. T., Ahn, N., Le, T. A., & Lee, K. (2016). Theoretical and experimental study on mechanical properties and flexural strength of fly ash-geopolymer concrete. *Construction and Building Materials*, 106, 65–77. [CrossRef]

[5] Amiri, A. M., Olfati, A., Najjar, S., Beiranvand, P., & Fard, M. N. (2016). The effect of fly ash on flexural capacity concrete beams. *Advances in Science and Technology Research Journal*, 10(30), 89–95. [CrossRef]

[6] Uma, K., Anuradha, R., & Venkatasubramani, R. (2012). Experimental investigation and analytical modeling of reinforced geopolymer concrete beam. *International Journal of Civil and Structural Engineering*, 2(3), 808. [CrossRef]

[7] Yost, J. R., Radlińska, A., Ernst, S., & Salera, M. (2013). Structural behavior of alkali activated fly ash concrete. Part 1: Mixture design, material properties and sample fabrication. *Materials and Structures*, 46(3), 435–447. [CrossRef]

[8] Yacob, N. S., ElGawady, M. A., Sneed, L. H., & Said, A. (2019). Shear strength of fly ash-based geopolymer reinforced concrete beams. *Engineering Structures*, 196, 109298. [CrossRef]

[9] Visintin, P., Ali, M. M., Albitar, M., & Lucas, W. (2017). Shear behaviour of geopolymer concrete beams without stirrups. *Construction and Building Materials*, 148, 10–21. [CrossRef]

[10] Mourougane, R., Puttappa, C. G., Sashidhar, C., & Muthu, K. U. (2012). Shear behavior of high strength GPC/TVC beams. Proceedings of International Conference on Advances in Architecture and Civil Engineering (AARCV 2012), 21st – 23rd June 2012, 21. 142.

[11] ACI Committee. (2002). *Building code requirements for structural concrete:(ACI 318-02) and commentary (ACI 318R-02)*. American Concrete Institute.

[12] Chang, E. H. (2009). Shear and bond behaviour of reinforced fly ash-based geopolymer concrete beams [Doctoral dissertation]. Curtin University.

[13] *Australian Standard* AJCS (2004). Australian Standard. AJCS Standards Australia.

[14] Ng, T. S., Amin, A., & Foster, S. J. (2013). The behaviour of steel-fibre-reinforced geopolymer concrete beams in shear. *Magazine of Concrete Research*, 65(5), 308–318. [CrossRef]

[15] Alfaiate, J., Pires, E. B., & Martins, J. A. C. (1997). A finite element analysis of non-prescribed crack propagation in concrete. *Computers & Structures*, 63(1), 17–26. [CrossRef]

[16] Mukherjee, D. (August 6, 2009). Impact of celebrity endorsements on brand image. https://papers.ssrn.com/sol3/papers.cfm?abstract_id=1444814

[17] Reitherman, R. (2008). The EERI oral history program. In Proceedings of the *14th World Conference on Earthquake Engineering* (pp. 12–17). [CrossRef]

[18] Halahla, A. (2018). Study the behavior of reinforced concrete beam using finite element analysis. In *Proceedings of the 3rd World Congress on Civil, Structural, and Environmental Engineering (April 2018)*. (Vol. 10). [CrossRef]

[19] Rajhgopal, A., Saranya, P., Nagarajan, P., & Shashikala, A. (2021). Performance evaluation of geopolymer concrete beam-column joints using finite element methods. In Singh, R. M., Sudheer, K. P., & Kurian, B. (Eds.). *Advances in Civil Engineering*. (pp. 677-690). Springer.

[20] Aksoylu, C., Yazman, Ş., Ozkilic, Y. O., Gemi, L., & Arslan, M. H. (2020). Experimental analysis of reinforced concrete shear deficient beams with circular web openings strengthened by CFRP composite. *Composite Structures*, 249, Article 112561. [CrossRef]

[21] Ozkilic, Y. O., Yazman, Ş., Aksoylu, C., Arslan, M. H., & Gemi, L. 2021. Numerical investigation of the parameters influencing the behavior of dapped end prefabricated concrete purlins with and without CFRP strengthening. *Construction and Building Materials*, 275, Article 122173. [CrossRef]

[22] Aksoylu, C., Ozkilic, Y. O., & Arslan, M. H. (2020). Damages on prefabricated concrete dapped-end purlins due to snow loads and a novel reinforcement detail. *Engineering Structures*, 225, Article 111225. [CrossRef]

[23] Gemi, L., Madenci, E., & Ozkilic, Y. O. (2021). Experimental, analytical and numerical investigation of pultruded GFRP composite beams infilled with hybrid FRP reinforced concrete. *Engineering Structures*, 244, Article 112790. [CrossRef]

[24] Gemi, L., Madenci, E., & Ozkilic, Y. O. (2020). Investigation of flexural performance of steel, glass FRP and hybrid reinforced concrete beams. *Duzce Universitesi Bilim ve Teknoloji Dergisi*, 8(2), 1470–1483. [CrossRef]

[25] Ozkilic, Y. O., Aksoylu, C., Yazman, S., Gemi, L., Arslan, M. H. (2022). Behavior of CFRP-strengthened RC beams with circular web openings in shear zones: Numerical study. Structures 2022. [Epub ahead of print].

[26] Gemi, L., Alsdudi, M., Aksoylu, C., Yazman, S., Ozkilic, Y. O., Arslan, M. H. (2022). Optimum amount of CFRP for strengthening shear deficient reinforced concrete beams. *Steel and Composite Structures*. 2022. [Epub ahead of print].

[27] Ozkilic, Y. O., Aksoylu, C., & Arslan, M. H. (2021). Numerical evaluation of effects of shear span, stirrup spacing and angle of stirrup on reinforced concrete beam behaviour. *Structural Engineering and Mechanics, An International Journal*, 79(3), 309–326.

[28] Ozkilic, Y. O., Aksoylu, C., & Arslan, M. H. (2021). Experimental and numerical investigations of steel fiber reinforced concrete dapped-end purlins. *Journal of Building Engineering*, 36, 102–119. [CrossRef]

[29] Aksoylu, C., Ozkilic, Y. O., Yazman, S., Gemi, L., & Arslan, M. H. (2021). Experimental and numerical investigation of load bearing capacity of thinned end precast purlin beams and solution proposals. *Technical Journal of Turkish Chamber of Civil Engineers*, 32(3), 10823–10858.

[30] Arslan, M. H., Yazman, Ş., Hamad, A. A., Aksoylu, C., Ozkilic, Y. O., & Gemi, L. (2022). Shear strengthening of reinforced concrete T-beams with anchored and non-anchored CFRP fabrics. *Structures*, 39, 527–542. [CrossRef]

[31] Mo, K. H., Alengaram, U. J., & Jumaat, M. Z. (2016). Structural performance of reinforced geopolymer concrete members: A review. *Construction and Building Materials*, 120, 251–264. [CrossRef]

[32] Venkatachalam, S., Vishnuvardhan, K., Amarapathi, G. D., Mahesh, S. R., & Deepasri, M. (2021). Experimental and finite element modelling of reinforced geopolymer concrete beam. *Materials Today: Proceedings*, 45, 6500–6506. [CrossRef]

[33] SOLID65 Element Description. (2022). https://www.mm.bme.hu/~gyebro/files/ans_help_v182/ans_elem/Hlp_E_SOLID65.html

Journal of Sustainable Construction Materials and Technologies
Web page info: https://jscmt.yildiz.edu.tr
DOI: 10.47481/jscmt.1117101

JSCMT
Journal of Sustainable Construction Materials and Technologies

Research Article

Numerical investigation of precast reinforced concrete beam–to–column joints by replaceable damper

Yalda DEHQAN NEZHAD[1], Sepanta NAİMİ[2*]

[1]*Department of Civil Engineering, İstanbul Aydın University Faculty of Engineering, İstanbul, Türkiye*
[2]*Department of Civil Engineering, Altınbaş University Faculty of Engineering and Arcitecture, İstanbul, Türkiye*

ARTICLE INFO

Article history
Received: 15 May 2022
Accepted: 02 June 2022

Key words:
Beam–to–column steel joint, finite element method, numerical simulation, precast concrete, replaceable damper

ABSTRACT

This study aimed to investigate the precast reinforced concrete beam-to-column joints behaviors through the replaceable damper under cyclic loading. The precast concrete specimens have been embedded with steel reinforcement and specially shaped connectors. After the application of the replaceable damper under cyclic loading, the energy dissipation shaped very well and increased the bearing capacity of precast specimens. The precast concrete beam–to–column joints were designed and analyzed to compare with the traditional reinforced concrete (RC) specimen. The analysis result of the loading based on the controlled displacement method showed that the precast specimen model with a damper has more hysterical behavior than the traditional RC frame. Also, the specimen (PS-1) is passed the 2.7% chord rotation, which showed higher performance, than the traditional RC specimen. The efficiency of the PS-1 specimen with a special connection has been elaborated with the finite element method (FEM) and simulated by ABAQUS software.

Cite this article as: Dehqan Nezhad, Y., Naimi, S. (2022). Numerical investigation of precast reinforced concrete beam–to–column joints by replaceable damper. *J Sustain Const Mater Technol*, 7(2), 81–87.

1. INTRODUCTION

The construction method of the precast specimens has increased widely by replacing them with the cast–in–sit reinforced concrete. Because of these significant advantages, which are the high quality of the specimen and making at the factories under traditional methods, with low cost. Also precast reinforced specimens could work even in the incompatible climate condition, and it has taken a little time for building, fewer workers need and has easily assembling possibility on-sit [1, 2]. Accordingly, the selection of the right technical method is very important for this aim. For the designer that's very important to receive a resolution, which receives the specimen to required performance in situations of the load-bearing capacity, and ductility [3]. Using the damper could increase the energy dissipation capacity [4]. The two different types of beams–to–column joints were presented with Precast Seismic constructions methods [5]. In this study analysis has done by applying cyclic loading on the concrete beam and column joints, which column was reinforced by (I) steel, the failure was reined by the good performance of the beam,

***Corresponding author.**
*E-mail address: sepanta.naimi@altinbas.edu.tr

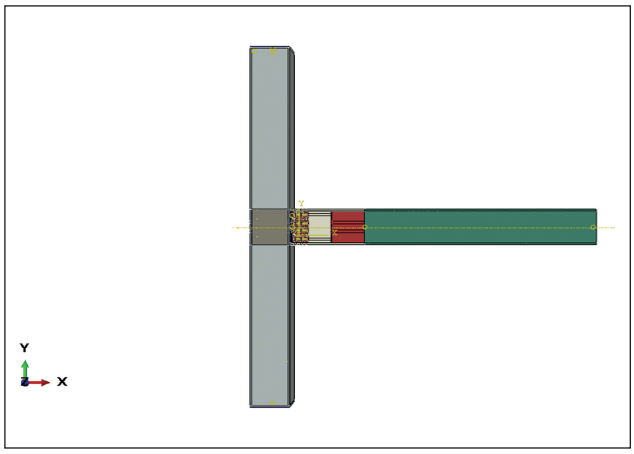

Figure 1. The type of connection between beam and column.

also, the connection valency relates to the shear valency of the beam [6]. The experimental test showed the negligible residual displacement at joints of beam–to–column, that is effect of pre-stressing force presented by steel strands. Hence the new type of beam–to–column joint expanded [7, 8]. On the other hand, the economic situation for transportation is also one of the most substantial parameters in the constructions industry, so using precast concrete may be use for subway construction [9]. The damper with friction presented for energy dissipation, which joints are showed a good self–centering capacity. For improving the energy dissipation capacity and loading capacity of self–centering capacity of beam–to–column joint was applied the replaceable mild steel bars [10]. This investigation had been used two structures to investigate the reinforcement's costs and the materials were utilized in this test. by using the nonlinear method and Sta4Cad achieved that building was reinforced by shear wall and had been shown better performance than the jacketed one [11]. The bamboo–shaped energy dissipater was used to present the energy dissipation capacity of the precast specimens, that showed the good performance [12]. Many experiments conducted, which are illustrated excellent behavior in the self–centering capacity and without strength degradation. Most of the time welded steel plates are used in the precast components because the steel plate joints commonly are useful for the integration of precast concrete structures. More experiments are shown excellent behavior in the self–centering capacity and without strength degradation. Most of the precast components were used the welded steels, because of that the steel joints commonly are useful to the integration of precast concrete structures [13]. As well as investigated the self–centering joints by using friction dampers and it has presented them in the experimental research [14]. Using four different precast sample connections with rigid, pinned, semi-rigid and new type connection to test strength, ductility and stiffness, the new connection type performed well as a semi-rigid joint [15].

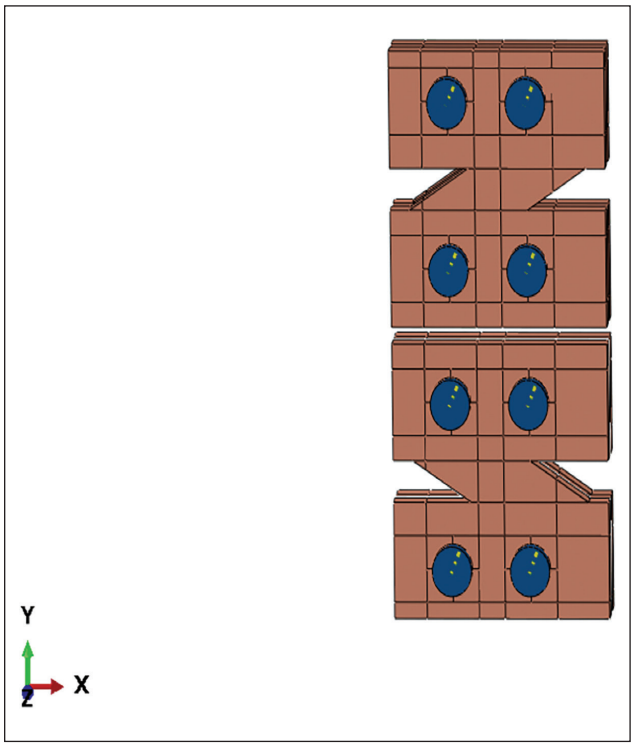

Figure 2. The damper shape.

This paper has investigated the behavior of Precast Concrete beam–to–column steel joints by using the replaceable damper under cyclic loading procedure. The main efficiency of this simulation is comparing to the monolithic model. The easy construction, the stiffness amount, the plastic hinge, increasing the energy dissipation of them, the ductility, energy dissipation factor, and strength of the specimen have been tested.

2. PROPOSED CONNECTION PARTS OF THE BEAM–TO–COLUMN

The type of connection parts of the beam–to–column joint simulation is illustrated in Figure 1. The special-shaped replaceable dampers are designed for energy dissipation capacity, which is shown in Figure 2. The special-shaped beam connector applied for connecting the beam to the column and utilized the special-shaped column connector part, which are shown in Figure 3. They are fastened together by bolts. The reinforcement bars, stirrups employed for resisting concrete, and the steel gusset plates are used for resisting the column. The two special designed plates are used for covering the concrete inside of cavity of the special shaped beam connector, which is shown in Figure 4. The cross-section areas of the precast beam–to–column joint and RC frame are illustrated in Figure 5. The gusset plates are used to avoid from the damage in column. All the parts dimensions are shown in Table 1.

Table 1. Parts dimension

Parts	Thickness (mm)	Height (mm)	Width (mm)	Length (mm)	Diameter (mm)	Web (mm)	Flange (mm)	Depth (mm)
Gusset	15	400	400	–	–	–	–	–
Covering plate	10	360	340	–	–	–	–	–
Bolts	–	–	–	–	21	–	–	–
Special B connector	–	–	250	750	–	12	20	400
Damper	15	165	165	–	–	–	–	–
Beam	–	400	250	3110	–	–	–	–
Column	–	400	400	4000	–	–	–	–

Table 2. Material properties

Material	Grade	Diameter Thickness (mm)	Yield strength (MPa)	Ultimate strength (MPa)
Reinforcement	HRB400	Ø8	407	644
	HRB400	Ø14	487	610
	HRB400	Ø16	436	634
Steel	Q345B	20	381	545
	Q235B	15	277	437
B concrete	–	–	–	40
C concrete	–	–	–	53

The moment expending along of the beam spend and the bending moment of the beam next to the steel joints, M_{C1}, and H steel at the free end M_{C2} [16].

$$M_{C1} \leq M_{CU1}$$

$$M_{C2} \leq M_{CU2}$$

The bending moment of concrete is shown by Mcu1 next to steel joints, and the bending moment of the concrete next to the H steel is shown by M_{cu2} [16].

The bending moment of the proposed steel connection joint equation could be obtained with:

$$x = \frac{\frac{L1}{2}+L2+L3}{L2+L2} \text{Mc1}$$

$$x = \frac{\frac{L1}{2}+L2+L3}{L2+L3} \text{Mc2}$$

Where L is the beam length, L1 is the connection steel joints length, L2 is the H steel length, and L3 is the concrete length without reinforcement and H steel [16].

The ultimate bending moment of the steel joint can receive by:

$$\text{Mpu} \leq \min\left(\frac{\frac{L1}{2}+L2+L3}{L2+L3}\text{Mcu1}, \frac{\frac{L1}{2}+L2+L3}{L2+L3}\text{Mcu2}\right)$$

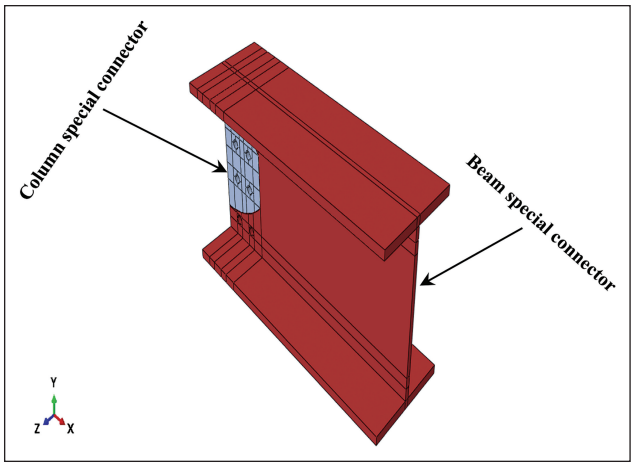

Figure 3. The beam and column special shaped connectors.

The dampers presented the bending moment of the steel joints after that, the ultimate bending moment in the damper's agreement with equation (5). In the tension and compression, the EDS of the dampers could be presented the bending moment capacity of the dampers [16].

$$2\sum_{i=1}^{3} \text{Ai Di fi} \leq \min\left(\frac{\frac{L1}{2}+L2+L3}{L2+L3}\text{Mcu1}, \frac{\frac{L1}{2}+L2+L3}{L2+L3}\text{Mcu2}\right)$$

Ai (i=1, 2, 3) is the DES area, Di (i=1, 2, 3) is the length between the DES, fi (i=1, 2, 3) is the stress at the EDS.

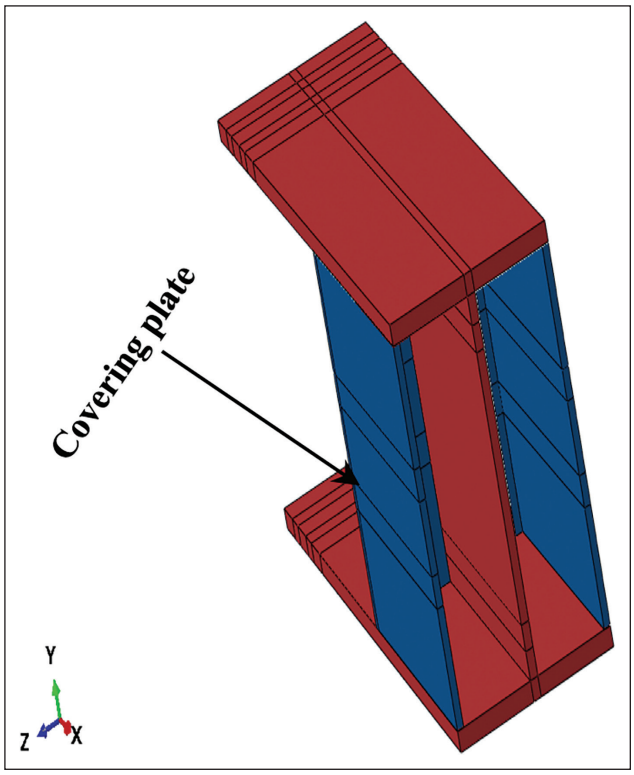

Figure 4. The special designed covering plates.

3. TEST STEP

The precast column boundary condition is located on the top and down by hinge support, and a 611 KN axial load is applied on the top of the column, which was equal to the 20% of the column bearing capacity. The displacement at top of the column could be controlled by using the supported beam at the top of the column, and this supported beam is fixed by the reaction wall. The jack and anchorage parts is applied on the top of the column since the beam could be raised in the location. A 50 Ton actuator had been bounded in the strong floor to exert the cyclic loading at end surface of the beam.

4. MATERIAL PROPERTIES

The HRB400 steel used for reinforcement, and the Q345B, and Q235B was utilized for all steel parts and damper. The all-steels tension behavior tested [17]. The compressive strength of the concrete for the beam and the compressive strength of concrete for the column were tested [18]. All the materials were given in Table 2.

5. TEST PROCEDURE

A new precast beam–to–column joint was designed based on Geng et al. 2020 experimental models [19]. Also, the precast specimen compared with RC frame. The Z damper is applied in the PS-1 specimen, that is replaceable, and the concrete damages could be very slight. So, the damper could change after applying cyclic load. The same analysis can be done to obtain the characteristic of PS-1 joints as well. In this analysis the displacement-controlled loading has been used in every cyclic loading at this simulation. This procedure was repeated three times under displacement levels. The 5% drift amplitudes is shown in Figure 3. ±0.25%, ±0.5%, ±0.75%, ±1%, ±1.5%, ±2%, ±2.5%±0.3%, ±0.4%, and 0.5% respectively [20, 21].

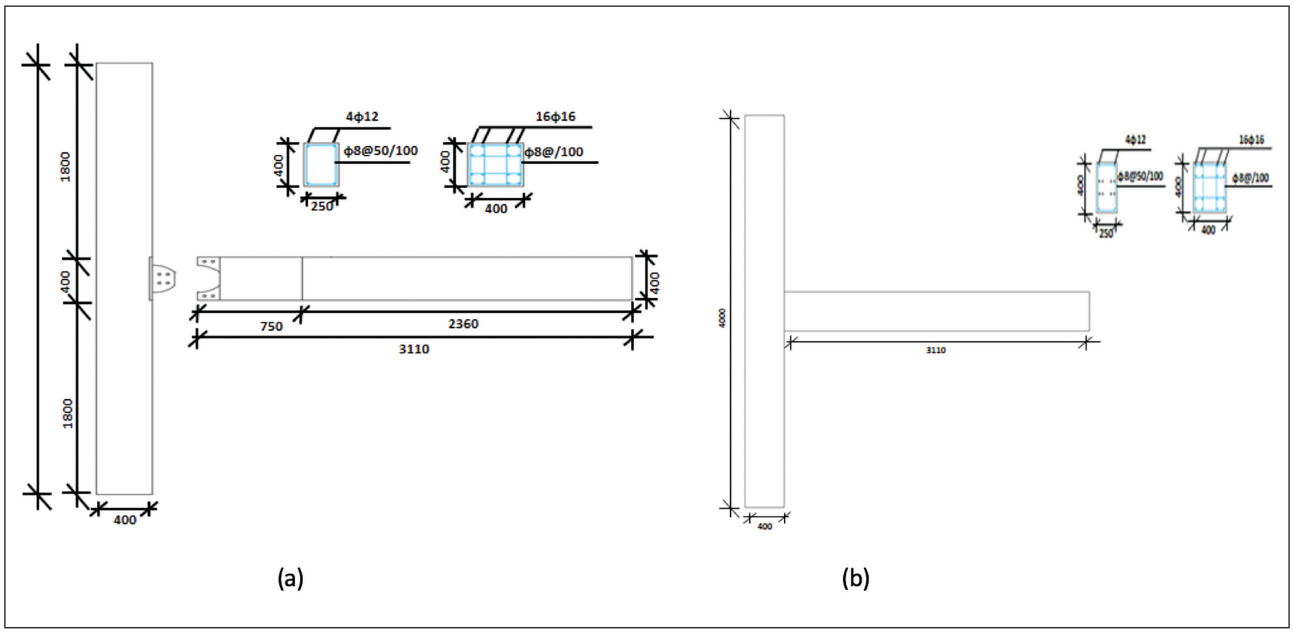

Figure 5. **(a)** The cross-section area of the precast concrete beam to column, and **(b)** the RC frame.

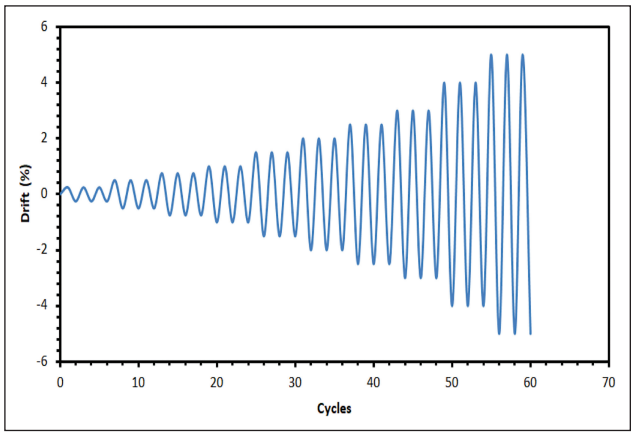

Figure 6. Loading protocol.

6. THE RESULT AND DISCUSSION

6.1. Load–Deformation

The moment rotation of the precast specimen PS-1, and the RC-1 frames are shown in the Figure 7. The moment rotation of the precast has compared with the RC frames.

The precast specimen model with damper was shown a greater hysteric behavior than the RC frame. The precast model was bounded with the replaceable damper and connected by special-shaped connectors. The precast specimen under cyclic loading was shown good performance. The chord rotation of the PS-1 has found as 2.7% and the RC-1 chord rotation has found as 2%, although, the resistance of the PS-1 has not increased.

6.2. The Stiffness Gradation

The stiffness of the PS-1 specimen was different from the RC-1, that has shown the different stiffness behavior. The equivalent stiffness was calculated by Secant stiffness of a point in the loading step. The equivalent stiffness specified the structure Elasto–Plastic state, that is illustrated in Figure 8.

The equivalent stiffness was analyzed in the maximum displacement point by first cycle of every level. The moment rotation of the specimens is shown in Figure 9.

The comparison of the rotation shows that the rotation of the PS-1 specimen is bigger than the rotation of RC-1, therefore the performance of PS-1 specimen is better than RC-1 specimen. The equivalent stiffness of the specimens is not sufficient to show the specifications of the specimens. The tangent stiffness of the two specimens is shown in Figure 10.

Because the damper has decresed the equivalent stiffness of the PS-1 specimen, where the equivalent stiffness of the RC-1 specimen was found 1.6 times greater than the PS-1 specimen.

Although, the PS-1 specimen presented less moment rotation than RC-1 specimens, the PS-1 sample with damper shows higher energy dissipation.

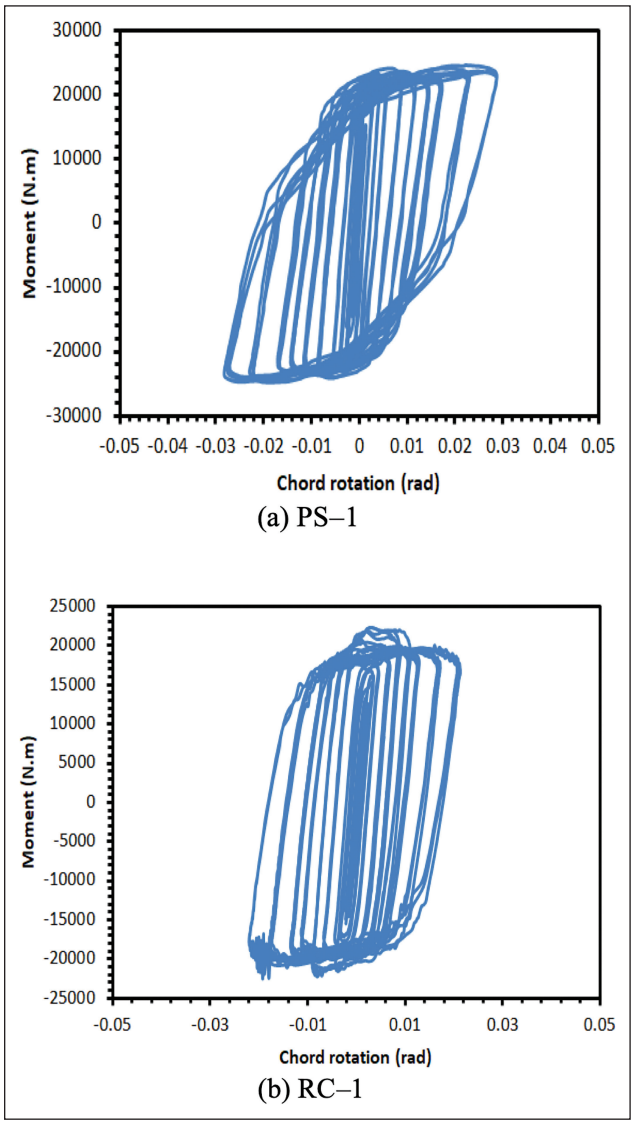

Figure 7. The moment rotation response of PS–1 **(a)**, and the moment rotation response of RC–1 **(b)**.

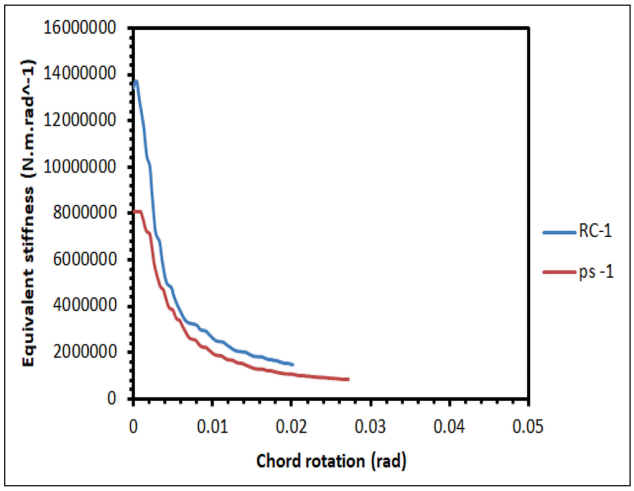

Figure 8. The equivalent stiffness of the PS-1 and RC-1.

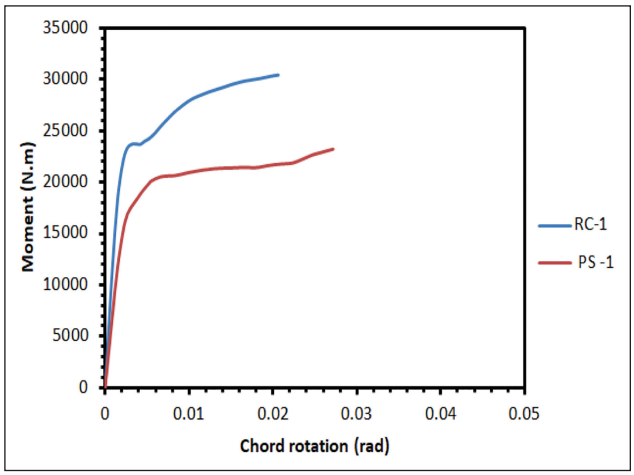

Figure 9. The moment rotation chord of PS-1 and RC-1.

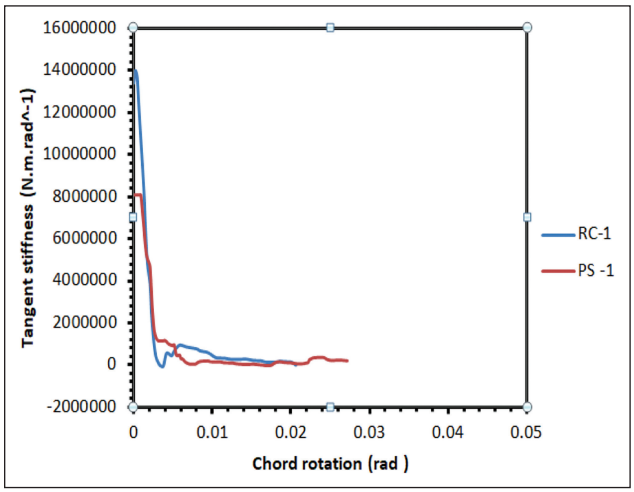

Figure 10. The tangent stiffness of PS-1 and RC-1 relationships with the moment chord rotation.

The chord rotation of the PS-1 specimen has been found greater than RC-1 specimens, which has illustrated that PS-1 specimen was saved the damage under loading procedure. That means the damper increased greatly the chord rotation of the PS-1.

6.3. The Dampers Information

In this simulation, the Z-type damper is used, and the design of the Z-type damper with the specially shaped energy dissipation strip's goal was to avoid the untimely failure of the damper. The analysis result is illustrated the good performance of the Z-type damper with negligible deformation in the special-shaped strips of the Z-type damper after unloading. The Z type damper at the approximately 2.7% chord rotation wasn't shown the fracture and big deformation on the strips. The Q235B steel is used for the Z-type damper.

7. NUMERICAL STUDY AND DISCUSSION

7.1. Designing Approach

In this study, the efficiency of the PS-1 specimen with special connection has elaborated with finite element (FE) and simulated by ABAQUS software. The C3D8R elements have been used for simulating the concrete part, damper, and special-shaped connections. Also, From the T3D2 elements have been used for simulating the longitudinal reinforcement bars and stirrups. The contact behavior between dampers, bolts, special connection parts, concrete with the connector, and column with gusset plates have been applied for the connections. The column and beam connector have been simulated by the "tie" constraint. The cavity of the special beam connector and the concrete connection was done with contact pairs. The hard contact applied for all surfaces, and the tangential behavior chosen from the Coulomb friction type. The friction of 0.6 is used for contact between concrete and steel surface, and the friction of 0.15 is used for contact between steel surfaces. The load transformation at the damper was via the shear force between the screw hole and bolt. The 0.25 clearance has applied between screw and bolt, which has very effective on the hysteric response under small rotation.

8. CONCLUSION

In this study the precast reinforced concrete beam–to–column joints with replaceable damper under cyclic loading has been studied.

The precast specimen model with damper has shown a greater hysteric behavior than the RC frame.

1. The chord rotation of the PS-1 was 2.7% approximately, and the RC-1 chord rotation was 2%, as well as the resistance of the PS-1 was increased than RC-1.
2. Therefore, the equivalent stiffness of the PS-1 specimen was not greater than the RC-1 frame. Because the damper has decreased the equivalent stiffness of the PS-1 specimen. The tangent stiffness of the PS-1 specimen has not been increased more than RC-1 specimens.
3. The analysis result is illustrated the good performance of the Z-type damper with negligible deformation in the special-shaped strips of the Z-type damper after unloading. The Z type damper at the approximately 2.7% chord rotation wasn't shown the fracture and big deformation on the strips.

DATA AVAILABILITY STATEMENT

The authors confirm that the data that supports the findings of this study are available within the article. Raw data that support the finding of this study are available from the corresponding author, upon reasonable request.

CONFLICT OF INTEREST

The authors declare that they have no conflict of interest.

FINANCIAL DISCLOSURE

The authors declared that this study has received no financial support.

PEER-REVIEW

Externally peer-reviewed.

REFERENCES

[1] Jaillon, L., Poon, C., & Chiang, Y. (2009). Quantifying the waste reduction potential of using prefabrication in building construction in Hong Kong. Waste Management, 29(1), 309–320. [CrossRef]

[2] Yee, A. A. (2001). Social and Environmental Benefits of Precast Concrete Technology. PCI Journal, 46(3), 14–19. [CrossRef]

[3] Breccolotti, M., Gentile, S., Tommasini, M., Materazzi, A. L., Bonfigli, M. F., Pasqualini, B., Colone, V., & Gianesini, M. (2016). Beam-column joints in continuous RC frames: Comparison between cast-in-situ and precast solutions. Eng Struct, 127, 129–144. [CrossRef]

[4] Dyke, S. J., Spencer, B. F., Sain, M. K., & Carlson, J. D. (1998). An experimental study of MR dampers for seismic protection. Smart Mater Struct, 7(5), 693–703. [CrossRef]

[5] M. J. N. (1988). Research needs for precast seismic structural systems. structural systems research (Report No: SSRP-88/0). University of California, San Diego.

[6] Sermet, F., Ercan, E., Hökelekli, E., Arisoy, B. (2020). Cyclic behavior of composite column-reinforced concrete beam joints. Sigma J Eng Nat Sci, 38(3), 1427–1445.

[7] Morgen, B. G., & Kurama, Y. C. (2007). Seismic Design of Friction-Damped Precast Concrete Frame Structures. J Struct Eng, 133(11), 1501–1511. [CrossRef]

[8] Morgen, B. G., & Kurama, Y. C. (2004). A friction damper for post-tensioned precast concrete moment frames. PCI J, 49(4), 112–133. [CrossRef]

[9] Vardar, T., Altan, M. F., & Naimi, S. (2017). Economic and technological evaluation of transportation system, new trends. J Sustain Const Mater Technol, 1(1), 83–88. [CrossRef]

[10] Elliot, S., Bucklow, I. A., & Wallach, E. R. (1980). An examination of diffusion bonded interfaces in a mild steel. J Mater Sci, 15(11), 2823–2833. [CrossRef]

[11] Olbak, M., Naimi, S. (2016). Kentsel dönüşüm uygulanmış 5 katlı iki yapı örneğinin deneysel verileri kullanılarak doğrusal olmayan analiz yöntemleri ile güçlendirme sonuçlarının irdelenmesi. İstanbul Aydın Üniversitesi Dergisi, 31, 145–166.

[12] Wang, C. L., Liu, Y., & Zhou, L. (2018). Experimental and numerical studies on hysteretic behavior of all-steel bamboo-shaped energy dissipaters. Eng Struct, 165, 38–49. [CrossRef]

[13] Shariatmadar H, Beydokhti E. Z. (2014). An investigation of seismic response of precast concrete beam to column connections: experimental study. Asian J Civ Eng 15(1), 41–59.

[14] Xu, L. H., Fan, X. W., & Li, Z. X. (2016). Cyclic behavior and failure mechanism of self-centering energy dissipation braces with pre-pressed combination disc springs. Earthq Eng Struct Dyn, 46(7), 1065–1080. [CrossRef]

[15] Noroozinejad Farsangi., E. (2010). Connections behaviour in precast concrete structures due to seismic loading. GU J Sci, 23(3), 315–325.

[16] Li, Z., Qi, Y., & Teng, J. (2020). Experimental investigation of prefabricated beam-to-column steel joints for precast concrete structures under cyclic loading. Eng Struct, 209, Article 110217. [CrossRef]

[17] GB/T 228.1. (2010). Metallic materials-tensile testing-Part 1: Method of test at room temperature. Standard Press. [Chinese]

[18] GB/T50081. (2002). General administration of quality supervision, inspection, and quarantine of the people's republic of China. Standard for test method of mechanical properties on ordinary concrete. China Architecture & Building Press. [Chinese]

[19] Li, Y., Geng, F., Ding, Y., & Wang, L. (2020). Experimental and numerical study of low-damage self-centering precast concrete frame connections with replaceable dampers. Eng Struct, 220, Article 111011. [CrossRef]

[20] Huang, X., Zhou, Z., Xie, Q., Guo, C., & Li, C. (2018). Seismic analysis of friction-damped self-centering coupled-beams for moment-resisting-frames without floor elongation. J Earthq Tsunami, 12(05), Artgicle 1850012. [CrossRef]

[21] Huang, L., Zhou, Z., Huang, X., & Wang, Y. (2020). Variable friction damped self-centering precast concrete beam–column connections with hidden corbels: Experimental investigation and theoretical analysis. Eng Struct, 206, Article 110150. [CrossRef]

Journal of Sustainable Construction Materials and Technologies
Web page info: https://jscmt.yildiz.edu.tr
DOI: 10.47481/jscmt.1093312

JSCMT
Journal of Sustainable Construction Materials and Technologies

Research Article

Influence of rice husk ash substitution on some physical, mechanical and durability properties of the metakaolin-based geopolymer mortar

Aigul KABİROVA[1*], Mucteba UYSAL[2]

[1]*Department of Civil Engineering, Karadeniz Technical University, Trabzon, Türkiye*
[2]*Department of Civil Engineering, Yıldız Technical University, İstanbul, Türkiye*

ARTICLE INFO

Article history
Received: 25 March 2022
Accepted: 01 June 2022

Key words:
Geopolymer mortar, ground granulated blast furnace slag, metakaolin, rice husk ash, substitution

ABSTRACT

In this study, it was investigated the influence of rice husk ash, which is a waste by-product of industrial production, on ultrasonic pulse velocity, compressive strength, flexural strength and high temperature endurance of the metakaolin-based geopolymer mortar. For this, the sand was substituted by rice husk ash (RHA) at the rate of 25%, 50% and 75% by wt. in the production of geopolymer mortar. A total of 4 series of metakaolin-based geopolymer mortars (reference series and three series with RHA substitution) were produced. In this study, the geopolymer, in other words, the binder of the mortar was produced by metakaolin and ground granulated blast furnace slag reacting with the mixture of sodium hydroxide (12M NaOH) and sodium silicate (Na_2SiO_3) solutions. The ratio of metakaolin and reactant mixture (12M NaOH + Na_2SiO_3) was determined for each series following the preliminary experiments. On the specimens produced as 50 mm cube and 40 x 40 x 160 mm prism, the intended experiments were carried out after specimens underwent curing in a dry oven at 60°C during 72 h and gained strength. The results have shown that RHA could be used as a filling material in metakaolin-based geopolymer mortars, and metakaolin-based geopolymer mortars with 50% RHA substitution can be an alternative to the pure metakaolin-based mortar.

Cite this article as: Kabirova, A., & Uysal, M. (2022). Influence of rice husk ash substitution on some physical, mechanical and durability properties of the metakaolin-based geopolymer mortar. *J Sustain Const Mater Technol*, 7(2), 88–94.

1. INTRODUCTION

Nowadays, the interest to geopolymers is increasing. This is because geopolymer technology allows an opportunity to obtain a construction material with higher engineering properties using waste materials, so that geopolymers can be an alternative to Portland cement. The recycling of waste materials provides for using natural resources economically. Another reason that makes geopolymers attractive is that much fewer CO_2 emissions occur during the production process [1–6]. Geopolymers were discovered through research on nonflammable and noncombustible plastic materials in the aftermath of various catastrophic fires involved common organic plastic in France between 1970–1972 and announced by Davidovits in 1978 [7]. Geopolymers are binders obtained as a result of the reaction

***Corresponding author.**
*E-mail address: zarakebir16@gmail.com

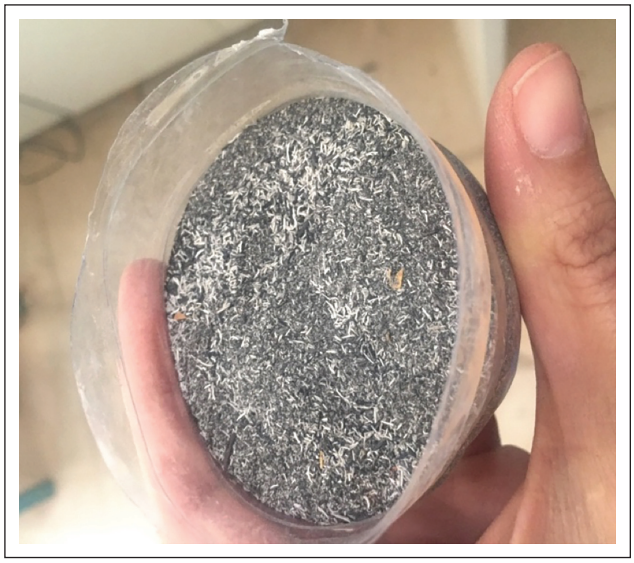

Figure 1. Burned rice husk (≥63 μm).

Figure 2. The prism specimens after curing.

Table 1. Chemical composition of pozzolans of the binder

Chemical composition (%)	SiO_2	Al_2O_3	Fe_2O_3	TiO_2	CaO	MgO	K_2O	Na_2O	L.O.I.
Metakaolin	56.10	40.25	0.85	0.55	0.19	0.16	0.55	0.24	1.11
GGBS	40.60	12.83	1.37	0.75	36.08	6.87	0.68	0.79	0.03

Table 2. Compounds of geopolymer mortars (for 1000 g MK)

Geopolymer mortar	12M NaOH solution	Na_2SiO_3	12 M NaOH: Na_2SiO_3 rate	MK	MK:RM rate	GGBS	RS	RHA	RHA:RS rate
MK	433.3	866.7	1:2	1000	1:1.3	133.3	2250	–	–
MK-RHA25	466.7	933.3	1:2	1000	1:1.4	133.3	1687.5	562.5	25:75
MK-RHA50	583.3	1166.7	1:2	1000	1:1.75	133.3	1125	1125	50:50
MK-RHA75	700	1400	1:2	1000	1:2.1	133.3	562.5	1687.5	75:25

of wastes such as blast furnace slag, fly ash or red mud, or calcined natural sources like kaolin, zeolite or bentonite (metakaolin, metazeolite or metabentonite) with alkaline solutions. Hydroxide solutions (NaOH, KOH, LiOH) and silicates (Na_2SiO_3 and K_2SiO_3) used in the production of geopolymer are defined as reactants [7], or reagents, in other words, hardeners [8].

Although Kriven (2017) [9] has stated the optimum strength gain time of geopolymer mortar as 24 h, there are few studies on the strength-time relationship for geopolymer mortars and geopolymer concrete. Duxson et al. (2007) [10] have observed a minimal change in the compressive strength of metakaolin-based geopolymer specimens between 7 and 28 days of ageing. Albidah et al. (2021) [11] have obtained the results where the metakaolin-based geopolymer concrete specimens at 7 days of ageing have achieved 89.1–95.3% of the compressive strength obtained at 28 days. Also, some geopolymer concrete specimens at 14 days had a compressive strength nearly equivalent to the 28-day compressive strength. In this study, the compressive strength was evaluated at 7 and 28 days for geopolymer mortars based on metakaolin, which is obtained by calcining purified kaolin clay and represents an amorphous aluminosilicate. Because of these, metakaolin is compatible with alkaline solutions and gains strength quickly. In addition to this, ground granulated blast furnace slag was used for faster gaining strength, according to [7].

The reason for using rice husk ash (RHA) as a substitution material is because it has the highest silica content (by up to 94%–95%) among all plant residues [12, 13]. And so it can be used as pozzolan. Bezerra et al. (2011) [14] have observed that RHA presents pozzolanicity and the mortars with incorporated RHA had values superior to the reference mixtures in relation to the physical and mechanical performance probably due to pozzolanic reactions. In developed countries, RHA is used to generate electricity, and biochar

Figure 3. **(a)** Universal press, some views from **(b)** compression tests and **(c)** three-point flexural tests.

is used in the production of high-performance concrete or ultra-high-performance concrete [12, 15, 16].

Nowadays, there are studies on the influence of partial replacement of chief binder material (e.g. metakaolin, fly ash) with RHA in the geopolymer [17–21]. Results of studies, where metakaolin (MK) was replaced by 20–30 wt% RHA, show that MK+RHA generates a compact pore structure, which contributes to improvement of compressive strength [17, 18]. Wen et al. (2019) [20] have investigated the viability of a novel geopolymer derived from non-calcined sludge and modified rice husk ash blend. Yomthong et al. (2019) [21] have improved the compressive strength of fly ash-based geopolymer through usage of RHA at 3 wt%. On the one hand, there are studies where the ratios of RHA were higher. Mrema and Mboya (2016) [13] have investigated the influence of RHA/Lime ratio on the strength properties of sand mortars. There were 40/60, 50/50, 60/40, 70/30 and 80/20 RHA/Lime ratios in the binder. It has been found out in the study that the optimum proportions are 60% RHA and 40% lime. The compressive strength was increased when the rate of RHA was increased from 40 to 60 wt%, and it was decreased when RHA was increased from 60 to 80 wt%. In this study, considering all of these, it is researched the potential of using RHA at the rate of 25%, 50% and 75% by wt. in the sand of metakaolin-based geopolymer mortar.

2. MATERIALS AND MIX DESIGN

In the production of geopolymer mortars, there were used metakaolin with specific gravity of 2.52, ground granulated blast furnace slag with specific gravity of 2.91, 12 molar sodium hydroxide (12M NaOH) solution, sodium silicate (Na_2SiO_3), 2 mm river sand and 63 μm rice husk ash. The molarity of NaOH solution was selected according the existing study [22]. The specific gravity of river sand (RS) is 2.67 and it is 2.14 for rice husk ash (RHA). In Figure 1, there is shown the burned rice husk (≥63 μm). It was used after passing through the sieve. The chemical properties of the pozzolans of the binder and the compounds of geopolymer mortars are given in Table 1 and Table 2, respectively.

In Figure 2, there are shown the specimens underwent curing in a dry oven at 60°C during 72 h.

3. TEST METHODS

Experimental studies consist of two stages. In the first stage, a total of 24 cubes of 50 mm, and a total of 24 prisms of 40 x 40 x 160 mm were produced for compression and flexural testing of the specimens at 7 and 28 days of ageing. Testing for compressive strength was performed according to ASTM C109/C109M-20a [23] on the

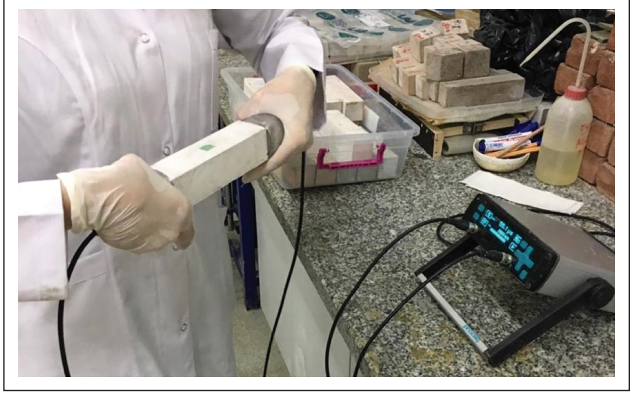

Figure 4. A view from ultrasonic pulse velocity tests.

Figure 5. Nabertherm B130 high temperature electric furnace.

Table 3. Compressive strength, ultrasonic pulse velocity (UPV) and flexural strength of geopolymer mortars at 7 and 28 days of ageing

Geopolymer mortar	Compressive strength (MPa)		Increase in compressive strength (%)		Flexural strength (MPa)		UPV (m/s)	
	7 days	28 days	7 days	28 days	7 days	28 days	7 days	28 days
MK	45.68	40.47	–	–	8.53	8.95	3403	3464
MK-RHA25	49.13	53.60	7.55	32.44	8.44	8.81	3381	3432
MK-RHA50	50.12	53.65	9.75	32.57	8.39	7.69	3118	3212
MK-RHA75	35.13	33.85	-23.1	-16.36	7.18	5.80	2725	2898

Table 4. The results for MK-RHA50 exposed to high temperatures

High temperature/ Geopolymer mortar	Weight loss (%)	UPV (m/s)		Flexural strength	Strength loss (%)
		Before test	After test		
200°C					
MK	0.48	3385	2630	3.62	57.56
MK-RHA50	–	3004	2855	3.86	53.99
400°C					
MK	3.57	3441	1396	1.89	77.84
MK-RHA50	5.02	2979	2215	1.49	82.24
600°C					
MK	5.84	3410	833	1.06	87.57
MK-RHA50	6.56	3008	2156	1.68	79.98
800°C					
MK	13.88	3400	0	0.73	91.44
MK-RHA50	7.35	2943	1688	0.97	88.44

cubes. Three-point flexural strengths of the prisms were obtained according to ASTM C349-18 [24].

In Figure 3, there are shown the universal press for compression and flexural testing, and some views from the testing.

In Figure 4, there is shown a view from the ultrasonic pulse velocity test performed according to ASTM C597-09 [25].

In the second stage, it was selected the highest value of the 7-day compressive strength from the series with RHA substitution, and the high temperature (200°C, 400°C, 600°C and 800°C) tests were performed on a total of 24 prisms (12 specimens each for both of MK and MK-RHA series). The high temperature testing was performed following the existing study [22]. Before the tests, oven dry prism specimens'

Figure 6. The prism specimens placed in the furnace.

weights and ultrasonic pulse velocities were determined. Then specimens were exposed to the effect of 200°C, 400°C, 600°C and 800°C in the Nabertherm B130 furnace shown in Figure 5. The applied temperature rise rate was 5°C/min. The specimens were kept at the target temperature for 60 min. After that, the heating was stopped and the furnace door was opened, and the specimens were cooled at the room temperature (23°C). In Figure 6, there are shown prism specimens placed in the furnace. Three days after the high temperature application, the specimens' weight, ultrasonic pulse velocity and flexural strength were obtained, and the losses were determined.

4. RESULTS AND DISCUSSIONS

The results from the first stage of experimental studies are given in Table 3 and Figure 7–9.

In Table 3, it is clearly seen that 25 and 50 wt% RHA substitution increases the metakaolin-based mortar compressive strength. The highest compressive strength was obtained by 50 wt% substitution. Also, the obtained results are shown that RHA increases the compressive strength and flexural strength, when it changes from 25 to 50 wt%, and RHA reduces both strengths, when it changes from 50 to 75 wt%. In existing studies, it is indicated that up to 60 wt% RHA added filling effects, and strong Si-O-Si bonds aid in enhancing strength [13, 17–19].

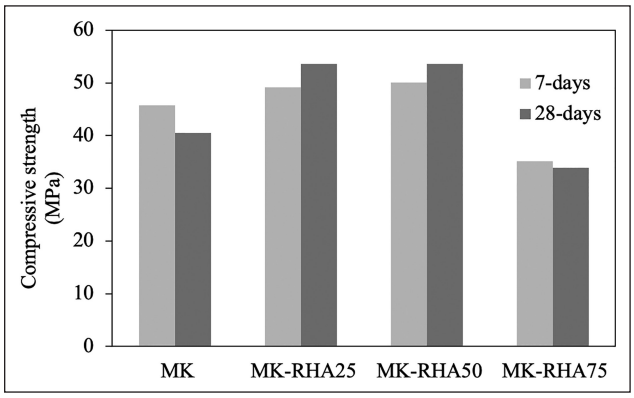

Figure 7. Compressive strength of geopolymer mortars at 7 and 28 days of ageing.

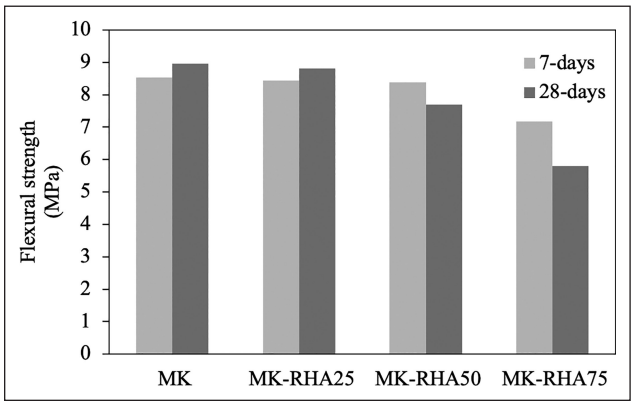

Figure 8. Flexural strength of geopolymer mortars at 7 and 28 days of ageing.

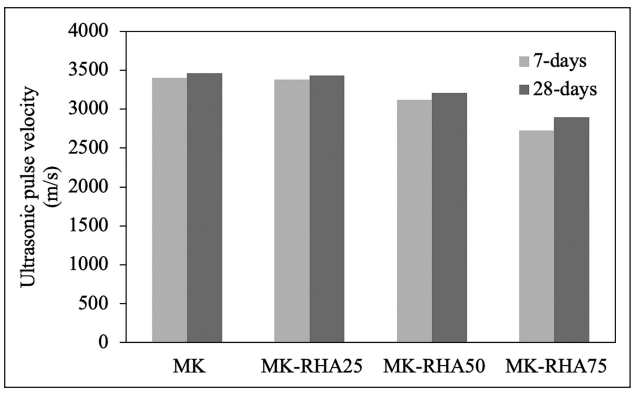

Figure 9. Ultrasonic pulse velocity of geopolymer mortars at 7 and 28 days of ageing.

In this study, also, no significant changes were noted at 28 days for both compressive strength and flexural strength. It is seen that the compressive strength of geopolymer mortars with 25 and 50 wt% RHA substitution at 7 days of ageing achieved 91.66% and 93.42% of the 28-day compressive strength, respectively. These results agree with the existing results [10, 11, 13].

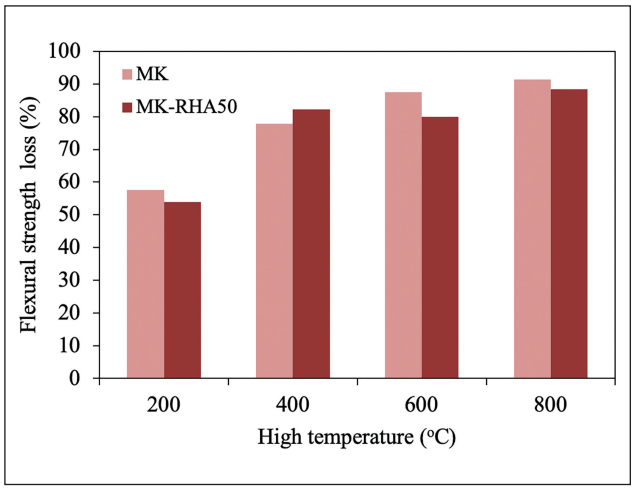

Figure 10. Flexural strength losses of MK-RHA50 exposed to high temperatures.

In this study, UPV values decreased with an increasing rate of RHA substitution. It agrees with the existing results, and it is because of a material with a low density has more voids and UPV will be longer in the material [12]. In the study, RHA, which had lower density, produced more voids in the mortar, and as a result, the lower UPV and flexural strength values were obtained.

According to the results obtained in the first stage, the geopolymer mortar with 50 wt% RHA substitution (MK-RHA50) was selected for the second stage. The results from the second stage of experimental studies are given in Table 4 and Figure 10.

According to the results given in Table 4, the geopolymer mortar with 50 wt% RHA substitution has better high temperature endurance. In Liang et al. (2019) [18], there is indicated that the pores of geopolymer were refined by the filling effects of RHA and enrichment of gel phases, which was the primary reason for the optimization of geopolymer thermal stability.

5. CONCLUSION

The current study was aimed to investigate the usability of rice husk ash (RHA) on the production of metakaolin-based geopolymer mortars. For this, it was determined ultrasonic pulse velocity, compressive strength, flexural strength and high temperature endurance of the geopolymer mortars, where RHA was used at rate 25%, 50% and 75% in the sand. The results have shown that RHA could be used as a filling material in metakaolin-based geopolymer mortars. On the other hand, it was seen that metakaolin-based geopolymer mortar containing 50 wt% RHA can be an alternative to pure metakaolin-based mortar and it will be beneficial in terms of the economic use of aggregate/sand.

DATA AVAILABILITY STATEMENT

The authors confirm that the data that supports the findings of this study are available within the article. Raw data that support the finding of this study are available from the corresponding author, upon reasonable request.

CONFLICT OF INTEREST

The authors declare that they have no conflict of interest.

FINANCIAL DISCLOSURE

The authors declared that this study has received no financial support.

PEER-REVIEW

Externally peer-reviewed.

REFERENCES

[1] Davidovits, J. (2013). A review on Geopolymer cement. www.geopolymer.org/library/technical-papers/21-geopolymer-cement-review-2013

[2] Geopolymer Institute (2006). Geopolymer Cement for mitigation of Global Warming. www.geopolymer.org/applications/global-warming

[3] McLellan, B. C., Williams, R. P., Lay, J., Riessen, A., & Corder, G. D. (2011). Costs and carbon emissions for geopolymer pastes in comparison to ordinary portland cement. Journal of Cleaner Production, 19(9–10), 1080–1090. [CrossRef]

[4] Thaarrini, J., & Dhivya, S. (2016). Comparative Study on the Production Cost of Geopolymer and Conventional Concretes. International Journal of Civil Engineering Research, 7(2), 117–124.

[5] Rajini, B., Narasimha Rao, A. V., & Sashidhar C. (2020). Cost Analysis of Geopolymer Concrete Over Conventional Concrete. International Journal of Civil Engineering and Technology, 11(2), 23–30. [CrossRef]

[6] Rintala, A., Havukainen, J., & Abdulkareem, M. (2021). Estimating the Cost-Competitiveness of Recycling-Based Geopolymer Concretes. Recycling, 6(3), 46. [CrossRef]

[7] Davidovits, J. (2008). Geopolymer chemistry and applications (Second Ed.). (pp. 584). Institut Géopolymère.

[8] Davidovits, J. (2017). Why alkali-activated materials are not geopolymers? www.geopolymer.org/faq/alkali-activated-materials-geopolymers

[9] Kriven, W. (2017). The geopolymer route to high tech ceramic. www.youtube.com/watch?v=9kqA-p9XrGWU

[10] Duxson, P., Mallicoat, S. W., Lukey, G. C., Kriven, W. M., & van Deventer, J. S. J. (2007). The effect of alkali and Si/Al ratio on the development of mechanical properties of metakaolin-based geopolymers. Colloids and Surfaces A: Physicochemical and Engineering Aspects, 292(1), 8–20. [CrossRef]

[11] Albidah, A., Alghannam, M., Abbas, H., Almusallam, T., & Al-Salloum Y. (2021). Characteristics of metakaolin-based geopolymer concrete for different mix design parameters. Journal of Materials Research and Technology, 10, 84–98.

[12] Zaki, A., & Sola, Ö. Ç. (2020). Investigation of Strength and Durability Properties of Mortars with Rice Husk Ash Additive. Alanya Alaaddin Keykubat University (ALKU) Journal of Science, 2(2), 54–61.

[13] Mrema, A., & Mboya, H. (2016, September 5–7). Strength properties of rice husk ash-lime mortars [Conference presentation]. The Sixth International Conference on Structural Engineering, Mechanics and Computation, Cape Town, South Africa. www.researchgate.net/publication/307935431_Strength_properties_of_rice_husk_ash-lime_mortars [CrossRef]

[14] Bezerra, I. M. T., De Souza, J., & De Carvalho, J. B. Q. (2011). Application of the rice husk ash in mortars for bricklaying. Revista Brasileira de Engenharia Agrícola e Ambiental, 15(6), 639–645. [CrossRef]

[15] Kang, S. H., Hong, S. G., & Moon, J. (2018). The use of rice husk ash as reactive filler in ultra-high performance concrete. Cement and Concrete Research, 115, 389–400. [CrossRef]

[16] Faried, A. S., Mostafa, S. A., Tayeh, B. A., & Tawfik, T. A. (2021). The effect of using nano rice husk ash of different burning degrees on ultra-high-performance concrete properties. Construction and Building Materials, 290, Article 123279. [CrossRef]

[17] Zhu, H., Liang, G., Zhang, Z., Wu, Q., & Du, J. (2019). Partial replacement of metakaolin with thermally treated rice husk ash in metakaolin-based geopolymer. Construction and Building Materials, 221, 527–538. [CrossRef]

[18] Liang, G., Zhu, H., Zhang, Z., & Wu, Q. (2019). Effect of rice husk ash addition on the compressive strength and thermal stability of metakaolin based geopolymer, Construction and Building Materials, 222, 872–881. [CrossRef]

[19] Hossain, Sk S., Roy, P. K., & Bae, C. J. (2021). Utilization of waste rice husk ash for sustainable geopolymer: A review. Construction and Building Materials, 310, Article 125218.

[20] Wen, N., Zhao, Y., Yu, Z., & Liu, M. (2019). A sludge and modified rice husk ash-based geopolymer: synthesis and characterization analysis. Journal of Cleaner Production, 226(44), 805–814. [CrossRef]

[21] Yomthong, K., Wattanasiriwech, S., & Wattanasiriwech, D. (2019). Rice husk ash-geopolymer composite. IOP Conference Series Materials Science and Engineering, 600(1), Article 012003. [CrossRef]

[22] Aygörmez, Y. (2018). Kolemanit atığı ve silis dumanı katkılı metakaolin tabanlı geopolimer harcın mekanik ve durabilite özelliklerinin incelenmesi [Unpublished Doctorial Thesis]. Yildiz Technichal Graduate School of Natural and Applied Sciences. [Turkish]

[23] ASTM C109/C109M-20a. (2020). Standard test method for compressive strength of hydraulic cement mortars (using 2-in. or [50-mm] cube specimens). https://webstore.ansi.org/Standards/ASTM/astmc109c109m20?gclid=Cj0KCQjw4uaUBhC8ARIsANUuDjXGZGLskNoj3J6_mBYWjsrrHCvYmpWnFgGQK9rntmlHKVZYg02lXPUaAmA4EALw_wcB

[24] ASTM C349-18. (2018). Standard test method for compressive strength of hydraulic-cement mortars (using portions of prisms broken in flexure). https://webstore.ansi.org/Standards/ASTM/astmc34918?gclid=Cj0KCQjw4uaUBhC8ARIsANUuDjXhvi1kMD7c3JXDlwPbOarJxVCibJ4--9GTWvPoXUmjS7zMCTgTpMsaAjKbEALw_wcB

[25] ASTM C597-09. (2009). Standard test method for pulse velocity through concrete. https://webstore.ansi.org/Standards/ASTM/astmc59709?gclid=Cj0KCQjw4uaUBhC8ARIsANUuDjVYjYrmaWofJIDtYc_dtJKmGMcouOBQMfsyaYv9B5avnZI-lI3TxrkaAgKnEALw_wcB

Journal of Sustainable Construction Materials and Technologies
Web page info: https://jscmt.yildiz.edu.tr
DOI: 10.47481/jscmt.1106592

JSCMT
Journal of Sustainable Construction Materials and Technologies

Research Article

Engineering properties and SEM analysis of eco-friendly geopolymer mortar produced with crumb rubber

Süleyman İPEK[1*], Kasım MERMERDAŞ[2]

[1]*Department of Architecture, Bingöl University, Bingöl, Türkiye*
[2]*Department of Civil Engineering, Harran University, Şanlıurfa, Türkiye*

ARTICLE INFO

Article history
Received: 20 April 2022
Accepted: 23 May 2022

Key words:
Crumb rubber, eco-friendly materials, geopolymer mortar, recycling, SEM

ABSTRACT

In the present study, the influence of the crumb rubber (CR) utilization as fine aggregate on the engineering properties of fly ash-based geopolymer mortar was experimentally investigated. In this context, the natural sand (NS) used in the production of geopolymer mortars was substituted with the CR, which comes out in the course of applying the retreading process to the end-of-life tires, at the substitution levels of 10%, 20%, 30%, 40%, and 50% by volume. In this way, 6 different geopolymer mixtures, one of which was the control mixture, were designed and produced. Then, the effect of CR on the fresh-state properties like flowability and fresh unit weight and the hardened-state properties like dry unit weight, compressive and flexural strengths of geopolymer mortars were examined. Besides, the properties of CR such as grading, specific gravity, water absorption capacity, fineness modulus as well as surface texture and particle shapes were compared with that of the river sand. In addition, the interfacial transition zone (ITZ) between fine aggregate particles (both NS and CR) and geopolymer paste was viewed using SEM images. When NS was substituted with CR at a 50% level, unit weights decreased significantly, which is considered lightweight mortar; however, no remarkable influence on the flowability was observed. The incorporation of CR, on the other hand, resulted in a reduction in the strength characteristics of the geopolymer mortar. Besides, a weaker ITZ was detected between the CR particles and geopolymer paste. Moreover, the visual appearance of the mixes revealed that the CR particles were well-distributed on the mortar cross-section, namely no bleeding and segregation problems were faced. As a consequence, it can be stated that the geopolymer mortar can be manufactured by substituting the NS with CR provided that it is at specified substitution levels. For instance, the flexural strength of the mortar was more than 3 MPa even at a 40% replacement level while the compressive strength of the geopolymer mortar dropped under 20 MPa at a 20% replacement level.

Cite this article as: İpek, S., & Mermerdaş, K. (2022). Engineering properties and SEM analysis of eco-friendly geopolymer mortar produced with crumb rubber. *J Sustain Const Mater Technol*, 7(2), 95–107.

***Corresponding author.**
*E-mail address: sipek@bingol.edu.tr

1. INTRODUCTION

One of the important problems of the 21st-century world is the growing waste piles. The United Nations Environmental Protection Agency classifies these waste piles as hazardous and non-hazardous waste materials. In this context, waste tires can be regarded as one of the most known and common contaminant materials. Although it is considered a non-hazardous waste material, it has a high potential of being a hazardous waste material, especially in the case of its uncontrolled burning. In addition, the pile of waste tires leads to be a nest for some animals like snakes, rodents, centipedes, etc., thereby, the natural habitat in the region where the waste tire is piled can be degraded. Therefore, recycling or reusing waste tires is an essential issue having importance because the decomposition of the tire rubber through natural ways takes a very long time [1].

As a consequence of this, many recycling and/or reusing methods were developed to decrease the amount of waste tire pile. Controlly burning the waste tires to obtain energy is one of the easiest and most beneficial ways of recycling the waste tires since they provide a high amount of heating energy [2]; however, it is limited or forbidden in many countries by laws due to its negative impact on nature such as releasing contaminant, hazardous, and toxic gases [3, 4]. In addition to burning them, there are alternative ways for recycling and/or reusing the waste tires like retreading them to obtain recapped tires, decomposing them by pyrolysis technique, and recycling them to achieve the materials or to produce tire-based products.

Apart from the aforementioned ways, using the end-of-life tires in civil engineering applications as filling material or aggregate is an innovative, environmentally friendly, and effective way of sweeping these idle tires away. To bring the waste tires into the form that can be used in such civil engineering applications, mechanically granulating is generally applied to the waste tires in order to obtain the idle tires in the sizes, commonly named tire chips and crumb rubber (CR) [5]. Among the civil engineering applications, using the waste tires as aggregate in the ready-mixed concrete sector having a large industrial volume with 160 million tons manufacturing in Turkey, 620 million tons manufacturing in Europe [6], and approximately 4.4 billion tons manufacturing in the world [7] can be regarded as the most effective way to get rid of these idle tires [8, 9].

Many scientists have investigated the influence of the aggregate derived from the waste tire on both fresh and hardened state properties of conventional concrete. However, incorporating rubber-derived aggregates into the geopolymer concrete, which was a material developed by French scientist Joseph Davidovits as an alternative to conventional concrete [10], is a completely new phenomenon, and there are some investigations about the rubber incorporated geopolymer concretes but the rubber percentage amount was limited. The difference between the traditional and geopolymer concretes is the paste phase of the mixture: in the traditional one, the cement (and mineral additives) and water constitute the paste phase while in the geopolymer one, the paste phase consists of aluminosilicate-rich material and alkaline solution. Here, it should be stated that sodium silicate (Na_2SiO_3)-sodium hydroxide (NaOH) and potassium silicate (K_2SiO_3)-potassium hydroxide (KOH) alkaline solution pairs are the pairs commonly used [11]. Thereby, a reaction named polymerization takes place between the aluminosilicate-rich raw materials and alkaline activator solution and as a result, the Si-O-Al-O bonds are formed, providing for the creation of geopolymers [12, 13]. One of the most significant pros of this new concrete concept is the possibility of being used of industrial waste materials like fly ash, blast furnace slag, bottom ash, etc. as the aluminosilicate-rich raw material, in other words, this concrete concept does not require the production of a specific raw material as in the traditional concrete. As a consequence, the production of such material leads to less energy consumption and greenhouse gas emissions, making this material a more energy-efficient and environmentally friendly construction material [13, 14].

There are just a few studies in the literature that evaluate the impact of CR incorporation on the performance of geopolymer mortars. Aly et al. [15], for example, employed waste rubber in the manufacture of geopolymer concrete and investigated the compressive and tensile strengths. Similarly, Aslani et al. [16] investigated the workability and mechanical performances of rubber aggregate-incorporated geopolymer concrete. Niş et al. [17] conducted a study in which the influence of CR incorporation on the mechanical characteristics of the geopolymer concrete and Eren et al. [18] carried out a study in which the possible utilization of CR in the self-compacting geopolymer concrete was investigated. Additionally, Wongsa et al. [19], on the other hand, looked at how CR affected the mechanical and thermal properties of geopolymer mortar, while Moghaddam [20] investigated the influence of sulfuric acid on CR-incorporated fiber-reinforced geopolymer concrete.

The target of the research presented herein is to manufacture a sustainable eco-friendly construction material and investigate its engineering properties. For this reason, an experimental study was carried out towards the reuse potential of the waste tire rubber as fine aggregate in geopolymer mortar production. For this reason, waste tire rubber named CR in fine size, coming out in the course of applying the retreading process to the end-of-life tires was incorporated into the fly ash-based geopolymer mortar instead of natural sand. Hereby, manufacturing an eco-friendly construction material was desired. For this reason, the possible influences of the incorporation of CR on the fundamental engineering properties of the geopolymer mortar were experimentally researched. Moreover, the interfacial transition zone between the fine aggregate particles (both river sand and crumb rubber) and geopolymer paste was also viewed using the scanning electron microscope (SEM) technique.

Table 1. Chemical compositions and physical properties of class F fly ash

Chemical composition, %									Physical properties	
CaO	SiO_2	Al_2O_3	Fe_2O_3	MgO	SO_3	Na_2O	K_2O	LOI*	Specific gravity	Specific surface area
1.69	55.46	26.33	6.71	2.42	0.05	1.08	4.22	1.2	2.00	2.018 m^2/g

*: LOI: loss on ignition.

Table 2. Chemical compositions of sodium hydroxide (NaOH)

Chemical composition, %				
NaOH (sodium hydroxide)	Na_2CO_3 (sodium carbonate)	NaCl (sodium chloride)	Fe (iron)	Specific gravity
≥98.0	≤0.5	≤0.02	≤0.001	1.254

Table 3. Chemical compositions and physical properties of sodium silicate (Na_2SiO_3)

Chemical composition, %		Density, g/ml	Module	Bome, °B
Na_2O (sodium oxide)	SiO_2 (silica)			
9.03	27.08	1.367	2.93	38.68

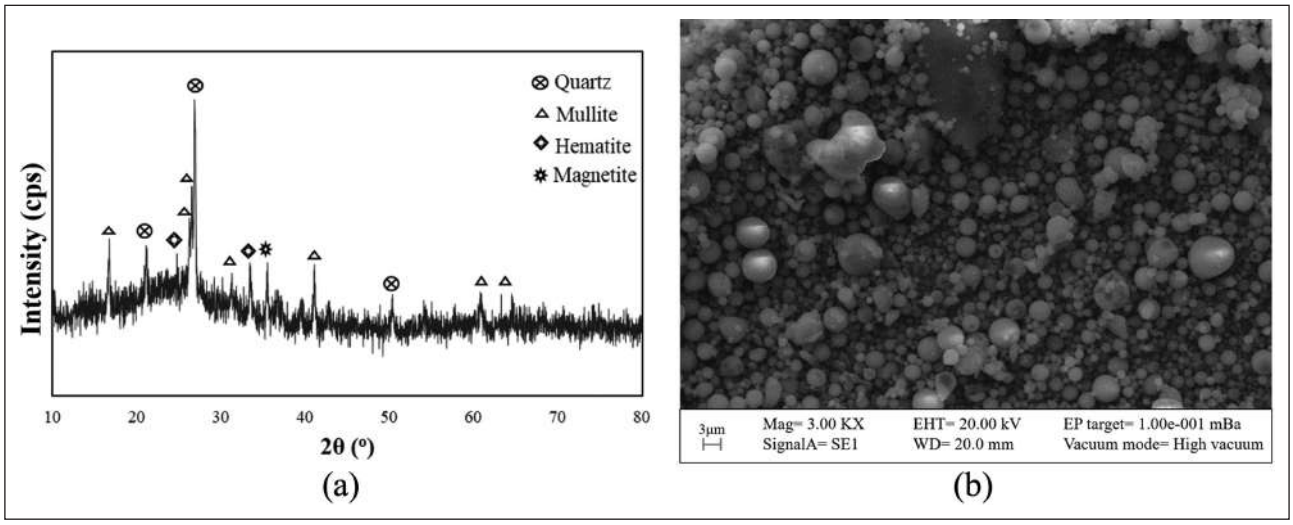

Figure 1. **(a)** X-ray diffraction (XRD) analysis result of fly ash and **(b)** scanning electron microscope (SEM) image of its particles

2. MATERIALS AND METHODS

2.1. Materials

Fly ash conforming to ASTM C311 [21] and regarded as class F according to ASTM C618 [22] was employed as an aluminosilicate-rich raw material in the production of geopolymer mortars. The chemical compositions and physical properties of fly ash, which was procured from the Çatalağzı thermal power plant in Zonguldak province of Turkey, are presented in Table 1. In addition, the X-ray diffraction (XRD) analysis result of fly ash is indicated in Figure 1a, and the image of its particles taken by scanning electron microscope (SEM) is demonstrated in Figure 1b. The main themes presented in these figures are components constituting the fly ash and particle sizes and shapes of fly ash. In regard to Figure 1a, it can be stated that the peak point in the intensity occurred at quartz crystal since the fly ash highly consists of SiO_2. On other hand, it can be seen in Figure 1b that the fly ash consists of generally particles smaller than 3 μm. Also, it should be emphasized that the particles of the FA are in a spherical shape.

As an alkaline activator, NaOH and Na_2SiO_3 pair with a ratio of 1-to-2 was used. The chemical compositions and properties of NaOH in spherical pellet form in white color and Na_2SiO_3 in the liquid form in light yellow color

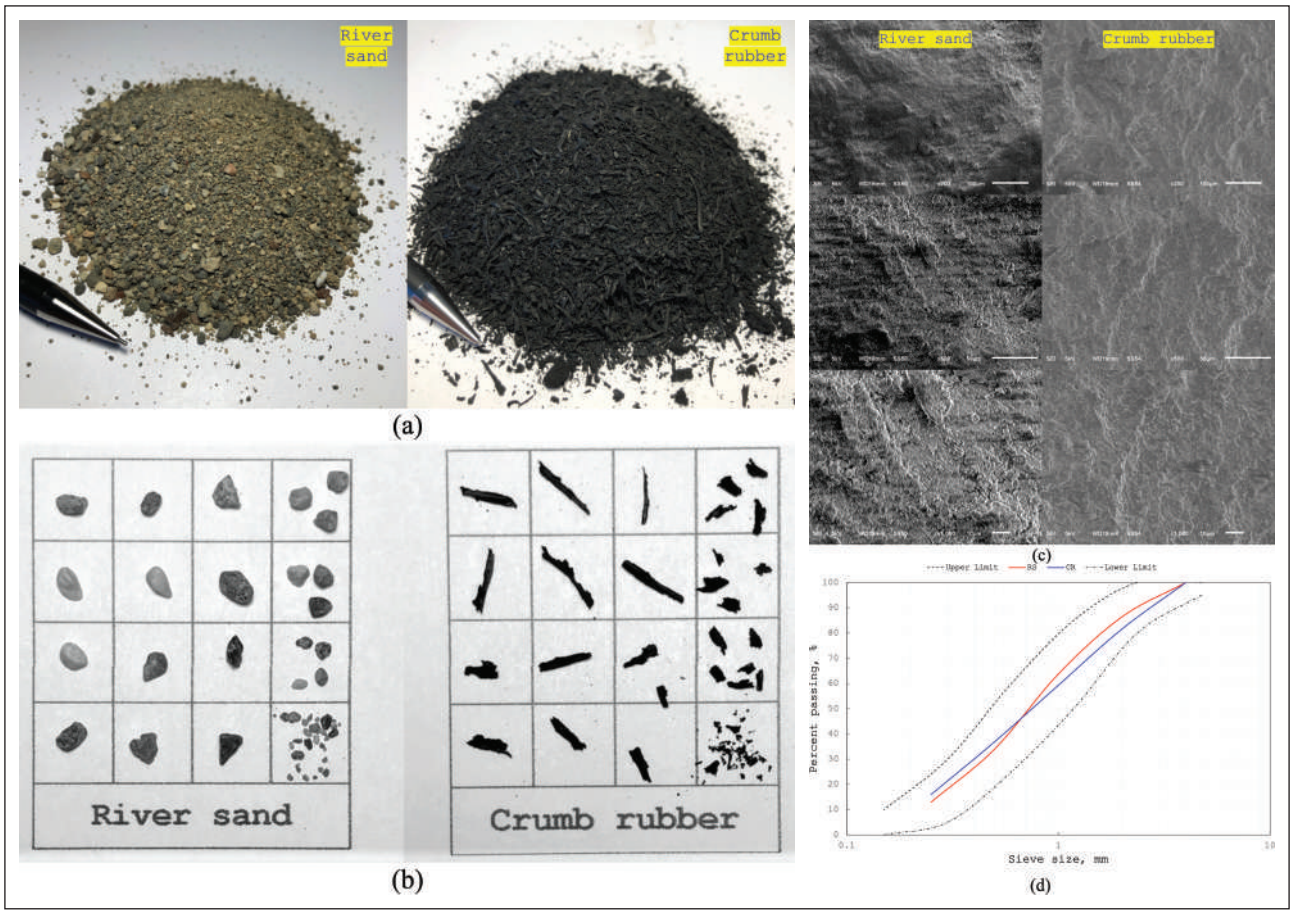

Figure 2. River sand and crumb rubber: **(a)** general photographic views, **(b)** photographic view of particles, **(c)** SEM images, and **(d)** sieve analysis results.

are presented in Tables 2 and 3, respectively. The NaOH pellets used to prepare the NaOH solution with a 12-M concentration had a purity of more than 98%. In addition to this, Na_2SiO_3 solution comprising of liquid and solid materials with respectively roughly 61.5% and 38.5% had a silica-to-sodium oxide ratio (SiO_2/Na_2O) of about 2.5.

As the last material, the superplasticizer with a commercial name of MGlenium 51 having a specific gravity of 1.07 was used to achieve geopolymer mixtures with sufficient flowability.

In the production of the geopolymer mortars of the present study, river sand (RS) with a maximum particle size of 4 mm and specific gravity of 2.74 was used. However, the waste tire rubber aggregate named crumb rubber (CR) having a specific gravity of 0.55 was substituted in some mixtures with river sand. The general photographic views of these two fine aggregates are given in Figure 2a whereas their particle shapes and sizes are shown in Figure 2b and their SEM images are indicated in Figure 2c. In addition, sieve analysis results (determined in accordance with ASTM C136 [23]) of RS and CR compared with the upper and lower limits for fine aggregate (proposed by ASTM C33 [24]) are shown in Figure 2d. The fineness modulus values of RS and CR were respectively 2.03 and 2.06. On the other hand, the water content and absorption values of RS were respectively about 0.94 and 2.31, whereas that of the CR were 0 which means the CR used in this study did not contain water and had no water absorption capability. As can be seen in Figures 2a and 2b, the CR consists of flaky and elongated particles. As the size of the particles decreases, the CR particles become angular and/or partly rounded. Besides, the CR particles are substantially softer than the RS particles, thus the elastic modulus of CR is less than that of the RS, which makes such materials structural unstable material. However, such characteristics may be useful for absorbing the energy such as impact energy, sound energy, heat energy, etc.

2.2. Mixture Proportions and Production

The mixtures in the present study were designed at a Na_2SiO_3-to-NaOH ratio of 2.0 and alkaline activator-to-aluminosilicate-rich raw material ratio of 0.5. The alkaline activator content and powder material (aluminosilicate-rich raw material) dosage were designated as 300 kg/m^3 and 600 kg/m^3, respectively. The superplasticizer content for the control mixture with sufficient flowability

Table 4. Mixture proportions for the rubberized geopolymer mortars, kg/m^3

Mixture name	FA	NH	NS	RS	CRSL, %	CR	SP
Plain mix	600	100	200	1231.1	0	–	21
Rubberized mix 1				1108.0	10	24.7	
Rubberized mix 2				984.9	20	49.4	
Rubberized mix 3				861.8	30	74.1	
Rubberized mix 4				738.7	40	98.9	
Rubberized mix 5				615.6	50	123.6	

FA: Fly ash; NH: Sodium hydroxide; NS: Sodium silicate; RS: River sand; CRSL: Crumb rubber substitution level; CR: crumb rubber; SP: superplasticizer.

was determined as 3.5% of powder material by mass after many trial batches. Since the rheological behavior of such materials is significantly influenced by variation in the superplasticizer content, all the mixtures in the present study were produced at a superplasticizer content of 3.5%. In the production of the plain geopolymer mixture, only the RS was used as fine aggregate; however, in the production of the geopolymer mixture containing crumb rubber, the RS was partially replaced with the CR at the levels of 10%, 20%, 30%, 40%, and 50% by volume. In this way, 6 geopolymer mortar mixtures were produced in total. Table 4 presents the detailed proportions of the geopolymer mortar ingredients.

Alkaline activator-to-fly ash ratio (Na_2SiO_3-to-NaOH), alkali activator molarity, fly ash dosage, and alkali activator content selected within the scope of the study carried out by Ekmen et al. [25], which is one of the most comprehensive studies in this context, in which the effects of the above-mentioned parameters on the fresh and hardened properties of geopolymer mortars were taken into consideration. Ekmen et al. [25] investigated the fresh and hardened properties of fly ash-based geopolymer mortars with 2 activator-to-fly ash ratios, 3 Na_2SiO_3-to-NaOH ratios, and 3 alkali activator molarities. Considering the consistency and strength findings obtained from this study, the mixture proportions in the current study were determined.

The same mixing procedure was applied to all geopolymer mortars during the production. This procedure consisted of two states: in the first stage, the alkaline activator solution was prepared and in the second stage, the geopolymer mortar was produced. First, the NaOH solution with 12-M concentration was prepared, and then, it was mixed with Na_2SiO_3 solution before almost 24-h of the beginning of the second stage. This solution was kept in a beaker till it was used in the production of geopolymer mortars. The second stage of the production procedure began by mixing the alkaline activator solution with fly ash in a mixer for about 3 minutes. Subsequently, the superplasticizer was poured into the mixer, and it was allowed to revolve for 2 minutes more. Thereafter, the RS in the plain mortar mixture and RS and CR mixture in the other mortars were gradually added to the mixer, and it was permitted to rotate the mixer extra 3 minutes after all fine aggregates were poured. Thereby, the production process of the geopolymer mortars was completed. The fresh-state properties of the geopolymer mortars were determined in terms of flowability measured by the flow table test, and fresh unit weight once the production process finished. After the fresh-state properties were determined, the mixtures were poured into the steel molds in two layers, of each which was vibrated for 30 seconds using a vibrating table. A heat curing of 60 °C for 24 hours was applied to the specimens taken and then, the demoulded specimens were kept in the laboratory condition where the temperature was 23±2 °C for the following 2 days. The specimens in the steel molds were put into the oven to be exposed to the heat curing regime and all the specimens were covered with a plastic bag to prevent water evaporation in the alkali solution during the heat curing. After the 3-day curing regime, the hardened-state tests were performed. Herein, it should be noted that one of the most important issues to be resolved regarding the applicability of geopolymer mortars is the high-heat curing required for the geopolymerization process and its application time. The main purpose of recent studies is to manufacture geopolymer mortar or concrete at lower curing temperatures as much as possible with application time. In terms of energy efficiency, 60°C as the curing temperature and 24 hours as the curing duration were selected according to research in the literature on the issue.

2.3. Testing Methods

The test apparatus shown in Figure 3a was employed to measure the flowability of the geopolymer mortar mixtures and ASTM C1437 [26] was followed during the application of the flow table test. During the determination of both fresh and hardened (1-day and 3-day) unit weights of the mixtures, ASTM C138 [27] was followed. A closed-loop testing machine shown in Figure 3b was used to perform the 3-day flexural strength test in regard to the ASTM C348 [28]. The 3-day compressive strength of the geopolymer mortar mixtures was determined per ASTM C109 [29] and ASTM C597 [30] was followed during measuring the 3-day UPV values of the mixtures as typically indicated in Figure 3c.

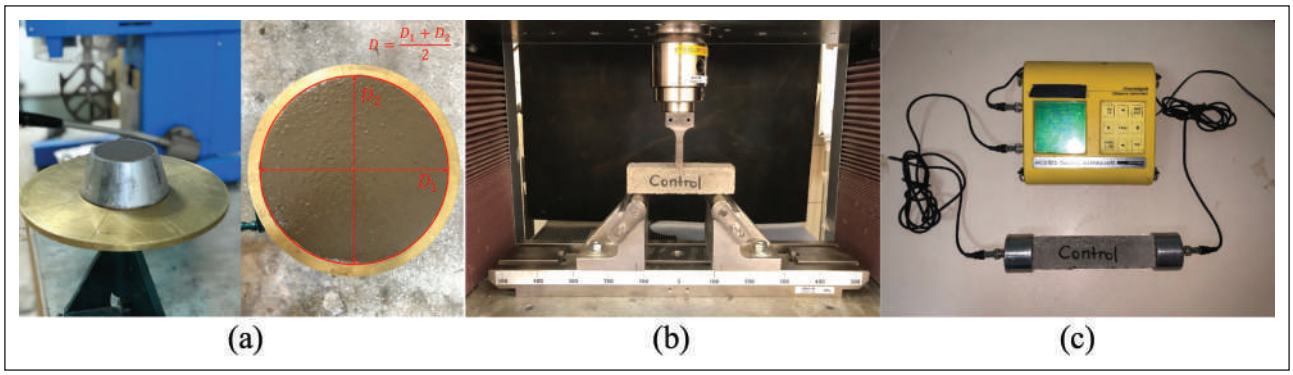

Figure 3. **(a)** Test apparatus of flow table test and measuring the flow diameter, **(b)** test device used in the measurement of flexural strength, and **(c)** UPV test device.

3. RESULTS AND DISCUSSION

3.1. Flowability Results

Based on the flow table test, the flowability of the mortars can be described in terms of mm or percentage. It should be noted that when the flowability is presented in mm the perfect flowability is 200 mm while when it is given in percentage this 200-mm flowability is defined as 100% flowability. The plain geopolymer mortar produced in this study had a flowing diameter of 210 mm which means 110% flowability. On the other hand, it was observed that substituting the RS with CR did not influence the flowability of geopolymer mortars. All the mixtures produced in the current study had a flowing diameter of 210 mm (namely 110% flowability). Since the CR particles have almost no water absorption capability, incorporating the CR into the geopolymer mortar did not affect the flowability characteristics of the mixtures. Besides, the CR particles that can be considered flaky and elongated may play a blockage role during the flowing but since the table is rammed 25 times in 15 seconds during performing the test, this role of the CR particles may have been minimized and/or eliminated. However, it should be stated that this finding is not consistent with the results reported in the literature. For example, when Aslani et al. [16] increased the crumb rubber replacement level from 10% to 20%, they observed a small decrease in the slump flow diameter values. In addition, Wongsa et al. [19] investigated how the crumb rubber incorporation influences the flowability, mechanical, and thermal properties of geopolymer mortar. They found that adding crumb rubber to geopolymer mortar mixtures made them less workable. On the other hand, Moghaddam et al. [20] reported a minor improvement in the flowability of geopolymer concrete after replacing natural sand with spherical crumb rubber derived from old tires. Similarly, Zhong et al. [31] achieved an enhancement in the workability of the geopolymer mortar from a general perspective. For this reason, the findings presented in the current study will contribute to the literature in this context.

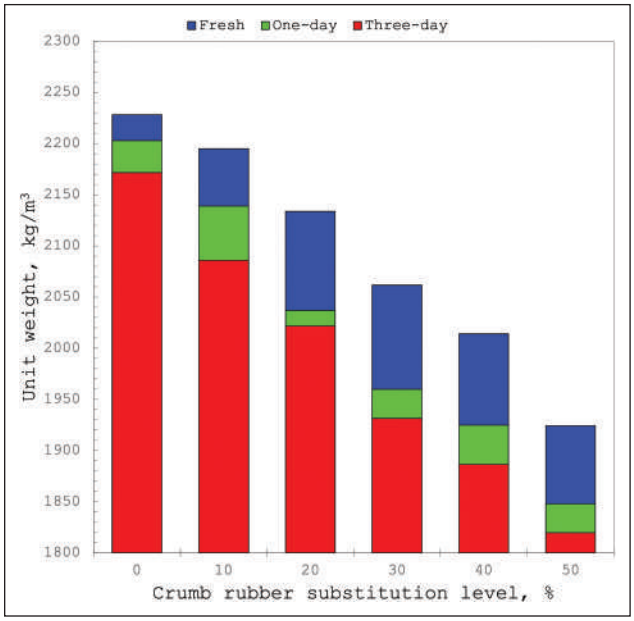

Figure 4. The variation in both fresh and dry unit weights of rubberized geopolymer mortars

3.2. Unit Weight Results

The change in both fresh and dry unit weight of the geopolymer mortars with respect to the CR substitution level is indicated in Figure 4. The fresh unit weight of the plain geopolymer mortar was about 2228 kg/m^3, whereas a systematic decrease in the fresh unit weight was observed by gradually substituting the RS with the CR. The fresh unit weights ranging between 2195 kg/m^3 and 1924 kg/m^3 were obtained for the geopolymer mortars containing CR. As expected, the CR incorporation into the geopolymer mortar led to a decrease in the unit weight of the mixtures because of its lighter weight than the RS. The highest decrease of 14% was observed when the RS was substituted with the CR at 50%. The drying of the geopolymer mortar mixtures resulted in weight loss as is expected. There were decreases to be ranging from about 1.0% to 5.0% in the unit weights of the mortars after 1 day. On the other hand, after 3 days, re-

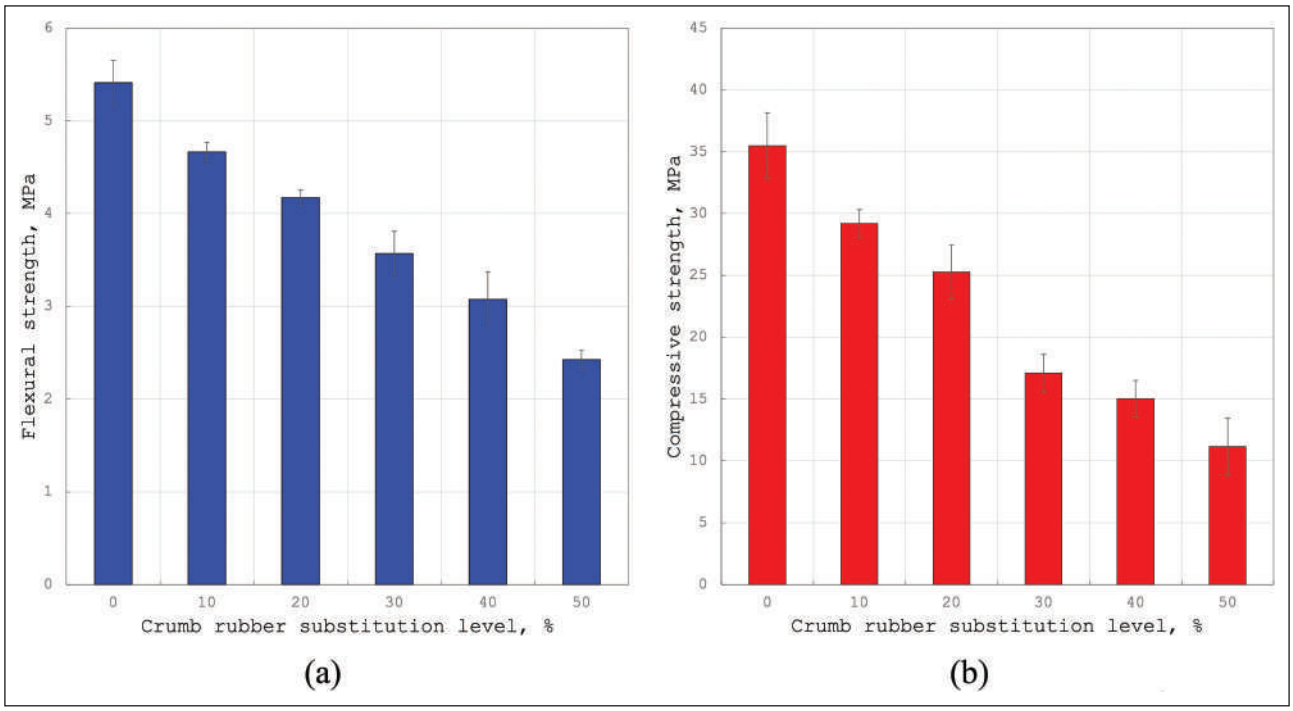

Figure 5. The variations in **(a)** flexural strength and **(b)** compressive strength of rubberized geopolymer mortars.

ductions between about 2.5% and 6.5% in the unit weights were observed. The lowest unit weight after the 3 days was obtained in the mixture produced with 50% CR as about 1820 kg/m^3 and on the same day, the control mixture had a unit weight of 2172 kg/m^3. TS EN 206-1 [32] regards the concrete having a unit weight (but oven-dry) of less than 2000 kg/m^3 and more than 800 kg/m^3 as lightweight concrete. Similarly, ACI Committee 213R-03 [33] classified the concretes as lightweight concrete when their unit weight (but air-dry) is less than 1950 kg/m^3. Since the geopolymer concretes (or mortars) have not been covered by any standard yet, these criteria can be taken into consideration to describe the geopolymer concretes (or mortars) based on the unit weight. In this context, it can be stated that the geopolymer mortar mixtures produced with 30%, 40%, and 50% CR can be definitely considered the lightweight geopolymer mortar when the 3-day unit weights were taken into consideration. Aslani et al. [16] and Wongsa et al. [19] characterized the geopolymer mortars incorporating crumb rubber manufactured in their studies as lightweight. Azmi et al. [34] reported a systematical reduction in the unit weight of the geopolymer concretes when the crumb rubber replacement level gradually increased from 0% to 20%. Besides, it should be stated that there are a limited number of studies in which the unit weight of the geopolymer mortar incorporating crumb rubber was investigated.

3.3. Flexural and Compressive Strengths

The variations occurring in flexural and compressive strengths of the geopolymer mortars because of the CR incorporation are shown in Figures 5a and 5b, respectively. The 3-day average flexural strength value of the control geopolymer mortar was about 5.41 MPa, and there was observed to be a systematical decrease in the average flexural strength of the mortars by substituting the RS with the CR and increasing the substitution level. The lowest 3-day average flexural strength value of 2.42 MPa was observed in the geopolymer mortar produced with a 50% CR substitution level. The reduction rates in the 3-day average flexural strength due to the CR incorporation were about 14%, 23%, 34%, 43%, and 55% when the substitution levels were 10%, 20%, 30%, 40%, and 50%, respectively. Wongsa et al. [19] investigated the properties of two types of geopolymer mortars: one was fully produced with RS and the other one was fully produced with CR. They reported a more than 75% reduction in the 28-day flexural strength when the RS was fully replaced with the CR. However, Zhong et al. [31] reported a slight increase in the flexural strength of the geopolymer mortar when the RS was replaced with the CR at the substitution level of 5% and a decrease after this substitution level.

Similarly, the compressive strength results revealed that incorporating the CR into the geopolymer mortar led to a decrease in the compressive strength. Also, increasing the CR substitution level yielded a systematic decrease in the compressive strength, see Figure 5b. The 3-day average compressive strength of the control geopolymer mortar was about 35.5% and incorporating 10% CR into the geopolymer mortar resulted in a nearly 18% decrease in the 3-day average compressive strength. Increasing the CR

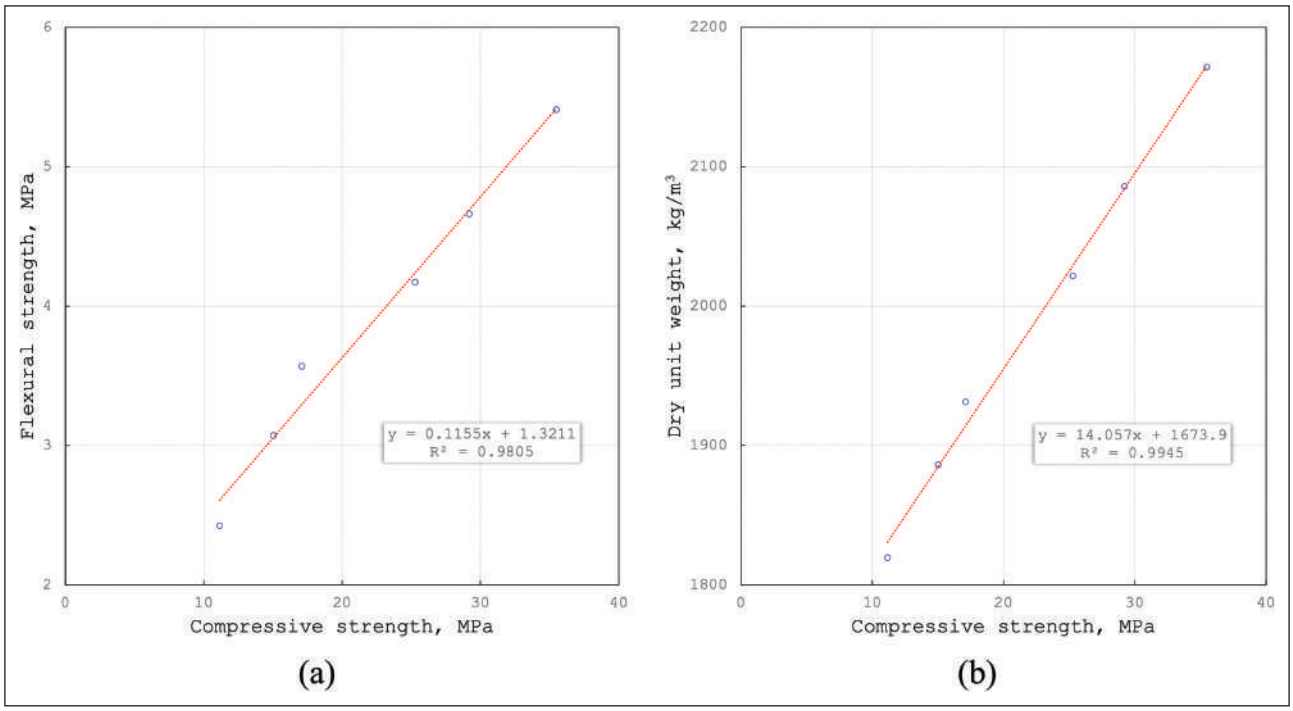

Figure 6. Correlation between **(a)** flexural and compressive strengths and **(b)** dry unit weight and compressive strength of rubberized geopolymer mortars.

substitution level from 10% to 50% diminished the compressive strength to 11.2 MPa. The results achieved from the study herein comply with the limited number of studies reported in the literature. For example, both Wongsa et al. [19] and Zhong et al. [31] reported a decrease in the 7-day and 28-day compressive strengths of the geopolymer mortar by substituting the natural sand with CR. In a similar manner, Azmi et al. [34] observed a nearly 65–75% decrease in the 7-day and 28-day compressive strengths at the CR substitution level of 20%.

One of the main reasons for the decrease in the strengths (both compressive and flexural) is that the interfacial transition zone occurring between geopolymer paste and rubber aggregate is larger than that occurring between the natural aggregate. Besides, the soft structure of the rubber aggregate will exhibit higher strain performance under loading compared to hardened geopolymer paste and natural aggregate. This means that in places where rubber aggregate is present, hardened geopolymer paste and/or natural aggregates will carry the most of the load, and the rubber aggregate will participate in the load-bearing role at even high strain levels, but at these strain levels, the hardened geopolymer paste has already cracked and the integrity of the mortar has deteriorated. Therefore, incorporating the rubber aggregate into the geopolymer mortar negatively influences its compressive strength.

Moreover, in Figure 6a, the correlation between the flexural and compressive strengths of the geopolymer mortars produced in the current study is presented. By taking into consideration the coefficient of determination (R^2) value given in this figure, it can be stated that there is a strong relationship and correlation between the flexural and compressive strengths of the geopolymer mortars of this study. A similar correlation was observed between the dry unit weight and compressive strength of the geopolymer mortars produced in this study as shown in Figure 6b. When the R^2 value given in this figure is considered, it can be stated that there is a directly proportional and strong relationship between the 3-day dry unit weight and compressive strength values.

3.4. UPV Values

The change in the UPV values of the geopolymer mortars depending on the CR substitution level is indicated in Figure 7a. The control mixture, which does not contain CR, had a UPV value of 3027 m/s. Since there is no qualifying scale for the cement-based and/or geopolymer mortars, the classification for the concrete given by Hwang et al. [35] can be used in this context to get an idea about the quality of the mortars produced in this study and to establish a relationship between the other engineering properties and UPV values. According to this classification, the geopolymer mortar produced in this study can be regarded as moderate-quality mortar. However, incorporating the CR into the geopolymer mortar caused decreases in the UPV values, correspondingly in the quality of mortar. The main reason behind this situation is the macro-scale porosity formations in the geopolymer mortar. Such porous structures in the

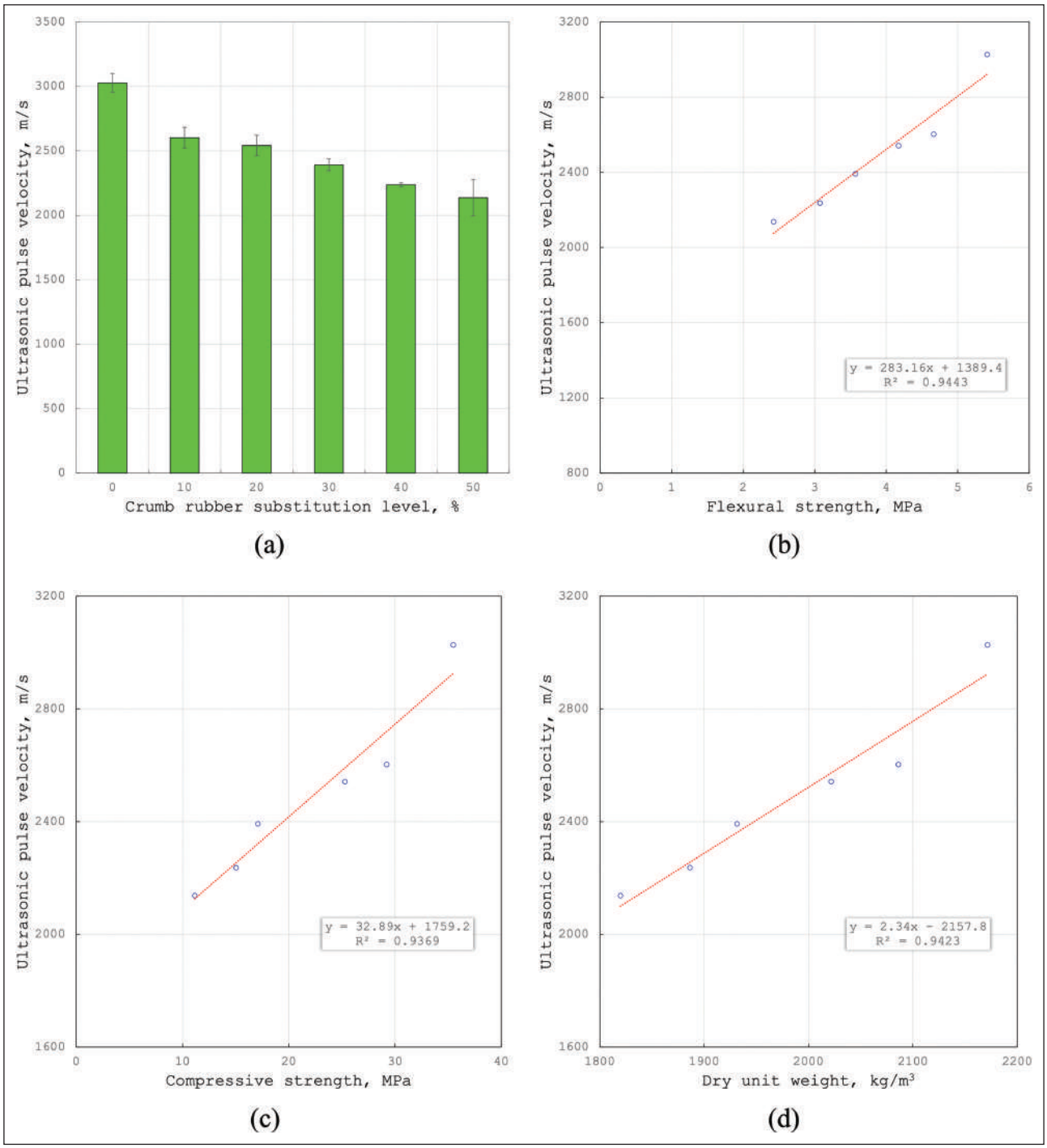

Figure 7. **(a)** Variation in UPV values of the geopolymer mortars due to the CR incorporation and the correlation between the UPV values and **(b)** flexural strength, **(c)** compressive strength, and **(d)** dry unit weight.

hardened mortar prevent and/or delay the transferring of the ultrasonic waves from the transmitter to the receiver. For this reason, there is to be a decrease in the UPV values. But it should be also stated that the decrease in UPV values of geopolymer mortar due to the CR incorporation may be also caused by the nature of the rubber. As it is well-known, the rubber material is a perfect isolation material for waves having any frequency. Therefore, the ultrasonic pulse waves may have been absorbed by the rubber particles during the transfer from the transmitter to the receiver. As can be seen in Figure 7a, the geopolymer mortars produced with CR had UPV values of less than 3000 m/s and more than 2100 m/s. About 30% reduction in the UPV value of geopolymer mortar was observed when the 50% of RS was substi-

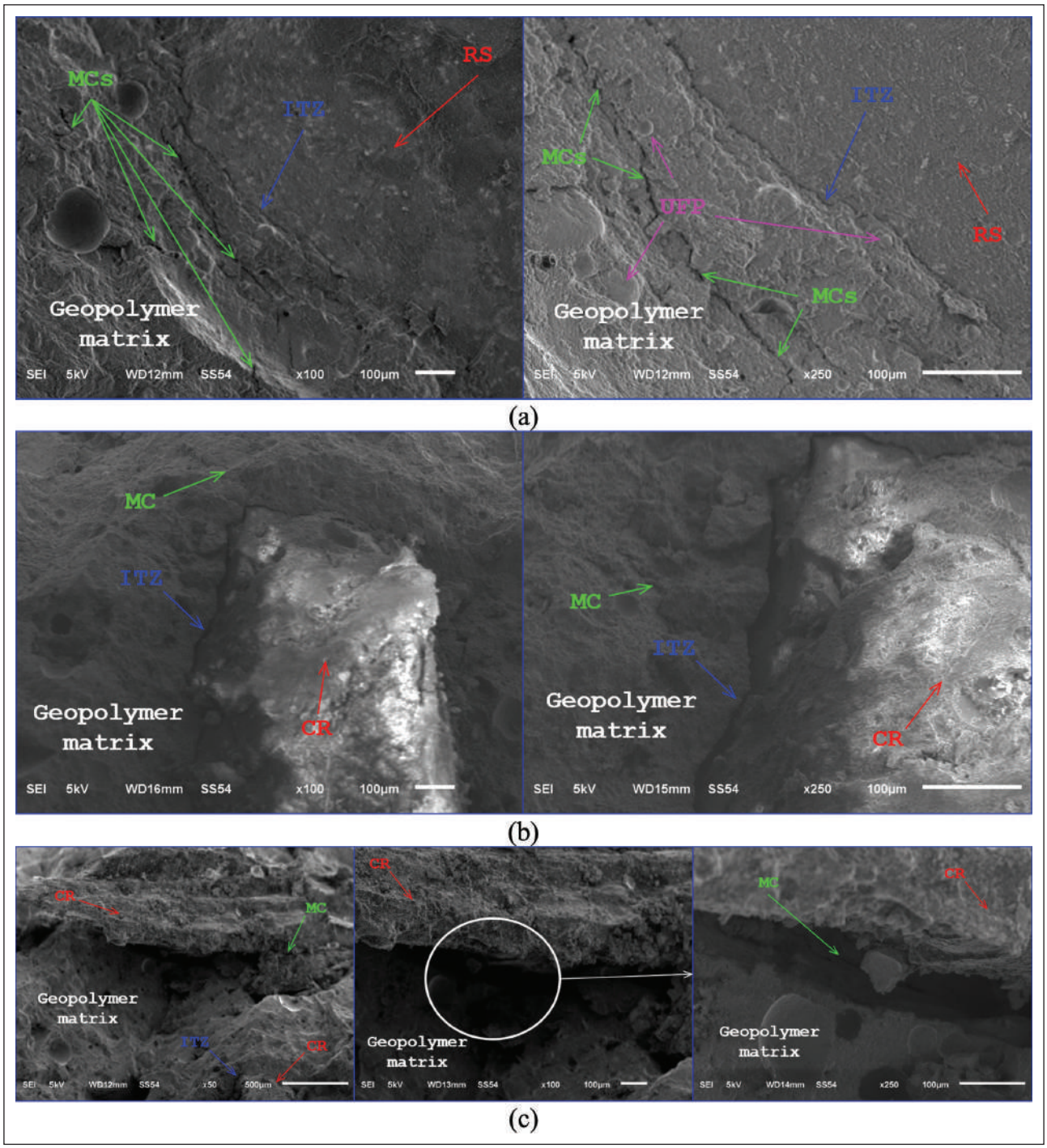

Figure 8. SEM images of **(a)** control geopolymer mortar mixture and **(b)** and **(c)** rubberized geopolymer mortar mixtures.

tuted with CR. In this context, the rubberized geopolymer mortars produced in the present study can be considered poor-quality mortars with respect to the classification presented by Hwang et al. [35].

On the other hand, in order to establish the relationship between the engineering properties of the geopolymer mortars and their UPV values, a binary correlation was used. In this regard, Figures 7b, 7c, and 7d indicate the correlations between UPV values and flexural strength, compressive strength, and dry unit weight, respectively. When the correlations between the UPV values and the aforementioned properties of the geopolymer mortars are investigated, it will be seen that there are strong relationships with the R2 values of more than 0.93 between the UPV values and the flexural strength, compressive strength, and dry unit weight of the geopolymer mortars. This does not only show how

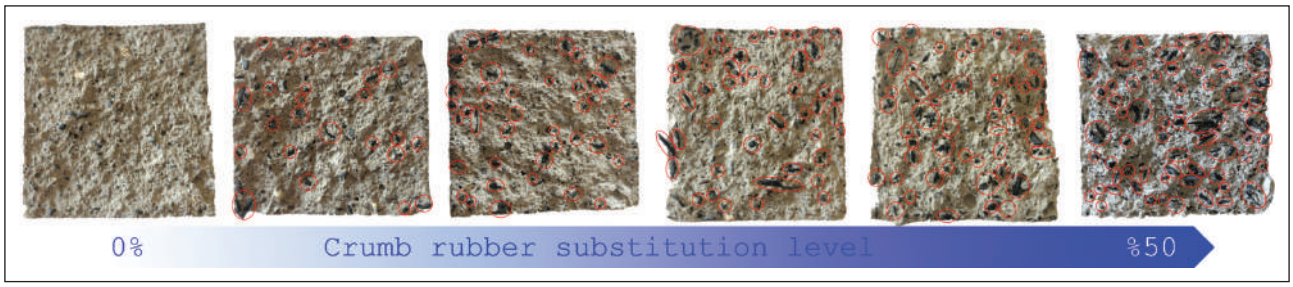

Figure 9. Cross-sections of hardened geopolymer mortar mixtures.

the interactive relations between these properties are well but also indicates that the experimental program conducted in this research has been properly carried out.

3.5. SEM Analysis and Visual Observation

Here, the SEM images of both control and rubberized geopolymer mortars are presented and discussed. Two SEM images (x100 and x250 zoom-in) of the control geopolymer mortar are given in Figure 8a. Similarly, the SEM images presented in the same zoom-in of the rubberized geopolymer mortar are given in Figure 8b; however, in addition to this, three SEM images (x50, x100, and x250 zoom-in) of another rubberized geopolymer mortar are presented in Figure 8c. When the SEM images of the control mixture are investigated, a distinct ITZ between the geopolymer paste and RS particle (as shown with blue arrows) can be noticed. Besides, there are detected to be microcracks (as shown with green arrows) and unreacted and partially reacted fly ash particles on the geopolymer matrix (as indicated with pink arrows). In a similar way, when the SEM images of rubberized geopolymer mortars are investigated, more distinct ITZs between the geopolymer paste and CR particles will be sighted. The ITZ between the CR and the geopolymer paste is more distent in the SEM pictures than it is between the RS and the geopolymer paste. Such distinct ITZ formations decrease the interlock between the particle and paste, thus resulting in lower mechanical performances. Furthermore, SEM scans revealed certain gap areas around the CR particles (Fig. 8c). Such gap regions around the fine particles reduce the permeability resistance of the geopolymer mortars.

In addition to the observation based on the microscopic scale, the CR distributions on the cross-section of the geopolymer mortars were visually observed. One of the difficulties faced during the production of such types of mortars is the bleeding in the mortar and relevantly the inhomogeneous distribution of rubber particles and segregation issues. Since the CR particles are lighter than the geopolymer paste, they have a tendency to move up, leading to the separation of the geopolymer paste and CR particles. As a result, in such types of materials, there occurs a layer consisting of CR particles and paste at the top of the cross-section, and there occurs another paste layer immediately below this layer. Such problems need a very sensitive mixture design. Figure 9 is presented to display the bleeding detection and distribution of rubber particles on the cross-section of mortars produced in the present study. When the cross-sections of the geopolymer mortars illustrated in this figure are investigated, it will be seen that these layers did not occur in any mortar mixtures, and besides, the visually detected CR particles are homogeneously distributed on the mortar cross-sections. In other words, it can be stated that no bleeding and relevant segregation problems were observed in the mortar mixtures produced in the current study.

4. CONCLUSIONS

Based on the findings given above, the following conclusions can be done:

- The flowability of geopolymer mortar was not affected by CR incorporation and increasing its substitution level.
- Substituting the RS with CR and increasing its level systematically decreased the unit weight of the geopolymer mortar. After a 30% substitution level, lightweight geopolymer mortar was achieved. As the geopolymer mortars dried, there was a unit weight loss ranging from 1% to 5% for the first day and ranging from 0.5% to 2.5% for the following two days.
- Incorporating the CR into the geopolymer mortar led to a reduction in both flexural and compressive strengths.
- UPV values of the geopolymer mortars decreased by incorporating the CR since the CR particles cause a porous structure in the hardened mortar and have a wave absorption nature.
- The binary correlation results revealed that there is a strong relationship between the investigated engineering properties.
- SEM images showed that the ITZ occurring between the CR particles and geopolymer matrix is more distinct than that occurring between the RS particles and geopolymer matrix.
- Visually inspection of the cross-sections of the rubberized geopolymer mortars indicated that no bleeding and relevant segregation problems occurred and the CR particles are homogeneously distributed on the mortar cross-sections.

DATA AVAILABILITY STATEMENT

The author confirm that the data that supports the findings of this study are available within the article. Raw data that support the finding of this study are available from the corresponding author, upon reasonable request.

CONFLICT OF INTEREST

The author declare that they have no conflict of interest.

FINANCIAL DISCLOSURE

The author declared that this study has received no financial support.

PEER-REVIEW

Externally peer-reviewed.

REFERENCES

[1] Ipek, S., Diri, A., & Mermerdas, K. (2021). Recycling the low-density polyethylene pellets in the pervious concrete production. *Journal of Materials Cycle and Waste Management*, 23, 272–287. [CrossRef]

[2] Holka, H., & Jarzyna, T. (2017). Recycling of car tires by means of waterjet technologies. *AIP Conference Proceedings* 1822, Article 020008. [CrossRef]

[3] Siddika, A., Al Mamun Md, A., Alyousef, R., Amran, YHM., Aslani, F., & Alabduljabbar, H. (2019). Properties and utilizations of waste tire rubber in concrete: A review. *Construction and Building Materials*, 224, 711–731. [CrossRef]

[4] Ipek, S., & Mermerdas, K. (2020). *Studying the impact of crumb rubber on the setting time of self-compacting mortar*. Proceeding Books: International Conference on Engineering & Natural Sciences-9, November 13- 15, Ankara-Turkey.

[5] Karger-Kocsis, J., Meszaros, L., & Barany, T. (2013). Ground tyre rubber (GTR) in thermoplastics, thermosets, and rubbers. *Journal of Materials Science*, 48(1), 1–38. [CrossRef]

[6] THBB. *Dünyada sektör*. (2021, 20 October). https://www.thbb.org/sektor/dunyada-sektor/ [Turkish]

[7] Hilburg, J. (2021, 20 October). *Concrete production produces eight percent of the world's carbon dioxide emissions*, The Architects' Newspaper. https://www.archpaper.com/2019/01/concrete-production-eight-percent-co2-emissions

[8] Güneyisi, E. (2010). Fresh properties of self-compacting rubberized concrete incorporated with fly ash. *Materials and Structures*, 43, 1037–1048. [CrossRef]

[9] Dondi, G., Tataranni, P., Pettinari., M., Sangiorgi, C., Simone, A., & Vignali, V. (2014). Crumb Rubber in cold recycled bituminous mixes: comparison between traditional crumb rubber and cryogenic crumb rubber. *Construction and Building Materials*, 68, 370–375. [CrossRef]

[10] Davidovits, J. (1994). Properties of geopolymer cements. in Proceedings First International Conference on Alkaline Cements and Concretes, Kiev, Ukraine, 131–149.

[11] Palomo, A., Blanco-Varela, M. T., Granizo, M. L., Puertas, F., Vazquez, T., & Grutzeck, M. W. (1999). Chemical stability of cementitious materials based on metakaolin. *Cement and Concrete Research*, 29(7), 997–1004. [CrossRef]

[12] Ma, C. K., Awang, A. Z., & Omar, W. (2018). Structural and material performance of geopolymer concrete: a review. *Construction and Building Materials*, 186, 90–102. [CrossRef]

[13] Mermerdas, K., Ipek, S., & Mahmood, Z. (2021). Visual inspection and mechanical testing of fly ash-based fibrous geopolymer composites under freeze-thaw cycles. *Construction and Building Materials*, 283, Article 122756. [CrossRef]

[14] Turner, L. K., & Collins, F. G. (2013). Carbon dioxide equivalent (CO2-e) emissions: A comparison between geopolymer and OPC cement concrete. *Construction and Building Materials*, 43, 125–130. [CrossRef]

[15] Aly, A. M., El-Feky, M. S., Kohail, M., & Nasr, E. S. A. R. (2019). Performance of geopolymer concrete containing recycled rubber. *Construction and Building Materials*, 207, 136–144. [CrossRef]

[16] Aslani, F., Deghani, A., & Asif, Z. (2020). Development of lightweight rubberized geopolymer concrete by using polystyrene and recycled crumb-rubber aggregates. *Journal of Materials in Civil Engineering*, 32(2), Article 04019345. [CrossRef]

[17] Nis, A., Eren, N. A., & Cevik, A. (2022). Effects of recycled tyre rubber and steel fibre on the impact resistance of slag-based self-compacting alkali-activated concrete. *European Journal of Environmental and Civil Engineering*, 2022. [Epub ahead of print]. doi:10.1080/19648189.2022.2052967[CrossRef]

[18] Eren, N. A., Alzeebaree, R., Cevik, A. Nis, A., Mohammedameen, A., & Gulsan, M.E. (2021). The effects of recycled tire rubbers and steel fibers on the performance of self-compacting alkali activated concrete. *Periodica Polytechnica Civil Engineering*, 65(3), 890–900. [CrossRef]

[19] Wongsa, A., Sata, V., Nematollahi, B., Sanjayan, J., & Chindaprasirt, P. (2018). Mechanical and thermal properties of lightweight geopolymer mortar incorporating crumb rubber. *Journal of Cleaner Production*, 195, 1069–1080. [CrossRef]

[20] Moghaddam, S. C., Madandoust, R., Jamshidi, M., & Nikbin, I. M. (2021). Mechanical properties of fly ash-based geopolymer concrete with crumb rubber and steel fiber under ambient and sulfuric acid conditions. *Construction and Building Materials*, 281,

Article 122571. [CrossRef]
[21] ASTM C311/C311M-18. (2018). *Standard test methods for sampling and testing fly ash or natural pozzolans for use in portland-cement concrete*. ASTM International.
[22] ASTM C618-19. (2019). *Standard specification for coal fly ash and raw or calcined natural pozzolan for use in concrete*. ASTM International.
[23] ASTM C136/C136M-19. (2019). *Standard test method for sieve analysis of fine and coarse aggregates*. ASTM International.
[24] ASTM C33. (2018). *Standard specification for concrete aggregates*. ASTM International.
[25] Ekmen, S., Mermerdas, K., & Algin, Z. (2021) Effect of oxide composition and ingredient proportions on the rheological and mechanical properties of geopolymer mortar incorporating pumice aggregate. *Journal of Building Engineering*, 34, Article 101893. [CrossRef]
[26] ASTM C1437-20. (2020). Standard test method for flow of hydraulic cement mortar. ASTM International.
[27] ASTM C138/C138M-17a. (2017). Standard test method for density (unit weight), yield, and air content (gravimetric) of concrete. ASTM International.
[28] ASTM C348-20. (2020). *Standard test method for flexural strength of hydraulic-cement mortars*. ASTM International.
[29] ASTM C109/C109M-20b. (2020). *Standard test method for compressive strength of hydraulic cement mortars (using 2-in. or [50 mm] cube specimens)*. ASTM International.
[30] ASTM C597-16. (2016). *Standard test method for pulse velocity through concrete*. ASTM International.
[31] Zhong, H., Poon, E. W., Chen, K., & Zhang, M. (2019). Engineering properties of crumb rubber alkali-activated mortar reinforced with recycled steel fibres. *Journal of Cleaner Production*, 238, Article 117950. [CrossRef]
[32] TS-EN 206-1. (2000). *Concrete Part 1*. Turkish Standard Institute.
[33] ACI Committee 213R. (2003). *American Concrete Institute. Guide for structural lightweight aggregate concrete. Manual of Concrete Practice*. Farmington Hills, Michigan.
[34] Azmi, A. A., Abdullah, M. M. B., Ghazali, C. M. R., Sandu, A. V., & Hussin, K. (2016). Effect of crumb rubber on compressive strength of fly ash based geopolymer concrete. *MATEC Web of Conferences*, 78, Article 01063. [CrossRef]
[35] Hwang, C. L., Bui, L. A. T., Lin, K. L., & Lo, C. T. (2012). Manufacture and performance of lightweight aggregate from municipal solid waste incinerator fly ash and reservoir sediment for self-consolidating lightweight concrete. *Cement and Concrete Composites*, 34(10), 1159–1166. [CrossRef]

Journal of Sustainable Construction Materials and Technologies
Web page info: https://jscmt.yildiz.edu.tr
DOI: 10.47481/jscmt.1106786

JSCMT
Journal of Sustainable Construction Materials and Technologies

Research Article

An investigation on effect of aggregate distribution on physical and mechanical properties of recycled aggregate concrete (RAC)

Hasan DİLBAS*

Department of Civil Engineering, Van Yüzüncü Yıl University, Van, Türkiye

ARTICLE INFO

Article history
Received: 21 April 2022
Accepted: 17 June 2022

Key words:
Aggregate gradation curve, entropy method, mechanical properties, physical properties, recycled aggregate, TOPSIS

ABSTRACT

The aim of this study was to optimize the aggregate gradation curve (AGC) for recycled aggregate concrete (RAC). Five different gradation curves such as three AGCs defined in TS802 (A16, B16, C16) and two proposed AGCs named G1 and G2 were employed. The concretes designed with AGCs consist of different mortar phases and included coarse aggregates such as coarse NA and coarse RA. Thus, three stages were considered and were progressed in the experimental program: the 1st stage included the evaluation of the properties of the mortars, and the effect of AGC on the mortar phase of the concrete was investigated. The mortars had the components of concrete such as cement, water, and fine aggregate (<4 mm) representing the mortar phase of concretes. The 2nd stage was the evaluation of the test results of the fresh and the hardened concretes and, in this stage, the effect of AGC on the properties of concrete was diagnosed. Also, an additional stage was the 3rd stage and was made on the experimental data to define the weights of the parameters of the concretes by using the Entropy Method and to select the best AGC with the help of a decision-support instrument, TOPSIS. Separately evaluation of the test results showed that C16 resulted in a durable RAC in terms of low water absorption capacity with high compressive strength. Besides, the results of the Entropy Method presented exciting findings, and the coarse aggregate ratio in the mix was found to be the most effective parameter among the investigated parameters. When all parameters were investigated together using the TOPSIS method, the best AGC was found as G2 for RAC, but A16 can be preferred instead of G2 according to the similar TOPSIS scores. In addition, this paper opens a path in the literature regarding the need for the development of AGC in RAC and further investigations should be made.

Cite this article as: Dilbas, H. (2022). An investigation on effect of aggregate distribution on physical and mechanical properties of recycled aggregate concrete (RAC). *J Sustain Const Mater Technol*, 7(2), 108–118.

1. INTRODUCTION

The sustainability approach gains importance around the world day by day and seems to be the savior of future resources. Recycling of construction wastes, especially recycling of waste concrete (WC), is one of the sustainability approaches, and sustainable economic growth and saving resource policies, nowadays, are on the policymakers' agenda [1].

***Corresponding author.**
*E-mail address: hasandilbas@yyu.edu.tr

Regulations on recycled aggregate (i.e., Technical Code for Application of Recycled Aggregate Concrete (DG/TJ07-008) [2]) and higher consumption advisory policies (i.e., Directive 2008/98/EC [3]) are some of the actions on WC. However, although many regulations have been made, the construction and demolition waste (CDW) amount has been increased due to urban renewals [4–8], natural disasters [9, 10] and wars [11] especially happened in the recent decades and 1950s. The solution to the mentioned problem by advanced techniques and approaches was an obligation and a necessity. The utilization of a higher amount of WC in a widely used material such as concrete sounds good and inspires many researchers to evaluate the effect of the use of WC as recycled aggregate (RA) in concrete [12, 13]. However, the most important criterion preventing the usage of RA in new concrete is the higher water absorption capacity of RA compared to natural aggregate (NA) [14] and it decreases not only the physical and mechanical performance of recycled aggregate concrete (RAC) but also the durability performance of RAC [15]. Thus, some measures (use of mineral additions [16], mixing methods (i.e., double-mixing method [17] and triple mixing method [18]), RA treatment methods (Shi et al., 2016), etc.) [19] have been developed and suggested by researchers in their studies. At this point, it was commonly stated that the use of 20~30% RA had a minor effect on the properties of RAC [20] and treatment may have increased the optimum utilization ratio of RA (i.e., up to 60% RA treated with optimized ball mill method [10, 21–24] and up to 50% RA with new combination method [25]). Thus, it is meaningful to consider RA with a treatment method instead of the use of RA in the mix only and it has advantages, as expected.

Besides, although many papers focused on the effect of RA on concrete properties increasing the optimum ratio of RA in the mix, few papers aimed to present the effect of design methods especially considering the aggregate properties (aggregate size, particle packing, etc.) (i.e., [26–30]). Duan et al. [31] proposed a modified design method for RAC, and the scatter of the compressive strength and the porosity of RAC were investigated. The size of RA such as 5–10 mm, 10–20 mm, and 5–20 mm was considered to have an aggregate gradation effect on RAC and aggregate gradation re-adjustment was suggested stating satisfactory test results [31]. Bui et al. [25] developed a new combination method and replaced natural aggregate (NA) with RA in consideration of the different sizes of aggregates, and the methodology resulted in a new and increased optimum ratio as 50%. McGinnis et al. [32] investigated the gradation effect of RA considering the average particle size of RA such as ASTM #8 (1.18–12.5 mm) and ASTM #57 (2.36–37.5 mm) and also used the literature data such as INDOT #8. It was found that the gradation impact of coarse NA and RA was similar, and a smaller average aggregate size made RAC stronger and also stiffer [32]. Based on the experiments of concretes including NA, it was also found that "5–10–14–18" mm and "5–10–18–22" mm bands result in better concrete in consideration of compressive strength and workability [33]. Although the studies considered the aggregate size effect and also gradation effect on the properties of RAC [25, 31, 32], the effect of AGC on the properties of RAC was rarely studied. The theoretical research (i.e., particle packing, random aggregate distribution in a unit volume/section) and author examinations on this topic showed that AGC affected the aggregate concentration of unit volume. Also, it was stated that the decrease of aggregate concentration in concrete decreased the mechanical performance of concrete [34] and it should have been considered in the mix design.

To fill the gap in the literature, optimization of AGC considering the standard curves such as A16-B16-C16 compatible with TS 802 [35] and two proposed curves (G1 and G2) were examined in consideration of the properties of the mortar phases of concrete and the concretes such as NACs and RACs. The concretes consisted of different mortar phases (M-G1, M-A16, M-B16, M-C16, and M-G2) due to the different AGCs and, also coarse aggregates such as coarse NA and coarse RA. Thus, three stages were considered and were progressed in the experimental program: The 1st stage included the evaluation of the properties of the mortar phase of the concretes, and the effect of AGC on the mortars was investigated. The mortars include the components of concrete representing the mortar phase of concretes. The 2nd stage was the evaluation of the test results of concretes such as the air content of fresh concrete, the density of the hardened state of concrete, the water absorption, and the compressive strength, and in this stage, the effect of AGC on the fresh and the hardened properties of concrete were determined. Also, an additional stage was the 3rd stage and was made on the findings and the parameters to define the weights of the parameters of the concretes by using the Entropy Method and to select the best AGC with the help of a decision-support instrument, TOPSIS.

2. MATERIAL AND METHOD

2.1. Materials

General-purpose CEM I 42.5 R compatible with TS EN 197-1 was utilized in the mixes (Table 1).

In the mixes, coarse NAs and RAs were employed. NA was a crushed calcareous stone. River sand (0–2 mm) and crushed stone (0–4 mm) as a fine aggregate were utilized (Table 2). RA was sourced from low strength WC (<20 MPa) [36]. Superplasticizer was used to enhance the low workability of fresh concretes (Table 3). S2 slump class (50–90 mm) was selected for whole mixes.

2.2. Method

In the design of concrete, TS 802's AGCs for maximum aggregate size of 16 mm (A16, B16, and C16) [35] and two proposed AGCs (G1 and G2) were considered (Table 4). AGC development studies usually have been dependent on Fuller's Curve, and AGC was developed for concrete mixtures to achieve optimum performance. The aim of the proposal of

Table 1. Properties of cement

Contents	Cement
SiO_2 (%)	18.9
CaO (%)	64.7
SO_3 (%)	3.42
Al_2O_3 (%)	4.8
Fe_2O_3 (%)	3.4
MgO (%)	1.4
K_2O (%)	0.4
Na_2O (%)	0.7
Density (g/cm^3)	3.11
Chlorine ratio (%)	0.0241
Specific surface area (m^2/kg)	3840
Loss on ignition (%)	1.82
Activity index (%)	–

Table 2. The properties of natural aggregates and recycled aggregates

Notation	Density, g/cm^3	Water absorption %	LA abrasion value %	Residual content %
Sand	2.56	0.64	–	–
Crushed sand	2.62	0.85	–	–
NA (11-16 mm)	2.70	0.32	26	–
NA (4-11 mm)	2.65	0.42	–	–
RA (11-16 mm)	2.21	8.10	46	45
RA (4-11 mm)	2.23	8.90	–	54

Table 3. The properties of superplasticizer

Content	Superplasticizer
Structure of material	Polycarboxylic ether
Color	Amber
Density (kg/l)	1.08-1.14
Alkaline ratio (%)	<3
Chlorine ratio (%)	<0.1

G1 and G2 gradation curves was to be observed the effect of non-consideration of the gradation curves given in TS 802. The ingredients of the designed mixtures were presented in Table 5. The specimens were produced under standard laboratory conditions according to TS EN 12390-2 [37]. Then, the freshly produced mixtures were cast in the molds and 15×15×15 cm cubic specimens were maintained in the molds for 24 hours for hardening purposes. Also, the fresh concrete was sieved through a 4 mm mesh sieve and the passing mixture was placed in 4x4x16 cm prismatic molds when the concretes including NA were produced. Thus, the mortar phases of the concretes were obtained. The specimens were cured in 22±2 °C water for 28 days according to TS EN 12390-2 [37]. At the age of 28 days, the experiments such as water absorption, density, and compressive strength tests for hardened concrete specimens, and bending and compressive strength tests for the mortars were conducted and compatible with the related standards [38–40].

The strength class of RACs and natural aggregate concretes (NACs) are determined according to Eq. 1–2 detailed in TS EN 206-1+A2 [41]:

$$f_{c,\,avg} \geq f_{ck} + 1.0 \quad (1)$$

$$f_{c,\,min} \geq f_{ck} - 4.0 \quad (2)$$

Here, f_{ck} is the characteristic compressive strength of group (MPa), $f_{c,\,avg}$ is the average compressive strength of group (MPa), and $f_{c,\,min}$ is the minimum compressive strength of group (MPa).

2.2.2. Entropy Method

The Entropy Method [42] was used to evaluate the weight factors of the experimental findings such as density, water absorption, coarse aggregate ratio, air content of fresh concrete, natural aggregate concentration, and fineness modulus and compressive strength. According to the method, the following calculation steps are considered.

If *i*; 1, 2, 3, …, m are alternatives, *j*; 1, 2, 3, …, n are evaluation criteria, x_{ij}=the value of ith alternative at jth evaluation criterion,

$$X = \begin{bmatrix} x_1(1) & \cdots & x_1(n) \\ \vdots & \ddots & \vdots \\ x_m(1) & \cdots & x_m(n) \end{bmatrix} \text{ and i = 1, 2, …, m and j= 1, 2, …, n} \quad (3)$$

Here, X is the matrix included alternatives and criteria. The first calculation is the normalization of the values of X matrix as follows:

$$p_{ij} = \frac{x_{ij}}{\sum_{j=1}^{n} x_{ij}} \quad (4)$$

Here, p_{ij} is the normalized value of ith alternative and jth criterion. In this method, the value of entropy E_i of the ith alternative is defined as [42]:

$$E_i = -\frac{\sum_{j=1}^{n} p_{ij} \cdot \ln(p_{ij})}{\ln n} \quad (5)$$

Here, E_i is between 0 and 1. Then, the determination of weight w_i can be done as:

$$w_i = \frac{1 - E_i}{\sum_{j=1}^{n} (1 - E_i)} \quad (6)$$

Also, weight w_i is between 0 and 1, and the sum of w_i is 1.

Table 4. Aggregate gradation curve details for standard curves such as A16, B16, and C16 [35], and proposed curves such as G1 and G2

Sieve size, mm	G1	TS 802			G2
		C16 (Upper AGC)	B16 (Ideal AGC)	A16 (Lower AGC)	
0.125	13	11	7	3	2
0.25	27	20	13	6	4
0.5	40	30	20	10	6
1	54	41	28	15	10
2	67	52	37	22	15
4	78	64	49	33	20
8	91	77	63	48	30
11.2	95	90	79	68	55
16	99	99	92	85	79
32	100	100	100	100	100

Table 5. Mix design of concretes

Parameters	Natural aggregate concretes					Recycled aggregate concretes				
Mixes	NAC-G1	NAC-C16	NAC-B16	NAC-A16	NAC-G2	RAC-G1	RAC-C16	RAC-B16	RAC-A16	RAC-G2
Components										
River Sand (0–2 mm), kg/m³	759	541	380	199	126	759	541	380	199	126
Crushed Stone (0–4 mm), kg/m³	808	698	533	349	276	808	698	533	349	276
Coarse Aggregatea (4–11 mm), kg/m³	207	489	546	716	603	169	400	447	586	494
Coarse Aggregate (11–16 mm), kg/m³	56	111	388	590	850	47	93	326	497	715
Cement, kg/m³	350	350	350	350	350	350	350	350	350	350
Water, kg/m³	175	175	175	175	175	175	175	175	175	175
Mix details										
Natural aggregate concentration, %	70.2	70.1	70.1	69.9	69.9	64.3	56.4	49.3	41.0	38.3
Attached old mortar content, %	0	0	0	0	0	6.0	13.7	20.8	28.9	31.6
Fresh properties										
Slump class	S2	S2	S2	S2	S2	S2	S2	S2	S2	S2
Air content of fresh concrete, %	1.1	1.3	1.3	1.4	1.5	1.3	1.7	1.8	2.0	1.7

2.2.3. Decision-Making Method: Technique for Order Preference by Similarity to Ideal Solution (TOPSIS)

Technique for Order Preference by Similarity to Ideal Solution (TOPSIS) is one of the multi-criteria decision-making methods [10, 24, 43–47]. The method works with many matrixes and the data is entered in the decision matrix in the first part. Also, it goes on objectively and, in the progress the method forms positive and negative ideal solutions. However, only weights of the criteria are subjectively formed in the system and the user selects the weighting coefficients for each data.

Decision matrix includes alternative values with i×j dimensions. Lines in the matrix are decision points and columns in the matrix are factors (Eq. 7).

$$A_{ij} = \begin{bmatrix} a_{11} & \cdots & a_{1j} \\ \vdots & \ddots & \vdots \\ a_{i1} & \cdots & a_{ij} \end{bmatrix} \quad (7)$$

Table 6. The test results of mortars

Notations	Air content of fresh mortar, %	Bending strength, MPa			Compressive strength, MPa		
		Average	Minimum	Standard deviation	Average	Minimum	Standard deviation
M-G1	2.4	9.17	9.07	0.12	45.2	43.0	1.57
M-A16	3.0	9.63	9.26	0.32	46.0	44.8	0.98
M-B16	3.1	9.09	8.60	0.43	44.8	43.2	1.40
M-C16	3.5	8.72	7.52	1.15	46.7	43.4	2.16
M-G2	3.7	8.53	8.16	0.33	44.0	43.0	0.65

Table 7. The test results of concretes

Notations	C_{NA}, %	C_{CNA}, %	I_m, mm	A_{fresh}, %	d, g/cm³	WA, %	f_c, MPa			
							Mean	Min.	Std. Dev.	Str. Class
NAC-G1	70.2	14	3.36	1.1	2.26	3.1	43.1	41.6	1.56	C30/37
NAC-C16	70.1	32	4.16	1.3	2.32	3.0	44.1	43.2	0.95	C30/37
NAC-B16	70.1	50	5.12	1.3	2.36	2.5	50.2	49.8	0.34	C35/45
NAC-A16	69.9	70	6.10	1.4	2.38	3.1	53.6	52.7	0.77	C40/50
NAC-G2	69.9	78	6.79	1.5	2.41	3.2	46.5	43.7	2.57	C35/45
RAC-G1	63.6	14	3.36	1.3	2.18	3.5	35.9	34.4	1.30	C25/30
RAC-C16	56.8	32	4.16	1.7	2.22	3.5	38.7	38.0	0.93	C30/37
RAC-B16	49.7	50	5.12	1.8	2.21	3.9	37.4	37.0	0.51	C30/37
RAC-A16	42.0	70	6.10	2.0	2.21	4.3	34.8	33.7	1.42	C25/30
RAC-G2	38.8	78	6.79	1.7	2.23	4.5	34.2	33.5	0.86	C25/30

C_{NA}: Ratio of natural aggregate volume to total volume; C_{CNA}: Coarse aggregate volume to total aggregate volume; I_m: Fineness modulus; A_{fresh}: Air content of fresh concrete; d: Density of hardened concrete; WA: Water absorption; f_c: Compressive strength.

Then, normalized matrix is formed considering decision matrix elements (a_{ij}) (Eq. 8–9).

$$N_{ij} = \frac{a_{ij}}{\sqrt{\sum_{i=1}^{n} a_{ij}^2}} \quad (i = 1,2,3,\dots,m \; ve \; j = 1,2,3,\dots,n) \tag{8}$$

$$N_{ij} = \begin{bmatrix} n_{11} & \cdots & n_{1j} \\ \vdots & \ddots & \vdots \\ n_{i1} & \cdots & n_{ij} \end{bmatrix} \tag{9}$$

The weighting coefficients are added to normalized matrix (Eq. 10).

$$V_{ij} = \begin{bmatrix} w_1 \times n_{11} & \cdots & w_n \times n_{1j} \\ \vdots & \ddots & \vdots \\ w_1 \times n_{i1} & \cdots & w_n \times n_{ij} \end{bmatrix} \rightarrow V_{ij} = \begin{bmatrix} v_{11} & \cdots & v_{1j} \\ \vdots & \ddots & \vdots \\ v_{i1} & \cdots & v_{ij} \end{bmatrix} \tag{10}$$

According to the problem condition, positive and negative ideal solution values are found considering maximization and minimization (Eq. 11–14). Positive ideal solution values:

$$A^+ = \{(max_i \, v_{ij})\} \tag{11}$$

$$A^+ = \{v_1{}^+, v_2{}^+, \dots, v_n{}^+\} \tag{12}$$

where, A^+ matrix includes maximum values for each column. Negative ideal solution values:

$$A^- = \{(min_i \, v_{ij})\} \tag{13}$$

$$A^- = \{v_1{}^-, v_2{}^-, \dots, v_n{}^-\} \tag{14}$$

where, A^+ matrix includes minimum values for each column. Then the distance from alternatives to negative and positive ideal solutions is calculated (Eq. 15–16). The distance to positive ideal solution:

$$S_i^+ = \sqrt{\sum_{j=1}^{n} \left(v_{ij} - v_j^+\right)^2} \tag{15}$$

The distance to negative ideal solution:

$$S_i^- = \sqrt{\sum_{j=1}^{n} \left(v_{ij} - v_j^-\right)^2} \tag{16}$$

At the last part, calculation of the relative proximity to the ideal solution is done for alternatives and the values vary between 0 and 1 (1 is absolute positive ideal solution) (Eq. 17).

$$G_i^* = \frac{S_i^-}{S_i^- + S_i^+} \quad (17)$$

3. Results and Discussion

The test results were properly evaluated in the separate sections. In this paper, the effect of AGC on the properties of mortars and the properties of concretes were investigated. The concretes designed by five AGCs such as G1, 16, B16, C16, and G2 consisted of the mortar phases such as M-G1, M-A16, M-B16, M-C16, and M-G2, respectively, and also coarse NA and RA. Thus, three stages were conducted to assess the properties of the mortars and concretes and select the best mix. The test results of the mortars and concretes are given in Tables 6 and 7, respectively.

3.1. The Results of The Stages

The stages of this study have separated evaluation parts as given below. Accordingly, the first stage included the evaluation of the strengths of the mortars in consideration of the effect of AGCs on the mortar phases of the concretes. The mortars included some components of concrete (i.e., cement, water, fine aggregate, admixture, and not coarse aggregate) representing mortar phase of concrete. The second stage was on the test results of concretes (i.e., the air content of fresh concrete, the density of the hardened state of concrete, water absorption, and compressive strength) with fruitful comments, and evaluations. In the third stage, an evaluation was made as an additional stage on the experimental data to select the best AGC for RAC by using a decision-making instrument, it was TOPSIS.

3.1.1. Results of the First Stage of the Experimental Program

The results of the mortars were given in Table 6. The mortar phase was the same for NAC and RAC if the same aggregate distribution curve was used. It has been observed in this study that the strength properties of mortars were dependent on the AGC. it has been determined that the bending strength of mortars decreased as they were changed from the upper aggregate distribution curve to the lower aggregate distribution curve. For example, the bending strength of the M-G1 mixture was determined as 9.17 MPa, while the bending strength of the M-B16 mixture was determined as 9.09 MPa, and the bending strength of the M-G2 mixture was also found to be 8.53 MPa. It is found that the fineness modulus of the mix increased as the aggregate distributions of the mix changed from G1 to G2, and this caused an increase in the fineness modulus (which means that the grain size of aggregates became larger) reduced their bending strength. Considering the effect of the aggregate distribution on all mortar bending strengths, it can be seen that the highest bending strength value was obtained as 9.63 MPa in the M-C16 mixture and the second was M-G1 with 9.17 MPa following the first. On the other hand, the standard deviations of the mortars decreased (except for M-G2) and the air content of the fresh mortar increased when the fineness modulus of the mix decreased. This may be caused due to the increase in the average aggregate size of the mix (the fineness modulus of the mix) and it was reported that the higher aggregate size in the mix caused the settling problem creating gaps in the medium and realized a decrease in the strengths [24, 36]. On the other hand, the compressive strength of mortars was not influenced by the AGC, and the strengths only changed between 44–46 MPa. According to the cement properties obtained from the producer as given in Table 1, the cement has minimum 42.5 MPa compressive strength and the addition of fine aggregate didn't decrease/increase the strength. In addition, it was reported that the fine particles (0.063–4 mm) had a minor influence on the compressive strength of the specimens except for powders (<0.063 mm) if these were added to the cement paste [24, 36]. Accordingly, it can be commented that the bending behavior (bending is the combination of tensile + compressive stresses through the cross-section of the specimen as well-known) may have been influenced by the AGC. Besides, the minimum compressive strength values showed a limited change between 43–44 MPa while the standard deviation of the specimen presented a similar behavior. As a consequence of the results mentioned, AGC had an effect on the bending strengths and, a minor change was observed in the compressive strengths due to the AGC.

3.1.2. Results of the Second Stage of the Experimental Program

The results of the concretes were given in Table 7. According to the physical test results, it was found that when the fineness modulus of the mix increased due to different AGC, the density of NAC and RAC increased from 2.26 to 2.41 g/cm^3 and from 2.18 to 2.23 g/cm^3, respectively, and the increase in the density of RAC was found limited due to the increase in the open porosity. Because the water absorption of RAC was found higher than that of NAC, the inclusion of coarse RA in the mix was the key factor. For instance, the water absorptions of NAC-G2 and RAC-G2 were determined as 3.2% and 4.5% while the same AGC consideration in the mix and the mentioned difference became clearer when the coarse aggregate concentration increased in the mix from 14 to 78%. As reported in the literature, RA had a porous structure with high-water absorption and low-density values [1, 10, 21, 48] and it shaped the resulting concrete properties when RA was used in the mix. On the other hand, it can be indicated that the high fineness modulus the high coarse aggregate

Table 8. Weights of concrete properties

Criteria	Density	Water abs.	Coarse agg. ratio	Air content	Nat. agg. cons.	Fineness mod. of mix	Mean comp. str.
Weight values for NACs	0.0014	0.0207	0.7554	0.0295	0.0000	0.1737	0.0193
Weight values for RACs	0.0001	0.0275	0.6773	0.0480	0.0859	0.1558	0.0054
Weight values for concretes	0.0026	0.0636	0.5865	0.0688	0.0922	0.1349	0.0513

concentration, but the low natural aggregate concentration was observed by changing AGC from G1 to G2. Thus, the skeleton of the RAC became weak compared to NAC, so not only the physical properties but also the mechanical properties of RAC were affected negatively. Hence, the compressive strength of the RAC was obtained lower than NAC while the same AGC was considered.

When different AGCs from G1 to G2 were used with different fineness modulus from 3.36 to 6.79 mm in the mix, the compressive strength increased up to 38.7 MPa for up to 4.16 mm fineness modulus then decreased down to 34.2 MPa for up to 6.79 mm fineness modulus. Hence, the peak/maximum compressive strength of RAC was determined for RAC-C16. It can be stated that RAC-C16 had 56.8% natural aggregate concentration, a low open porosity (3.5%), and a high density (2.22 g/cm^3). However, the results showed that the highest compressive strength of NAC was obtained for RAC-A16 as 53.6 MPa with 69.9% natural aggregate concentration. It can be noted that the coarse aggregate concentration in the RAC caused high entrained air content, high open porosity, and settling problem decreasing the compressive strength while it supported the skeleton of NAC increasing the compressive strength of NAC although increasing a minor air content of the mix. Besides, although the mentioned positive effect of coarse NA on the strength was observed, the comments cannot be made for RA. Because RA had an additional part (AOM) compared to NA, AOM had low physical and mechanical properties compared to NA [21]. Therefore, RA had three ITZ: old ITZ between NA in RA and old AOM, new ITZ between NA in RA and cement paste, and new ITZ between AOM and cement paste [6, 24]. Thus, the inclusion of coarse RA cannot have acted as similar as the coarse NA and the increase in the compressive strength of RAC cannot have been observed due to AOM and the higher ITZ volume compared to that of NAC. In addition, based on the compressive strength test results, the strength classes of concretes were determined according to TS EN 206-1+A2 (Turkish Standards Institution, 2021), and the strength classes of the concretes were given in Table 7. According to the findings, it can be stated that the consideration of RA in the mix decreased not only the compressive strength but also the strength class of concrete. Besides, it is interesting that the strength class of not only NAC but also RAC were dependent on the aggregate type [24, 36] and the AGC. Also, the scatter of test results of compressive strength was observed due to the AGCs. The strength class of NACs was not the same and differed from C30/37 to C40/50. Similar comments can be made for RACs.

Thus, the fine particle proportion rather than coarse particle may have a great role in the results of RAC-C16, and AGC influenced RAC and NAC in a different way. Hence, the parameters mentioned above can be considered properly while the design of the RAC mix.

3.1.3. The Results of the Third Stage of the Experimental Program

In this section, the properties of concretes were evaluated in a holistic manner. First, the weights of the concrete results were determined using the Entropy Method and the importance of the parameters according to their weights was examined. In addition, considering the concrete results and parameters examined in the article, the best concrete series was determined using TOPSIS. Then, the results were compared together.

3.1.3.1. Entropy Method Results

The Entropy Method is a weighting method working objectively and is widely used in many areas from management to engineering. The output data of the method (weights) eases and accelerates decision-making with a low decision time. Hence, the weights of the parameters of concretes such as density, water absorption, coarse aggregate ratio, air content of fresh concrete, natural aggregate concentration, fineness modulus, and compressive strength were calculated to compare the importance level of each parameter in this study (Table 8). As a result, the weights of the properties of concretes were determined in consideration of the mentioned parameters.

The effect of the AGC on the properties of concretes was investigated in this study and the most important first and second criteria among the mentioned properties were determined by the Entropy Method such as that the first was the coarse aggregate ratio in the mix and the second was the fineness modulus of the mix aggregate. As mentioned in the previous section, it was found that the physical and the mechanical properties of not only NAC but also RAC were influenced by the coarse aggregate ratio of the mix and the natural aggregate concentration, and the findings were given in Table 8 proved these statements.

In addition, the comparison of the weights of the properties of NAC and RAC showed that the influence of the

Table 9. Weights of criteria (Scale from 1 to 10 imply that higher is important)

Criteria	Mortar		Concrete						
	Bending strength	Compressive strength	Coarse aggregate concentration	Natural aggregate concentration	Fineness modulus	Density	Water absorption	Air content	Compressive strength
Weights[a]	3	9	7	7	7	5	9	9	9

[a]: High is important.

Table 10. TOPSIS results

Concretes	NAC-G1	NAC-C16	NAC-B16	NAC-A16	NAC-G2	RAC-G1	RAC-C16	RAC-B16	RAC-A16	RAC-G2
Gi[a]	0.535	0.567	0.618	0.641	0.635	0.514	0.539	0.554	0.564	0.573

[a]: High is good.

AGC on the compressive strength of NAC was higher than that of RAC while a relatively minor influence of the AGC on the density of RACs and the natural aggregate concentration of NACs was found. Besides, when the weights of the concrete properties were compared, the weights of the water absorption and the air content of fresh concretes were nearly the same.

3.1.3.2. TOPSIS Results

TOPSIS is a method to determine the effectiveness and the suitable choice considering the criteria of the choices with their weights. Hence, when TOPSIS is intended to use, the weights of the criteria of the choice. In this paper, accordingly, the weights of criteria were determined as given in Table 9 and the results were evaluated in the TOPSIS using the weights which weights were formed according to the author's experiences. The scale for weights was performed from 1 to 10, and here the higher was more important. The mechanical performance and the durability performance were kept at the forefront. Hence, compressive strength and open-pore related properties such as the water absorption and the air content in the fresh concrete were decided as more important and 9 was specified. Besides, it is well-known that the natural aggregate concentration influences the mechanical performance of concrete [34] and 7 was specified for the concentrations.

After an examination of the parameters in TOPSIS, the results were found as given in Table 10. Separately evaluation of the test results showed that A16 resulted in a denser NAC with higher compressive strength, while C16 resulted in a durable RAC in terms of low water absorption capacity with higher compressive strength. However, when all parameters were investigated together using the TOPSIS the best AGCs were found as A16 for NAC and G2 for RAC, respectively. According to the TOPSIS results, RAC-G2 and RAC-A16 had 0.573 and 0.564 scores, respectively, and it can be noted that RAC-A16 can also be preferred instead of RAC-G2 due to the similar TOPSIS scores. When the TOPSIS results of RACs were compared with that of NAC, although RAC-G2 was the best in RACs, it is interesting that RAC-G2 was superior to the worse concrete among NACs.

4. CONCLUSION

In this paper, the effect of aggregate gradation curves (AGCs) detailed in TS 802 (A16, B16, and C16) on recycled aggregate concrete (RAC) was investigated. Also, two AGCs (G1 and G2) were proposed to examine the effect of the rest of the region detailed in TS 802 (A16, B16, and C16). Accordingly, a comprehensive experimental program was conducted including three stages for the evaluation of the properties of the mortar phase of concrete, the concrete, and the selection of the best concrete mix. Hence, after conducting the several tests on the specimens, the following conclusions and discussions were made based on the evaluations of the test results:

1) AGC had an effect on the bending strengths, and a minor change was found in the compressive strengths due to the effect of AGC.
2) Different AGCs required different fine and coarse aggregate proportions in the mix and five AGC were employed in the mix design of concretes. Accordingly, the fine particle ratio in the mix rather than the coarse particle ratio in the mix may have a great role in the results of RACs, and AGC affected RAC and NAC in a different manner. Thus, the parameters investigated in this paper can be considered properly in RAC mix design to achieve a high compressive strength value.
3) The Entropy results showed that the influence of the AGC on the compressive strength of NAC was higher than that of RAC while a relatively minor influence of the AGC on the density of RACs and the natural aggregate concentration of NACs. Also, the most important criterion was found as the coarse aggregate ratio in the mix and the fineness modulus of the mix aggregate followed the first.

4) Separately evaluation of the test results and holistic evaluation of all results presented different findings for RAC but the same for NAC. Accordingly, a separate evaluation of the test results showed that A16 resulted in a denser NAC with higher compressive strength, while C16 resulted in a durable RAC in terms of low water absorption capacity with higher compressive strength. However, when all parameters were investigated together using the TOPSIS the best AGCs were found as A16 for NAC and G2 for RAC, respectively. RAC-A16 can also be preferred instead of RAC-G2 due to the similar TOPSIS scores.

5. FURTHER ASPECTS

A16 AGC resulted in a denser NAC with higher compressive strength and can be suitable to use for NAC. However, further investigations should be conducted including the durability tests. C16 AGC can be offered to decrease the open pore content of RAC in terms of water absorption and thus this can lead to durable concrete. However, further investigations including durability parameters should be conducted. Because RA has pores, this leads to a weak link in the medium.

The Entropy Method, in this paper, gives the important level of the parameters and emphasizes that the coarse aggregate ratio in the mix was an important parameter and can be considered in the design of RAC. Besides, the importance level of the investigated properties of concretes should be enlarged by adding the other physical, mechanical, and durability properties. Thus, more comprehensive, understandable, and comparable findings can be achieved. Also, the weights of the concrete properties can be determined by using other weighting methods (i.e., SWARA, CILOS, IDOCRIW) and the results of the methods can be compared to each other. Also, the advantages and the disadvantages of the methods in the current area can be argued.

The AGCs such as A16, B16, and C16 considered in this paper were selected according to the maximum aggregate size (it was 16 mm). However, the effect of AGCs for the maximum aggregate sizes such as 8 mm, 32 mm, and 64 mm as given in TS 802 can be investigated in further studies RAC. Besides, in this paper, RA was sourced from low strength (<20 MPa) waste concrete. The medium strength (20–40 MPa) and the high strength (40 MPa>) waste concrete sources can be examined to observe the difference in the effect of the AGCs.

DATA AVAILABILITY STATEMENT

The author confirm that the data that supports the findings of this study are available within the article. Raw data that support the finding of this study are available from the corresponding author, upon reasonable request.

CONFLICT OF INTEREST

The author declare that they have no conflict of interest.

FINANCIAL DISCLOSURE

The author declared that this study has received no financial support.

PEER-REVIEW

Externally peer-reviewed.

REFERENCES

[1] de Brito, J., & Saikia, N. (2013). *Recycled aggregate in concrete use of industrial, construction and demolition waste*. Springer. [CrossRef]

[2] Li, X. (2008). Recycling and reuse of waste concrete in China: Part I. material behaviour of recycled aggregate concrete. *Resources, Conservation and Recycling*, 53, 36–44. [CrossRef]

[3] European Parlement (2008). Directive 2008/98/EC of The European Parliament and of The Council of 19 November 2008 on waste and repealing certain directives. *Official Journal of the European Union*, 312, 82–208.

[4] Dilbas, H., Şimşek, M., & Çakır, Ö. (2014). An approach for construction and demolition (C&D) waste disposal through concrete using silica fume. *EurAsia Waste Management Symposium*, Istanbul.

[5] Dilbas, H. (2014). *An examination on mechanical behaviour of a cantilever beam produced with recycled aggregate concrete* [Unpublished Master Thesis]. Graduate School of Natural and Applied Science, Yildiz Technical University.

[6] Dilbas, H., Şimşek, M., & Çakır, Ö. (2014). An investigation on mechanical and physical properties of recycled aggregate concrete (RAC) with and without silica fume. *Construction and Building Materials*, 61, 50–59. [CrossRef]

[7] Akça, K., Çakır, Ö., İpek, M., & Ipek, M. (2015). Properties of Polypropylene Fiber Reinforced Concrete Using Recycled Aggregates. *Construction Building Materials*, 98, 620–630. [CrossRef]

[8] Orhan, A.E. (2018). *Accounting for greenhouse gases emission from cement production* [Unpiblished Master Thesis]. Hacettepe University.

[9] Awchat, G. D., & Kanhe, N. M. (2013). Experimental studies on polymer modified steel fibre reinforced recycled aggregate concrete. *International Journal of Application or Innovation in Engineering & Management*, 2, 126–134. [CrossRef]

[10] Çakır, Ö., & Dilbas, H. (2021). Durability properties of treated recycled aggregate concrete: effect of optimized ball mill Method. *Construction and Building Materials*, 268, Article 121776.

[11] Wikipedia. (2022). 2. Dünya Savaşı. https://tr.wikipedia.org/wiki/II._Dünya_Savaşı [Turkish]

[12] Behera, M., Bhattacharyya, S.K., Minocha, A.K., Deoliya, R., & Maiti, S. (2014). Recycled aggregate from C&D waste & its use in concrete - a breakthrough towards sustainability in Construction Sector: A review. *Construction and Building Materials*, 68, 501–516. [CrossRef]

[13] Xiao, J., Li, W., Poon, C., Jianzhuang, X., Wengui, L.I., Chisun, P., Xiao, J., Li, W., & Poon, C. (2012). Recent studies on mechanical properties of recycled aggregate concrete in China-A review. *Science China Technological Sciences*, 55, 1463–1480. [CrossRef]

[14] Shaban, W. M., Yang, J., Su, H., Mo, K. H., Li, L., & Xie, J. (2019). Quality improvement techniques for recycled concrete Aggregate: A review. *Journal of Advanced Concrete Technology*, 17, 151–167. [CrossRef]

[15] Guo, H., Shi, C., Guan, X., Zhu, J., Ding, Y., Ling, T.C., Zhang, H., & Wang, Y. (2018). Durability of Recycled Aggregate Concrete – A Review. *Cement and Concrete Composites*, 89, 251–259. [CrossRef]

[16] Ramyar, K., Mardani-Aghabaglou, A., Inan, G., İnan Sezer, G., & Ramyar, K. (2014). Comparison of fly ash, silica fume and metakaolin from mechanical properties and durability performance of mortar mixtures view point. *Construction and Building Materials*, 70, 17–25. [CrossRef]

[17] Abd Elhakam, A., Mohamed, A. E., Awad, E., Elhakam, A. A., Mohamed, A.E., & Awad, E. (2012). Influence of Self-Healing, Mixing Method and Adding Silica Fume on Mechanical Properties of Recycled Aggregates Concrete. *Construction and Building Materials*, 35, 421–427. [CrossRef]

[18] Corinaldesi, V., & Moriconi, G. (2009). Behaviour of Cementitious Mortars Containing Different Kinds of Recycled Aggregate. *Construction and Building Materials*, 23, 289–294. [CrossRef]

[19] Shi, C., Li, Y., Zhang, J., Li, W., Chong, L., & Xie, Z. (2016). Performance enhancement of recycled concrete aggregate – A review. *Journal of Cleaner Production*, 112, 466–472. [CrossRef]

[20] Xiao, J., Li, W., Fan, Y., & Huang, X. (2012). An overview of study on recycled aggregate concrete in China (1996–2011). *Construction and Building Materials*, 31, 364–383. [CrossRef]

[21] Dilbas, H., Çakır, Ö., & Atiş, C.D. (2019). Experimental investigation on properties of recycled aggregate concrete with optimized ball milling method. *Construction and Building Materials*, 212, 716–726, [CrossRef]

[22] Dilbas, H., & Çakır, Ö. (2020). Influence of basalt fiber on physical and mechanical properties of treated recycled aggregate concrete. *Construction and Building Materials*, 254, Article 119216. [CrossRef]

[23] Dilbas, H., Çakır, Ö., & Yıldırım, H. (2020). An experimental investigation on fracture parameters of recycled aggregate concrete with optimized ball milling method. *Construction and Building Materials*, 252, Article 119118. [CrossRef]

[24] Dilbas, H. (2020). *An investigation of the effect of recycled aggregate use on concrete properties* (Unpublished Doctoral Thesis). Istanbul Yildiz Technical University.

[25] Bui, N. K., Satomi, T., Takahashi, H. (2017). Improvement of mechanical properties of recycled aggregate concrete basing on a new combination method between recycled aggregate and natural aggregate. *Construction and Building Materials*, 148, 376–385. [CrossRef]

[26] sharifi, E., Sadjadi, S.J., Aliha, M. R. M., & Moniri, A. (2020). Optimization of high-strength self-consolidating concrete mix design using an improved taguchi optimization method. *Construction and Building Materials*, 236, Article 117547. [CrossRef]

[27] Omary, S., Ghorbel, E., Wardeh, G., & Nguyen, M.D. (2018). Mix design and recycled aggregates effects on the concrete's properties. *International Journal of Civil Engineering*, 16, 973–992. [CrossRef]

[28] Pepe, M., Toledo Filho, R. D., Koenders, E. A. B., & Martinelli, E. (2014). Alternative Processing Procedures for Recycled Aggregates in Structural Concrete. *Construction and Building Materials*, 69, 124–132. [CrossRef]

[29] Amario, M., Santana, C., Pepe, M., Dias, R., & Filho, T. (2017). Optimization of normal and high strength recycled aggregate concrete mixtures by using packing model. *Cement and Concrete Composites*, 84, 83–92. [CrossRef]

[30] Pradhan, S., Kumar, S., & Barai, S. V. (2017). Recycled aggregate concrete: Particle packing method (PPM) of mix design Approach. *Construction and Building Materials*, 152, 269–284. [CrossRef]

[31] Duan, Z., Li, B., Xiao, J., & Guo, W. (2020). Optimizing mix proportion of recycled aggregate concrete by readjusting the aggregate gradation. *Structural Concrete*, 22(Suppl 1), E22–E32. [CrossRef]

[32] McGinnis, M. J., Davis, M., de la Rosa, A., Weldon, B. D., Kurama, Y. C. (2017). Strength and stiffness of concrete with recycled concrete aggregates. *Construction and Building Materials*, 154, 258–269. [CrossRef]

[33] Ashraf, W.B.; Noor, M.A. (2011). Performance-evaluation of concrete properties for different combined aggregate gradation approaches. *Procedia Engineering*, 14, 2627–2634. [CrossRef]

[34] Kocatürk, A. N., Haberveren, S., Altıntepe, A., Bayramov, F., Ağar, A. Ş., & Taşdemir, M. A. (2003). Agrega konsantrasyonunun betonun aşınma direncine Etkisi. 5. *Ulusal Beton Kongresi*, Istanbul. [Turkish]

[35] Turkish Standards Institution (2016). TS 802 Design of Concrete Mixes; Ankara.
[36] Mehta, P. K., & Monteiro, P. J. M. (2006). Concrete: Microstructure, properties and Materials. (Third Ed.). The McGraw-Hill.
[37] Turkish Standards Institution (2010). *TS EN 12390-2 Testing Hardened Concrete - Part 2: Making and Curing Specimens for Strength Tests*, Ankara.
[38] Turkish Standards Institution (2013). *TS EN 12390-7 Tests for Mechanical and Physical Properties of Aggregates - Part 6: Determination of Particle Density and Water Absorption*, Ankara.
[39] Turkish Standards Institution (2010). *TS EN 12390-3 Testing Hardened Concrete - Part 3 : Compressive Strength of Test Specimens*, Ankara.
[40] Turkish Standards Institution (2012). *TS EN 197-1 Cement – Part 1: Composition, Specification and Conformity Criteria for Common Cements*, Ankara.
[41] Turkish Standards Institution (2019). *TS EN 206-1 Concrete - Specification, Performance, Production and Conformity*, Ankara.
[42] Zhu, Y.; Tian, D.; Yan, F. (2020). Effectiveness of Entropy Weight Method in Decision-Making. *Mathematical Problems in Engineering*, 2020, Article 3564835. [CrossRef]
[43] Rashid, K., Razzaq, A., Ahmad, M., Rashid, T., & Tariq, S. (2017). Experimental and analytical selection of sustainable recycled concrete with ceramic waste aggregate. *Construction and Building Materials*, 154, 829–840. [CrossRef]
[44] Rashid, K., Hameed, R., Ahmad, H. A., Razzaq, A., Ahmad, M., & Mahmood, A. (2018). Analytical framework for value added utilization of glass waste in concrete: Mechanical and environmental performance. *Waste Management*, 79, 312–323. [CrossRef]
[45] Şimşek, B. & Uygunoğlu, T. (2016). Multi-response optimization of polymer blended Concrete: A TOPSIS based taguchi application. *Construction and Building Materials*, 117, 251–262. [CrossRef]
[46] Byun, H. S., & Lee, K. H. (2005). A decision support system for the selection of a rapid prototyping process using the modified TOPSIS method. *International Journal of Advanced Manufacturing Technology*, 26, 1338–1347. [CrossRef]
[47] Olson, D. (2004). Comparison of weights in TOPSIS models. *Mathematical and Computer Modelling*, 40, 721–727. [CrossRef]
[48] Dilbas, H., & Güneş, M. Ş. (2021). Mineral addition and mixing methods effect on recycled aggregate concrete. *Materials*, 14, 907. [CrossRef]